Molecular Dynamics and Orientation in Mixtures of Low-mass Molecules and Polymers

A Doctoral Thesis

by

Shogo Nobukawa

Submitted to

The Graduate School of Science, Osaka University

February, 2011

Acknowledgements

This thesis study was carried out during the period of 2005-2011 at the Department of Macromolecular Science, the Graduate School of Science, Osaka University. The author would like to express his sincere gratitude to Professor Dr. Tadashi Inoue and Associate Professor Dr. Osamu Urakawa for their cordial guidance and warm encouragement throughout this study. Grateful acknowledgements were also made to Associate Professor Dr. Toshiyuki Shikata for his helpful discussions and valuable comments.

The author would like to thank Assistant Professor Dr. Kenji Nakamura of the Graduate School of Science and Engineering, Ristumeikan University, Dr. Yousuke Ono of Mitsui Chemicals, Inc. and Mr. Yuichi Satokawa of DIC Co. for their helpful suggestions. The author sincerely thanks Ms. Keiko Saeki for her clerical support during his study. The author also thanks all members of Inoue laboratory for their helpful discussions and kind friendship.

The author would like to thank Professor Dr. Hiroshi Watanabe and Assistant Professor Dr. Yumi Matsumiya of the Institute for Chemical Research, Kyoto University for allowing him to use their Rheometer and for their valuable suggestions.

The author appreciates the financial supports from the BMC program (Integrated Educational program for Biological Sciences, Macromolecular Science, and Chemistry) of Osaka University (April, 2008 – March, 2009), and the Global COE (center of excellence) program, "Global Education and Research Center for Bio-Environmental Chemistry" of Osaka University (April, 2009 – March, 2011). The author also thanks to the grant from the Sasakawa Scientific Research Grant from the Japan Science Society (No. 21-350, April, 2009 – March, 2010).

Finally, the author wishes to express his gratitude to his family members for their constant and warm encouragements.

February, 2011

信川省吾

Shogo Nobukawa

Contents

Chapter I
General Introduction

I-1. Glass transition and cooperative dynamics

Glass transition phenomenon was found for many kinds of molecular liquids, including low-mass molecules and polymers, and it has been extensively studied so far.[1-6] Some molecular liquids turn into glasses *via* a supercooled state without crystallization. In such the glass forming materials, molecular dynamics exhibits the non-Arrhenius type temperature dependence as depicted in Fig. I-1.[6] In order to explain this anomalous temperature dependence, the notion of "cooperative molecular motion" in which a certain number of molecules are involved due to the *inter*-molecular interaction, was introduced by Adam and Gibbs.[3] The region where molecular motion is cooperative is called "cooperative rearranging region (CRR)". Their theory was quite successful, so that the notion of CRR is now widely accepted. However, it is not clear to apply the CRR concept to polymers because not only the *inter*-molecular but also the *intra*-molecular interactions are involved. The *intra*-molecular cooperativity governed by the internal rotational potential around the main chain carbon-carbon bonds should determine the size of the motional unit of a polymer in a single polymer chain, so called "segment". Thus, there are two key sizes to determine the dynamics of polymers: the segment size and CRR size. It is essential to clarify how these two types of cooperativity affect polymer dynamics around the glass transition for understanding the glass transition of the polymeric materials.

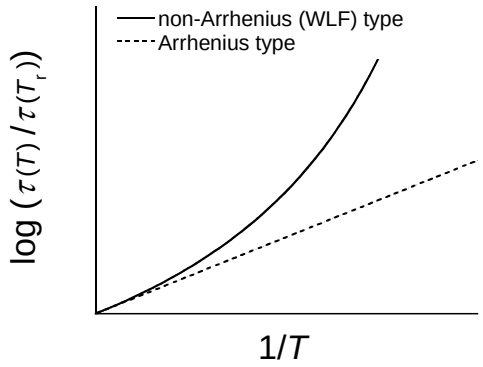

Figure I-1. Arrhenius and non-Arrhenius type temperature dependences for the molecular dynamics in glass forming liquids. τ is a characteristic relaxation time, which means the timescale of the molecular motion. T_r is a reference temperature.

Recently, it has been reported that some polymer/polymer or polymer/low-mass molecule (LMs) blends show heterogeneous glass transitions as if each component had their own distinct glass transition temperatures, T_g, even in the miscible state. This phenomenon is called "dynamic heterogeneity (DH)".[7] The component dynamics in such the miscible system are not completely coupled to each other and thus DH is observed. The DH phenomenon would be partly related to the chain connectivity (segment size of each component), and the mismatch in sizes between two constituent segments might be responsible for the DH. Understanding DH behavior of a two-component system (A/B) based on the CRR idea is a complex and challenging subject in the field of polymer dynamics because there are three types of *inter*-molecular interactions (A-A, B-B, and A-B) and two types of *intra*-molecular interaction (in A and B components). In order to shed light on this complicated situation, it is necessary to examine the glassy dynamics of polymer blends with changing both the segmental size and CRR size in a systematic way. However, these sizes in polymeric systems cannot be controlled so easy. In this thesis, the reorientation dynamics of rod-like low-mass molecules (LM) dissolved in flexible polymers are investigated, since LM dynamics in dilute state will be governed only by

the *inter*-molecular cooperativity between LM and polymer. Furthermore, LM has a well-defined molecular size so that by using the relaxation time of the LM component as an internal measure in the mixture systems, a relevant length scale for the glassy dynamics could be estimated.

Macroscopic deformation of polymeric materials induces the orientation of polymer chains. The rigid rod-like molecules dissolved in a deformed (oriented) polymer matrix are forced to align parallel to the direction of the polymer chain. The orientational coupling between the LM and the polymer will be evaluated, and the relationship between cooperative molecular orientation and dynamics will be discussed. In the following sections in this chapter, the detailed features related to the glass transition phenomena, dynamically heterogeneous behavior, and orientational correlation in some blend systems will be briefly reviewed. At the end of this chapter, the scope of this thesis is described.

I-2. Polymer dynamics in the vicinity of glass transition

Polymeric materials have been widely-used in our life as many kinds of commercial products. The mechanical and physical properties of polymers in the glassy state, such as an elastic modulus and the glass transition temperature, T_g, especially play important roles for industrial applications. Since T_g is independent of molecular weight, M, in a high M region where the degree of polymerization exceeds 100-1000, the glass transition is related to micro Brownian motion of chain portions over several repeating units. These molecular motions are called local chain motions, and they are considered to be "cooperative motions" of several repeating units under restriction of the internal rotational potential along the covalent carbon-carbon bonds due to the chain connectivity. The cooperative unit is called "segment" and the relaxation due to the segmental motion is often referred to as "α-relaxation" or "segmental relaxation" which can be observed by a wide variety of experimental

techniques: nuclear magnetic resonance (NMR)[8-10], dielectric relaxation (DR)[10-17], viscoelastic relaxation (VR)[18-21] and birefringence[20, 22-23] measurements, quasi-elastic neutron scattering (QENS)[24-25], fluorescence recovery after photobleaching (FRAP)[26-27], and other techniques. Irrespective of the measurements, the observed α relaxations of polymers are almost identical to each other and the α relaxation time, τ_α, shows quite similar temperature dependence described by the Williams-Landel-Ferry (WLF)[6, 28] function as follows using a reference temperature ,T_r,

$$\log\left(\tau_\alpha(T)/\tau_\alpha(T_r)\right) = -\frac{c_1(T-T_r)}{c_2+T-T_r} \qquad \text{(I-1)}$$

In earlier studies, temperature dependence of τ_α had been considered to be expressed by a universal WLF equation for typical polymeric materials if T_g was chosen as T_r: c_1 = 17.44 and c_2 = 51.6 K taking $T_r = T_g$ irrespective of polymer species.[29] However, now it has been widely recognized that the c_1 and c_2 are not universal but slightly depend on polymer structures.[30-32] The CRR sizes at T_g are also found to depend on polymer species.[32] Probably both the *intra*- and *inter*-molecular cooperativities, which might determine the CRR size, are dependent on polymer structures. For the case of polymer blends, the cooperative dynamics are much more complicated than simple alone systems because of three types of *inter*-molecular cooperativity as explained in the following section.

I-3. Dynamic heterogeneity in polymer/polymer and polymer/low-mass molecule blends

Recently, many researchers revealed that some miscible blends of polymer/polymer and polymer/low-mass molecule (LM) were dynamically heterogeneous. In this section, the details of the “dynamic heterogeneity” are firstly explained and then the purposes of this thesis are described.

Miscible polymer-polymer blends having large difference in T_g exhibit very broad glass transition as revealed by thermal and various types of relaxation measurements. These polymer blends are called dynamically asymmetric blends. The broadening of the glass transition is caused by two effects: a concentration fluctuation and the existence of two different *effective* T_gs for each of the blend components. Particularly, the idea of the *effective* T_g introduced by Lodge and MacLeish was able to explain successfully the glass transition behavior of polymer blends by considering "self-concentration" of the component polymer.[33-35] The key concept is "self-concentration" which describes that each component polymer feels different effective local concentrations due to the chain connectivity. Near a given repeating units, the probability for finding the same kind of repeating units becomes higher than the average concentration because both sides of the repeating unit are connected with the same kind of repeating units. The self-concentration, in their original theory, is estimated by regarding the statistical Kuhn segment as the dynamical unit related to the glass transition. This assumption that the Kuhn segment can be regarded as the dynamical segment unit, comes from the experimental finding by Inoue et al.[36-37] They found that the Kuhn segment had the similar size to the Rouse segment, which is a coarse grained unit in a bead-spring model and can be estimated by using a rheo-optical method. They also showed that the molecular motions responsible for the glass transition (referred to as "glass mode") was not related to the Rouse segment motion but related to more local unit, i.e., the twisting motion of a repeating unit.[23] Based on these findings, one may think that the Kuhn segment is not a suitable parameter to use as the dynamical unit related to the glass transition, and the self concentration model cannot perfectly explain the "dynamic heterogeneity" in polymer blends. Actually, the related length scale parameters in the Lodge-McLeish model are often regarded as just fitting parameters for quantitative description of data. Therefore, to modify the self-concentration model, it is necessary

to clarify the relationship between the length scale and structure related to the glassy dynamics of polymers.

Low-mass molecules (LMs) having a rod-like structure have fewer degrees of dynamical freedom than polymers. Also, no *intra*-molecular cooperativity works for rod-like LM dynamics, and thus the polymer/LM mixtures can be regarded as a model system to investigate the glass transition in the "dynamic heterogeneous blends". Do any LMs exhibit cooperative dynamics with polymer dynamics in the mixtures?

Adachi et al.[38-40] studied the dynamic heterogeneity of polymer solution, polystyrene (PS)/toluene (Tol) mixtures, through NMR, dielectric relaxation, and heat capacity measurements. They concluded that the Tol/PS mixtures are dynamic heterogeneous since the rotational motion of Tol was decoupled from the α-relaxation of PS and the heat capacity data showed a double step glass transition process. Therefore, the *inter*-molecular cooperativity between Tol and PS is not strong enough to exhibit a cooperative glass transition with a single T_g. In contrast, Urakawa et al. reported that PS/rod-like LM mixtures showed "dynamic homogeneity" unlike PS/Tol mixture.[41-42] They concluded that the difference between PS/rod-like LM and PS/Tol mixtures came from the size difference between Tol (much smaller) and rod-like LMs; the LMs they used were larger than Tol and comparable with the Kuhn segment size of PS. However, as mentioned above, it is unclear whether the Kuhn segment is comparable to the size of motional units for the glassy dynamics or not.

As a well-established technique called a fluorescence probe method, molecular motions of trace amount of fluorescent dyes dissolved in polymer matrices have been intensively investigated to probe the dynamics of matrix polymers especially near the glass transition by optical methods.[26] In those studies, the probe motion was implicitly assumed to be cooperative with the polymer motion. However, the above studies on PS mixtures suggest that there are two kinds of LMs: one can probe the polymer matrix dynamics but the other cannot. This difference would be in the size

of probe molecules: the large size LMs can be used as probes. It is necessary to clarify how the timescales of cooperative dynamics for LMs with various sizes are and how much the dynamics of small molecules (uncooperative LMs) is affected by matrix polymer dynamics.

In this thesis, the rotational relaxation of LMs and the α relaxation of polymers in the mixtures are examined by using broadband dielectric spectroscopy and dynamic mechanical relaxation measurements to compare directly the dynamics of LM and polymer. It would be worthwhile to note that the dielectric spectroscopy can sensitively detect rotational motions of LMs in much wider range of frequency (or timescale) than any other kinds of dynamic measurements. This makes it possible to discuss temperature dependence of rotational times over a wide temperature region. From the obtained results, the length scales or timescales of the glassy dynamics for various polymers are estimated and discussed in relation to the reported CRR sizes.

I-4. Correlation of molecular orientation between polymer and LM

Dynamic homogeneity (cooperative dynamics) of mixtures has been discussed based on the difference in the component relaxation times or friction coefficients at the segmental level including their temperature dependencies.[7, 33, 43-50] On the other hand, there is another cooperative phenomenon in miscible blends, i.e., local orientational coupling referred to as a nematic interaction (NI), which is observed as an enhancement of the optical anisotropy in applying the deformation on polymer materials. NI acts between the adjacent anisotropic molecules to be oriented in the same direction[51-56], leading to the cooperative orientation between the components to some extent in mixtures. Naturally, the following question arises. "Is there a correlation between dynamical cooperativity (homogeneity) and orientational coupling in mixtures?" If strong NI acts between component species, the component dynamics will become cooperative. However, strong NI will not necessarily be the origin of

the cooperative dynamics since the dynamically homogeneous state just requires both components to have similar friction coefficients in the mixture and does not require local orientational coupling. In order to ascertain the truth of these considerations, we choose the systems used in chapter II as a model system, in which the component dynamics is known to be cooperative as mentioned before and compare the NI parameter of this mixture with the typical values of that reported for chemically identical polymer blends with different molecular weights.[55] (Strictly speaking, the components do not have the same chemical structure, since one component is deuterated.)

For the evaluation of the NI effect, optical anisotropy measurements, such as birefringence and absorption dichroism, have been made so far,[52, 55-56] based on the theory proposed by Doi et al.[51] for single component entangled polymers. Afterward, Zawada et al.[56] extended their theory to be applicable to binary polymer blends and determined the NI parameter in a miscible polyisoprene/poly(vinyl ethylene) blend. Concerning the NI in polymer/LM mixtures, there is no study as far as we know. In such mixtures, LM component contributes not to the stress but to the birefringence through the NI in the rubbery-to-terminal region. Therefore, alternative theoretical equation is necessary to determine the NI parameter in polymer/LM mixtures.

In this thesis, a modified version of Zawada's equation to be applicable to polymer/LM systems will be proposed. The equation will be used to evaluate the NI parameters which quantify the orientational correlation between LM and polymer.

I-5. Scope of this doctoral thesis

As mentioned in previous sections, this thesis focuses on the dynamics of the components responsible for the glass transition in polymer/low-mass molecule (LM) mixtures to elucidate detailed molecular origin of cooperativity in polymer glasses. We chose LMs having a polar (cyano) group directly bound to the rigid aromatic group

because of the following reason. In order to observe selectively the rotational motion of the LM component in polymer/LM mixtures by dielectric measurements, the cyano group having larger dipole moment than apolar polymers was necessary. Furthermore, the rigid aromatic groups, such as biphenyl and terphenyl groups, can diminish the internal rotation degrees of freedom, so that these LMs suit our purpose to evaluate the cooperative dynamics between LM and polymers. In order to observe polymer dynamics, viscoelastic relaxation measurements are suitable and effective. When the polymer composition is high, the observed complex modulus almost reflect the polymer component contribution. In this way, the relaxation times of both components in the mixtures can be determined. Comparing the timescales for the component dynamics, the dynamic cooperativity (or uncooperativity) in the mixtures by changing the size of LMs, the polymer flexibility, and side-chain structure of polymers will be discussed. The LMs have rod-like structures, so that they will be cooperatively oriented parallel to the long axis of local chain segments of the polymer component due to the "nematic interaction". This cooperative orientation will be possibly related to the cooperative dynamics in polymer/LM mixtures.

In chapter II, the details of the rotational dynamics of 4-pentyl-4'-cyano-biphenyl (5CB, Fig. I-2) and 4-pentyl-4'-cyanoterphenyl (5CT, Fig. I-2) dissolved in a polystyrene (PS, Fig. I-2) matrix at several concentrations (5 ~ 27 wt%) are described. In particular, the relaxation mechanism of the LMs will be discussed by compared with the polymer chain dynamics. Discussion will be also made on the length scales

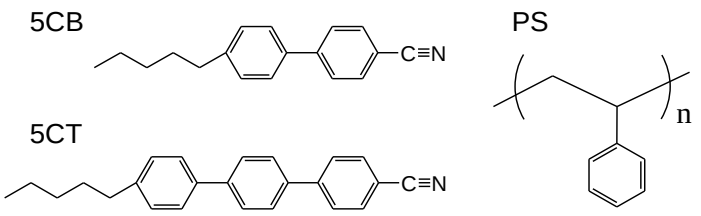

Figure I-2. Chemical structures of 4-pentyl-4'-cyanobiphenyl (5CB), 4-pentyl-4'-cyanoterphenyl (5CT), and polystyrene (PS).

relevant to the local chain motion of PS and the rotational motion of LM from the comparison of relaxation times for LMs and that for the Rouse segments. Furthermore, the dependence of the rotational relaxation behavior for 5CB molecules on the concentration is also investigated.

In chapter III, the effects of chain flexibility and side-chain bulkiness of polymers on the LM dynamics are examined. In order to change the flexibility, poly(1,2-butadiene) (1,2-PB), PS, poly(4-methyl styrene) (P4MS), and poly(4-*tert*-butyl styrene) (PtBS), shown in Fig. I-3, were used as polymer component, and the dynamics of 5CB dissolved in these polymers is compared. The effect of the Kuhn segment and side-chain sizes on the component dynamics is discussed. On top of that, we discuss how the side-chain bulkiness of polymers affects the LM dynamics in the mixtures. Furthermore, the dynamical scale of glass-mode relaxation for polymers, which dominates the cooperative motion of the LM, is also evaluated by comparing the relaxation time of 5CB with that of the viscoelastic glass-mode based on the Rouse[57] and rotational diffusion[58] theories.

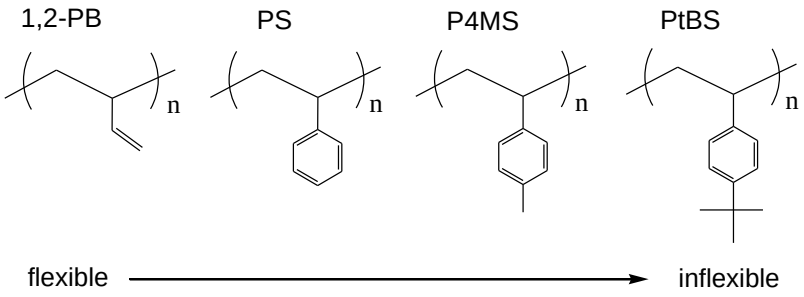

Figure I-3. Chemical structures of poly(1,2-butadiene) (1,2-PB), polystyrene (PS), poly(4-methyl styrene) (P4MS), and poly(4-*tert*-butyl styrene) (PtBS). The order of chain flexibility is also shown.

In chapter IV, nematic interaction (NI) between LM and polymer chain is estimated by using viscoelastic and birefringence data. The orientational correlation

via NI is compared with the cooperative dynamics described in the previous chapters and the origin of the cooperative dynamics in LM/polymer mixtures is discussed.

Finally, in chapter V, the obtained results in this thesis are summarized.

References

1. Ferry, J. D., *Viscoelastic Properties of Polymers*. 3rd ed.; Wiley: New York, 1980.
2. Fox, T. G.; Flory, P. J. *Journal of Polymer Science* **1954,** 14, 315-319.
3. Adam, G.; Gibbs, J. H. *Journal of Chemical Physics* **1965,** 43, 139-146.
4. Donth, E. *Journal of Non-Crystalline Solids* **1991,** 131, 204-206.
5. Angell, C. A. *Journal of Non-Crystalline Solids* **1991,** 131, 13-31.
6. Williams, M. L.; Landel, R. F.; Ferry, J. D. *Journal of the American Chemical Society* **1955,** 77, 3701-3707.
7. Alegria, A.; Colmenero, J.; Ngai, K. L.; Roland, C. M. *Macromolecules* **1994,** 27, 4486-4492.
8. Gisser, D. J.; Glowinkowski, S.; Ediger, M. D. *Macromolecules* **1991,** 24, 4270-4277.
9. Tracht, U.; Heuer, A.; Spiess, H. W. *Journal of Chemical Physics* **1999,** 111, 3720-3727.
10. Cendoya, I.; Alegria, A.; Alberdi, J. M.; Colmenero, J.; Grimm, H.; Richter, D.; Frick, B. *Macromolecules* **1999,** 32, 4065-4078.
11. Kremer, F.; Schönhals, A., *Broadband Dielectric Spectroscopy*. Springer-Verlag: Berlin, 2003.
12. Mansour, A. A.; Happ, E.; Wolf, T.; Stoll, B. *Colloid and Polymer Science* **1994,** 272, 894-902.
13. Runt, J. P.; Fitzgerald, J. J., *Dielectric Spectroscopy of Polymeric Materials*. American Chemical Society: Washington, DC, 1997.
14. Bergman, R.; Alvarez, F.; Alegria, A.; Colmenero, J. *Journal of Non-Crystalline Solids* **1998,** 235, 580-583.
15. Hirose, Y.; Urakawa, O.; Adachi, K. *Macromolecules* **2003,** 36, 3699-3708.
16. Hirose, Y.; Urakawa, O.; Adachi, K. *Macromolecules* **2004,** 37, 10215-10216.
17. Yano, O.; Wada, Y. *Journal of Polymer Science Part a-2-Polymer Physics* **1971,** 9, 669-686.

18. Inoue, T.; Cicerone, M. T.; Ediger, M. D. *Macromolecules* **1995,** 28, 3425-3433.
19. Roland, C. M.; Ngai, K. L.; Santangelo, P. G.; Qiu, X. H.; Ediger, M. D.; Plazek, D. J. *Macromolecules* **2001,** 34, 6159-6160.
20. Inoue, T.; Okamoto, H.; Osaki, K. *Macromolecules* **1991,** 24, 5670-5675.
21. Tyagi, M.; Alegria, A.; Colmenero, J. *Journal of Chemical Physics* **2005,** 122, 244909.
22. Inoue, T.; Mizukami, Y.; Okamoto, H.; Matsui, H.; Watanabe, H.; Kanaya, T.; Osaki, K. *Macromolecules* **1996,** 29, 6240-6245.
23. Inoue, T. *Nihon Reoroji Gakkaishi* **2000,** 28, 167-175.
24. Inoue, R.; Kanaya, T.; Nishida, K.; Tsukushi, I.; Shibata, K. *Physical Review Letters* **2005,** 95.
25. Inoue, R.; Kanaya, T.; Nishida, K.; Tsukushi, I.; Taylor, J.; Levett, S.; Gabrys, B. J. *European Physical Journal E* **2007,** 24, 55-60.
26. Ediger, M. D.; Inoue, T.; Cicerone, M. T.; Blackburn, F. R. *Macromolecular Symposia* **1996,** 101, 139-146.
27. Hwang, Y.; Inoue, T.; Wagner, P. A.; Ediger, M. D. *Journal of Polymer Science Part B-Polymer Physics* **2000,** 38, 68-79.
28. Ferry, J. D.; Landel, R. F.; Williams, M. L. *Journal of Applied Physics* **1955,** 26, 359-362.
29. Olabisi, O.; Robeson, L. M.; Shaw, M. T., *Polymer-Polymer Miscibility*. Academic Press, Inc.: New York, 1979.
30. Sokolov, A. P.; Novikov, V. N.; Ding, Y. *Journal of Physics-Condensed Matter* **2007,** 19.
31. Kunal, K.; Robertson, C. G.; Pawlus, S.; Hahn, S. F.; Sokolov, A. P. *Macromolecules* **2008,** 41, 7232-7238.
32. Ellison, C. J.; Mundra, M. K.; Torkelson, J. M. *Macromolecules* **2005,** 38, 1767-1778.
33. Lodge, T. P.; McLeish, T. C. B. *Macromolecules* **2000,** 33, 5278-5284.
34. Hirose, Y.; Urakawa, O.; Adachi, K. *Journal of Polymer Science Part B-Polymer Physics* **2004,** 42, 4084-4094.
35. Urakawa, O.; Ujii, T.; Adachi, K. *Journal of Non-Crystalline Solids* **2006,** 352, 5042-5049.
36. Inoue, T.; Matsui, H.; Osaki, K. *Rheologica Acta* **1997,** 36, 239-244.
37. Inoue, T. *Macromolecules* **2006,** 39, 4615-4618.
38. Adachi, K.; Fujihara, I.; Ishida, Y. *Journal of Polymer Science Part B-Polymer Physics* **1975,** 13, 2155-2171.
39. Taniguchi, N.; Urakawa, O.; Adachi, K. *Macromolecules* **2004,** 37, 7832-7838.

40. Yoshizaki, K.; Urakawa, O.; Adachi, K. *Macromolecules* **2003,** 36, 2349-2354.
41. Urakawa, O.; Ohta, E.; Hori, H.; Adachi, K. *Journal of Polymer Science Part B-Polymer Physics* **2006,** 44, 967-974.
42. Hori, H.; Urakawa, O.; Adachi, K. *Polymer Journal* **2003,** 35, 721-727.
43. Colby, R. H. *Polymer* **1989,** 30, 1275-1278.
44. Chung, G. C.; Kornfield, J. A.; Smith, S. D. *Macromolecules* **1994,** 27, 5729-5741.
45. Leroy, E.; Alegria, A.; Colmenero, J. *Macromolecules* **2002,** 35, 5587-5590.
46. Urakawa, O.; Fuse, Y.; Hori, H.; Tran-Cong, Q.; Yano, O. *Polymer* **2001,** 42, 765-773.
47. Haley, J. C.; Lodge, T. P.; He, Y. Y.; Ediger, M. D.; von Meerwall, E. D.; Mijovic, J. *Macromolecules* **2003,** 36, 6142-6151.
48. Lutz, T. R.; He, Y. Y.; Ediger, M. D.; Cao, H. H.; Lin, G. X.; Jones, A. A. *Macromolecules* **2003,** 36, 1724-1730.
49. Haley, J. C.; Lodge, T. P. *Colloid and Polymer Science* **2004,** 282, 793-801.
50. Watanabe, H.; Urakawa, O. *Korea-Australia Rheology Journal* **2009,** 21, 235-244.
51. Doi, M.; Pearson, D.; Kornfield, J.; Fuller, G. *Macromolecules* **1989,** 22, 1488-1490.
52. Kornfield, J. A.; Fuller, G. G.; Pearson, D. S. *Macromolecules* **1989,** 22, 1334-1345.
53. Doi, M.; Watanabe, H. *Macromolecules* **1991,** 24, 740-744.
54. Watanabe, H.; Kotaka, T.; Tirrell, M. *Macromolecules* **1991,** 24, 201-208.
55. Tassin, J. F.; Baschwitz, A.; Moise, J. Y.; Monnerie, L. *Macromolecules* **1990,** 23, 1879-1881.
56. Zawada, J. A.; Fuller, G. G.; Colby, R. H.; Fetters, L. J.; Roovers, J. *Macromolecules* **1994,** 27, 6851-6860.
57. Rouse, P. E. *Journal of Chemical Physics* **1953,** 21, 1272-1280.
58. Doi, M.; Edwards, S. F., *The Theory of Polymer Dynamics*. Oxford University Press: New York, 1986.

Chapter II

Component dynamics in mixtures of low-mass compounds and polymers

II-1. Introduction

Urakawa et al.[1-3] examined dielectric relaxation behaviors of polystyrene (PS)/low-mass molecule (LM) mixtures. They showed that the rotational motion of LM became cooperative with the α (dielectric segmental) relaxation of PS when the LM size was similar to the Kuhn segment size of PS.[1, 3] One unsolved but important concern in their conclusion is the assumption that the α relaxation of PS component takes place in the vicinity of T_g for the mixtures at a high PS content, since the dielectric α relaxation of PS could not be detected directly due to its low dielectric intensity. In order to provide more definite evidence whether both the motions are cooperative or not, it is necessary to compare the temperature dependence of relaxation times for both components.

In this chapter, the temperature dependence of both the relaxation times of PS and rod-like molecules in model mixtures are examined. Since the dielectric relaxation intensity of PS is much weaker than that of LMs (having large dipole moment), viscoelastic relaxation measurements were conducted to observe the PS chain motions. Quantitative comparison between the relaxation times of LM and PS enables us to understand deeply the dynamical cooperativity of these two components. The fundamental process of the cooperative motion will be also discussed.

II-2. Experimental

Samples Polystyrene (PS) was synthesized by living anionic polymerization of styrene (Wako Pure Chemical Industries, Ltd.) in benzene using *sec*-butyl lithium (Sigma-Aldrich) as an initiator. The weight average-molecular-weight (M_w) and molecular- weight distribution index (M_w/M_n) of PS were determined to be 15.9×10^3 and 1.07, respectively, by gel-permeation-chromatography (GPC) using PS standard samples (Tosoh). Two LM samples, 4-pentyl-4'-cyanobiphenyl (5CB, purity > 97 %) and 4-pentyl-4"-cyanoterphenyl (5CT, purity > 97 %), were also purchased from Wako Pure Chemical Industries, Ltd. and used as received. PS/5CB and PS/5CT mixtures were prepared by freeze-drying method from a benzene solution and subsequent removal of the residual solvent at an elevated temperature (100 ~ 150 ºC) in vacuo. Since all samples were transparent, components were homogeneously mixed.

The weight fractions of 5CB and 5CT in the mixtures, W_{5CB} and W_{5CT}, were determined by ^{1}H-NMR spectroscopy using Excalibur-270 (JEOL Ltd., Tokyo, Japan) for the deuterio-chloroform solutions. A typical ^{1}H-NMR spectra for PS/5CB system at W_{5CB} of 0.27 are shown in Fig. II-1. W_{5CB} and W_{5CT} were estimated from the peak areas indicated by alphabets (A to G) in this figure. The obtained values are listed in Table II-1.

Measurements Dielectric relaxation (DR) measurements of the PS/5CB and PS/5CT mixtures at various temperatures (−25 ~ 150 °C) were carried out by using two LCR meters, 4284A (Hewlett Packard, USA, angular frequency $\omega = 1.26\times10^2$~5.03×10^6 s^{-1}) and 7600 (Quad Tech, USA, $\omega = 62.8$~1.26×10^7 s^{-1}), and a homemade apparatus consisting of a Current Amplifier 428 (Keithley, USA) and a Fast-Fourier-Transform (FFT) Analyzer VC-2440 (Hitachi, Japan) which covers the frequency range of $\omega = 1.57\times10^{-2}$ ~ 6.28×10^3 s^{-1}. Samples were set in a parallel plate cell with a glass spacer and annealed at T_g+50 K in vacuo for 2 hours.

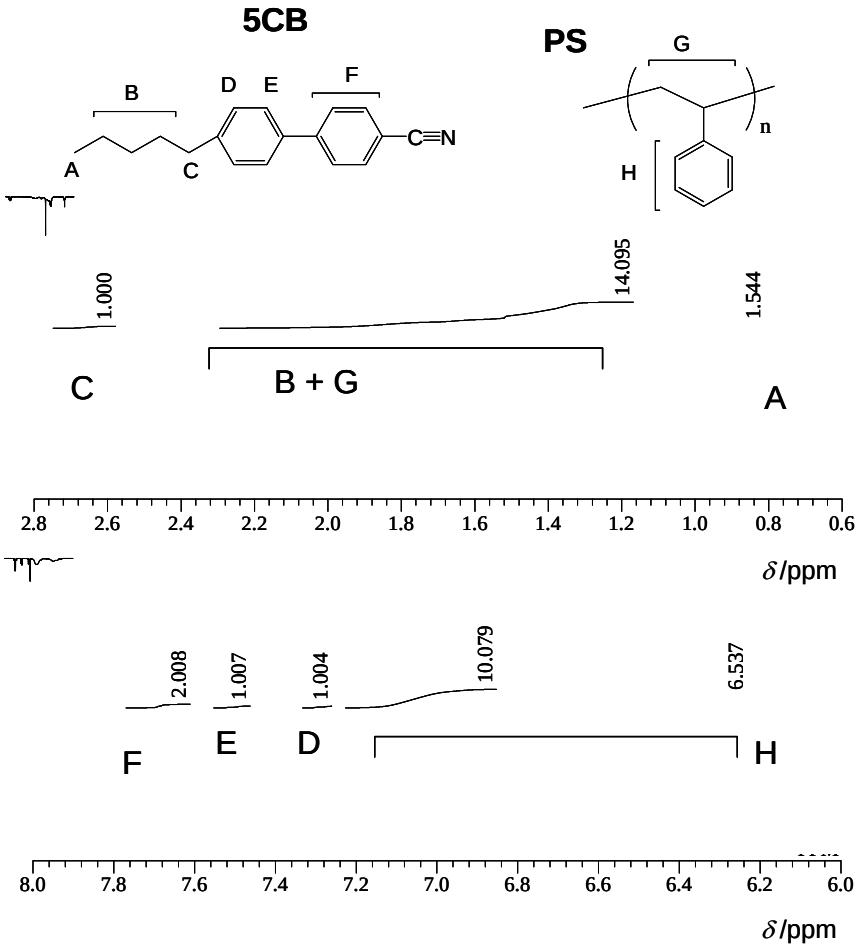

Figure II-1. ^{1}H-NMR spectra of PS/5CB in deuterated chloroform with concentration of 1 wt%. From integrated area of A, C~F, and H (except B and G), the weight fraction of 5CB was determined to be 0.27 in this system.

A dynamic viscoelastic relaxation (VR) measurement was carried out above the T_g of mixtures with two Dynamic Stress Rheometers (SR-500R, or SR-200, Rheometrics Inc., USA) using 25 mm parallel plates fixture after the DR measurement.

The glass transition temperature T_g for each mixture was determined by differential scanning calorimetry (DSC 6220, EXSTAR-6000, Seiko Instruments Inc., Japan) in the heating process with a rate of 10 K min^{-1}. For all the samples, the T_g values were checked to be unchanged before and after the DR and VR measurements to confirm that the composition change and the sample degradation did not occur.

Table II-1. Weight fractions of low-mass components (W_{5CB}, W_{5CT}), glass transition temperatures (T_g) dielectric relaxation intensities, $\Delta\varepsilon$, and activation energies, E_a, in PS/5CB or PS/5CT mixtures.

code	W_{5CB} or W_{5CT}	T_g / K	$\Delta\varepsilon_{\text{theo}}$ a)	$\Delta\varepsilon_{\text{total}}$ b)	$\Delta\varepsilon_{\text{slow}}$ b)	$\Delta\varepsilon_{\text{fast}}$ b)	E_a / kJmol^{-1}
PS	–	373	0.039	0.04	–	–	126 c)
PS/5CB	0.067	348	0.72	0.90	0.40	0.50	180 d)
	0.13	331	1.34	1.35	0.35	1.00	135 d)
	0.19	319	2.10	2.08	0.48	1.60	130 d)
	0.27	301	3.35	3.58	0.64	2.94	124 d)
PS/5CT	0.040	364	0.31	0.37	–	–	–
	0.11	352	0.95	0.75	–	–	–

a) Theoretical values were calculated by Onsager theory represented by eq. II-5 at T_g + 20 K for each mixture.

b) These values were obtained by fitting with eq. II-6 at T_g + 20 K.

c) β relaxation of PS

d) fast relaxation mode of 5CB

II-3. Results and Discussion

II-3-1. Composition dependence of glass transition temperature

Fig. II-2 shows DSC traces for bulk PS and PS/5CB mixtures. For all samples, a single glass transition was observed, indicating that the PS/5CB mixtures were homogeneously mixed without undergoing phase separations. The glass transition temperature, T_g, was determined from the flection point of the curve as indicated with arrows in Fig. II-2. Table II-1 summarizes T_gs of PS/5CB and PS/5CT mixtures. It is seen that T_g decreases with increasing 5CB or 5CT concentration, meaning that 5CB and 5CT work as ordinary plasticizers. Since the T_g of PS/5CB was lower than that of PS/5CT at the same composition, the ability of plasticization of 5CB is stronger than that of 5CT.

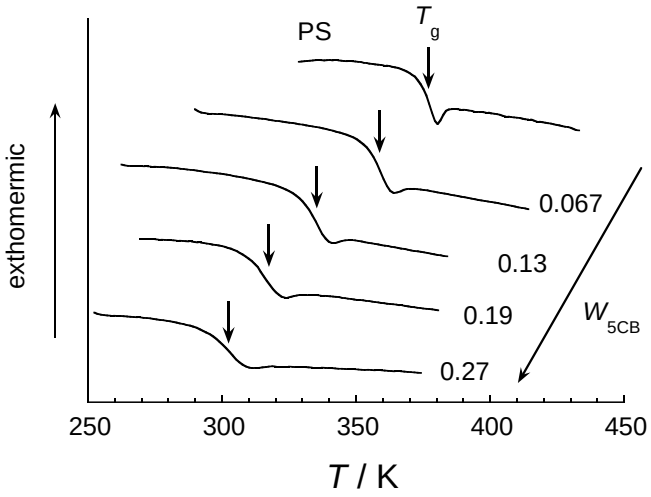

Figure II-2. DSC curves of bulk PS and PS/5CB mixtures at various compositions. The number represents the weight fraction of 5CB, W_{5CB}. The glass transition, T_g, is shown with arrows.

II-3-2. Viscoelastic relaxation behavior of PS/5CB and PS/5CT mixtures

Fig. II-3 displays the composite curves of the complex shear modulus, $G^*(\omega) = G'(\omega) + iG''(\omega)$ for bulk PS and PS/5CB mixtures at the reference temperature of 373 K. $G'(\omega)$ and $G''(\omega)$ are storage and loss moduli, respectively. Since molecular weight of PS is 15.9×10^3 being lower than the entanglement molecular weight (M_e ~ 20,000), the obtained viscoelastic curves are compared with the Rouse Model[4], which is known to reproduce the viscoelastic relaxation spectra very well for non-entangled polymers. The Rouse model explains the viscoelastic relaxation behavior of non-entangled polymers; it assumes that a polymer chain is composed of N+1 beads linearly connected with springs as shown in Scheme II-1, and considers the Brownian motion of the beads. The expression for G' and G'' is given by,

$$G'(\omega) = \frac{c\,R\,T}{M}\sum_{p}^{N}\frac{(\omega\tau_p)^2}{1+(\omega\tau_p)^2} \qquad \text{(II-1)}$$

$$G''(\omega) = \frac{c\,R\,T}{M}\sum_{p}^{N}\frac{\omega\tau_p}{1+(\omega\tau_p)^2} \qquad \text{(II-2)}$$

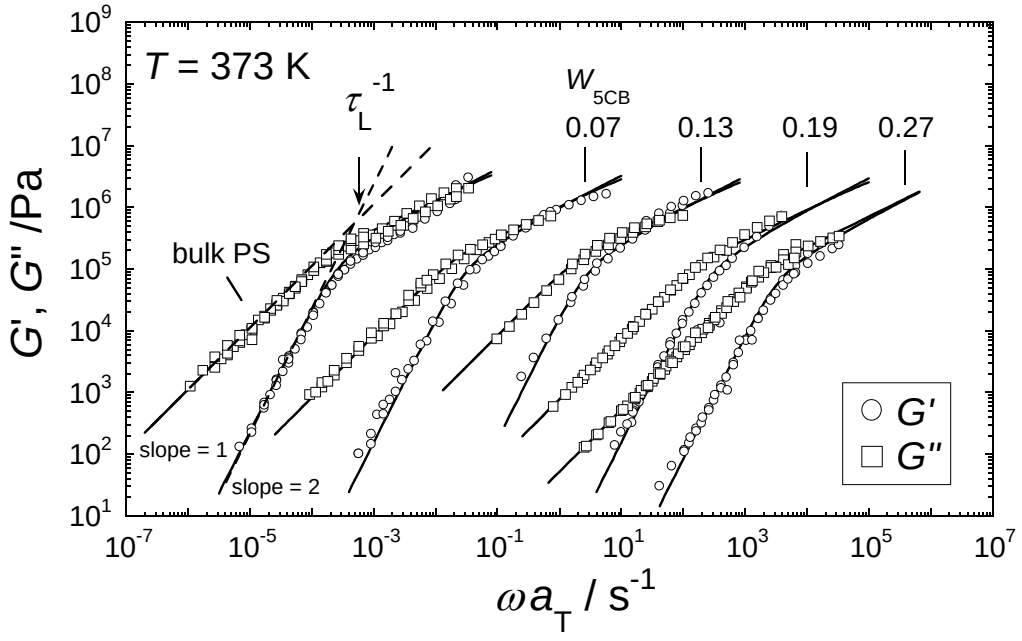

Figure II-3. Composite curves of bulk PS and PS/5CB mixtures at 373 K. Solid lines are the fitted result by using the Rouse model represented in eqs. II-3–II-5. Dotted lines on G' and G'' data represent the power law relations; $G' \propto \omega^2$ and $G'' \propto \omega^1$.

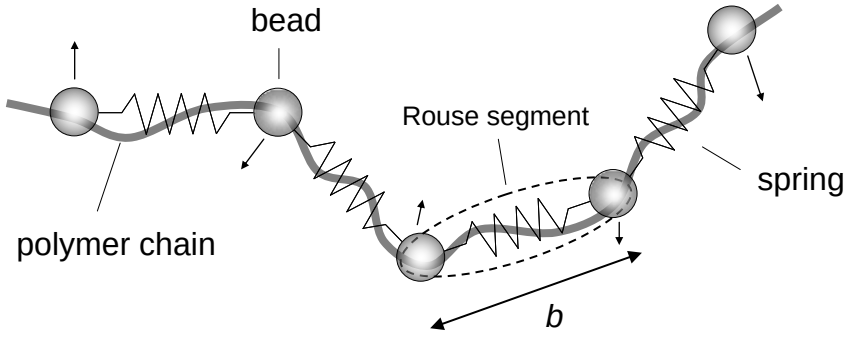

Scheme II-1 Schematic illustration of the Rouse model. N+1 beads are linearly connected with N springs. b is the bond length of the Rouse segment.

Here, c, R, T and M are the polymer concentration, gas constant, absolute temperature and molecular weight of the polymer, respectively. In the Rouse model, the chain dynamics is considered as coupled oscillations and the relaxation time of the p'th normal (Rouse) mode, τ_p, is given by

$$\tau_p = \frac{\tau_1}{p^2} = \frac{\zeta b^2 N^2}{6\pi^2 p^2 k_B T} \qquad \text{(II-3)}$$

Here, ζ, b, N, and k_B are friction factor, effective bond length, number of the Rouse segments, and the Boltzmann constant, respectively. Particularly, τ_1 is the longest relaxation time approximately equal to the terminal relaxation time, τ_L, determined by the viscoelastic measurement. Furthermore, the fastest mode corresponding to the case of $p = N^2$ in eqs. II-1 and II-2 is the fundamental process for the Rouse dynamics: the Rouse segment relaxation. The fastest relaxation time, τ_N, can be obtained to be τ_1/N^2 from eq. II-3. As seen in Fig. II-3, the G' and G'' curves could be fitted by the Rouse model (solid lines). The terminal relaxation time, τ_L, was determined from the crossing frequency of two lines represented by $G'(\omega) \propto \omega^2$ and $G''(\omega) \propto \omega^1$, as shown by the dotted lines in Fig. II-3.

Fig. II-4 illustrates the temperature dependence of τ_L for PS and PS/5CB at various compositions. With increasing 5CB concentration, τ_L curve shifts to lower temperatures, reflecting a decrease in T_g. In Fig. II-5, τ_L values are plotted against temperature difference, $T–T_g$. All the τ_L values overlap and can be expressed by a single universal curve as a function of $T–T_g$. In Figs. II-4 and II-5, the solid lines represent curves calculated by the following Williams-Landel-Ferry (WLF) equation.[5]

$$\log\left(\tau_L(T)/\tau_L(T_r)\right) = -\frac{c_1(T-T_r)}{c_2+T-T_r} \qquad \text{(II-4)}$$

Here, c_1 and c_2 are constants and T_r is a reference temperature. The obtained c_1 and c_2 values were c_1=12 and c_2=60 K at $T_r=T_g$, which are not so different from the generally reported vales; c_1=17.44 and c_2=51.6 K for ordinary polymers.[6]

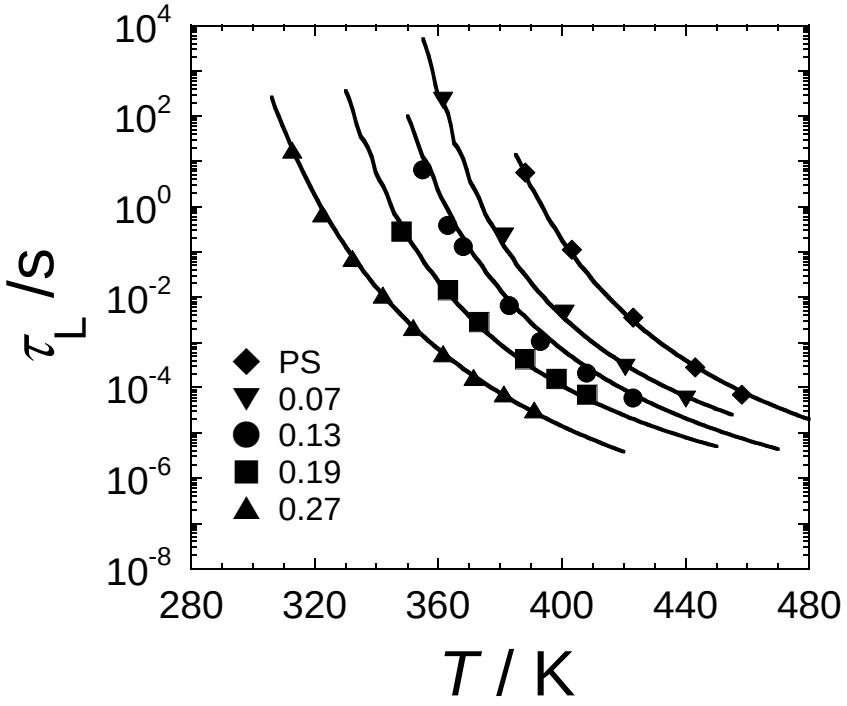

Figure II-4. Temperature dependence of τ_L for PS and PS/5CB at various compositions. Solid curves represent the fitted results by using the WLF equation given by eq. II-6.

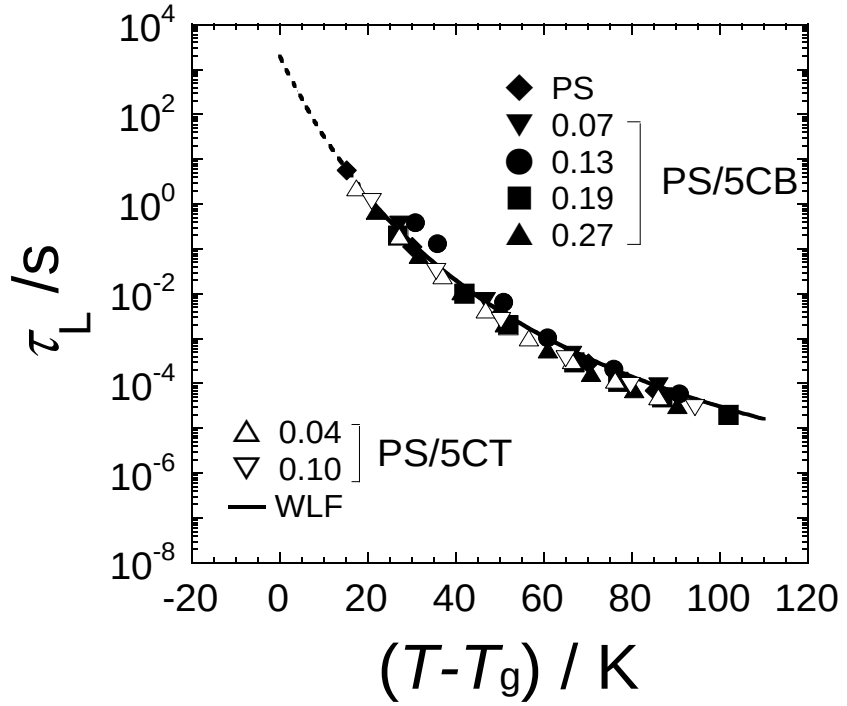

Figure II-5. Dependence of τ_L on $T–T_g$. A solid line is a curve calculated by the WLF equation (eq. II-6) with c_1=12.5, c_2=60 K and T_r=T_g.

II-3-3. Dielectric relaxation behavior of PS/5CB mixtures

Fig. II-6 shows dielectric loss spectra for PS/5CB mixture with W_{5CB}=0.13 at several temperatures. With decreasing temperature, the dielectric spectra become broader. This indicates breakdown of time-temperature-superposition (TTS) principle for the ε'' curve of PS/5CB mixtures. In addition to that, the ε'' spectra exhibit bimodal distribution particularly in the vicinity of and below T_g. Other PS/5CB mixtures at different compositions (W_{5CB} = 0.07, 0.19, and 0.27) also showed the similar trend concerning the temperature dependence of the spectrum shape.

Fig. II-7 shows the comparison of the ε'' spectra for PS/5CB mixtures with various compositions around the T_g of each mixture. In this figure, ε'' reduced by W_{5CB} (ε''/W_{5CB}) are compared since, as discussed later, the observed dielectric relaxation can be attributed to the motion of only 5CB. From Fig. II-7, it can be noted that the peak frequencies of two relaxation (slow and fast) modes do not change so much but the relative intensity of the two modes changes with composition: the fast mode becomes stronger with increasing W_{5CB}.

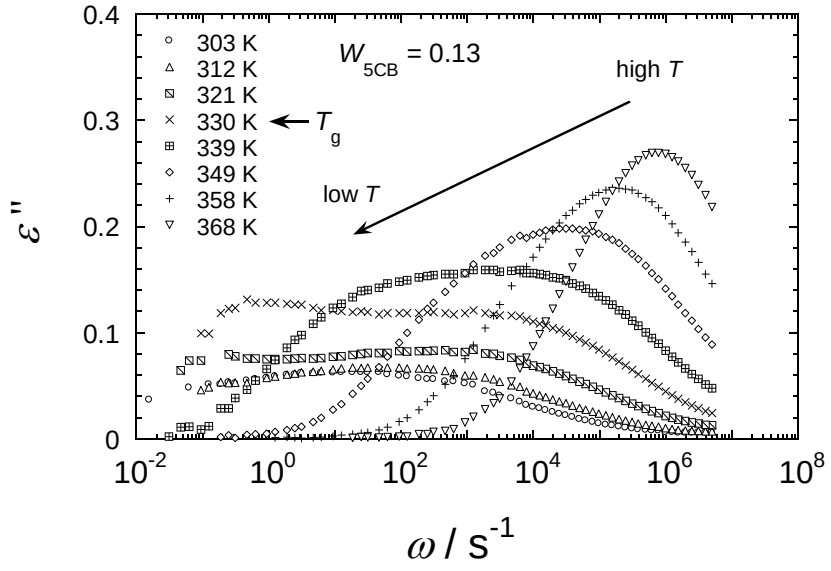

Figure II-6. Angular frequency, ω, dependence of dielectric loss, ε'', for PS/5CB (W_{5CB} = 0.13) at various temperatures.

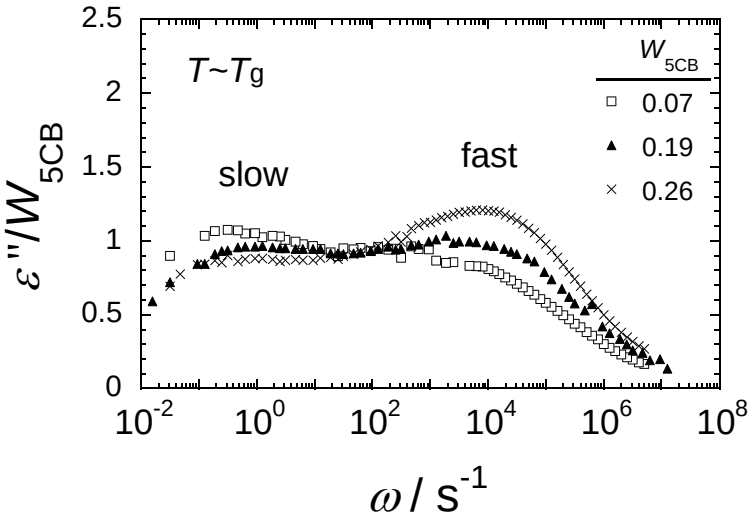

Figure II-7. Comparison of dielectric spectra for PS/5CB mixtures at various compositions. The vertical axis is reduced by the weight fraction of 5CB, W_{5CB}, for each mixture. With increasing W_{5CB}, slow component became weaker (fast component became stronger).

According to Onsager[7], a dielectric relaxation intensity, $\Delta\varepsilon\,(=\varepsilon(0)-\varepsilon_\infty)$, due to a polar molecule is given by,

$$\frac{(\varepsilon(0)-\varepsilon_\infty)(2\varepsilon(0)+\varepsilon_\infty)}{\varepsilon(0)(2+\varepsilon_\infty)^2}=\frac{\rho\phi_i N_A}{M}\frac{\mu^2}{9\varepsilon_0 k_B T} \qquad \text{(II-5)}$$

Here, $\varepsilon(0)$ and ε_∞ are dielectric permittivities at $\omega = 0$ and ∞, respectively, ε_0 is the electric constant (or the vacuum permittivity), N_A is Avogadro's number, and ρ is the density. M and ϕ_i are the molecular weight and the volume fraction of a polar molecule i having the electric dipole moment, μ, in the mixture, respectively. The densities of PS and 5CB are almost the similar ($\rho_{PS} = 1.04$ and ρ_{5CB}[8] $= 1.01$ at the isotropic state), thus ϕ_i can be replaced by the weight fraction, W_i. From eq. II-5, the dielectric intensities, $\Delta\varepsilon$, of PS and 5CB components in the mixtures can be estimated by using the μ values; μ(PS, repeating unit) = 0.21 D and μ(5CB) = 4.4 D (1 D =

3.33564×10^{-30} C m), which were calculated by WinMopac software (Fujitsu). Thus calculated theoretical values of dielectric intensities, $\Delta\varepsilon_{theo}$, are summarized in Table II-1. $\Delta\varepsilon_{theo}$ for bulk PS (0.039) is less than 1/18 of that for 5CB (0.72 for $W_{5CB} = 0.07$) at all mixtures in this study. This large difference in dielectric intensities indicates that the contribution of PS relaxation is negligibly small, so that only the 5CB relaxation is observed in the dielectric spectra for the mixtures. In conclusion, both the fast and slow modes in the bimodal spectra can be attributed to the relaxations of the 5CB molecule.

Fig. II-8 shows the dielectric spectra of PS/5CB mixture ($W_{5CB} = 0.13$) at 330.5 and 349.5 K. As seen in these spectra, the dielectric relaxations of the mixtures were much broader than the Debye type relaxation[9] (the single mode relaxation shown by a dotted line). Therefore, the broad dielectric spectra were fitted by the sum of the two Cole-Cole type relaxation functions[10-11] given by eq. II-6.

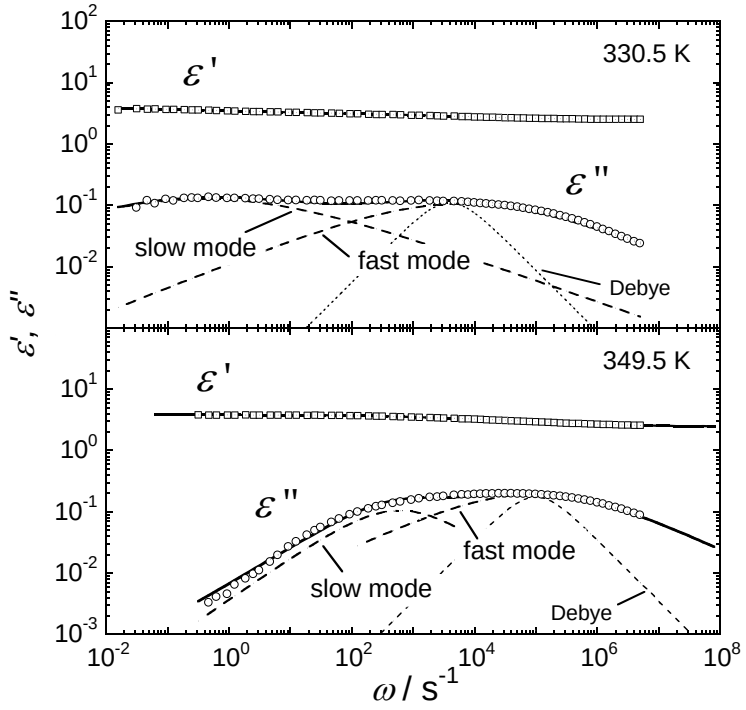

Figure II-8. Typical dielectric spectra of PS/5CB mixture ($W_{5CB} = 0.13$) at 330.5 and 349.5 K. The solid line represents the best fitted curves obtained by using eq. II-6. The broken lines show the Cole-Cole function. The dotted line represents a single Debye type relaxation.

$$\varepsilon^*(\omega) = \varepsilon_\infty + \sum_{j=\text{s 1 of w s}} \frac{\Delta\varepsilon_j}{1+(\mathrm{i}\omega\tau_j)^{\alpha_j}} \qquad \text{(II-6)}$$

The fit curves for PS/5CB (W_{5CB} = 0.13) are shown by solid lines in the figure. Here, α_j is the symmetric broadening parameter for j mode. In the case of the Debye type function, this parameter is equal to 1. α_{slow} and α_{fast} in Fig. II-8 were 0.35 and 0.33 for 330.5 K, and 0.55 and 0.42 for 349.5 K, respectively. Therefore, the dielectric relaxation spectra of these two modes became broader with decreasing temperature, indicating the broadening of the relaxation time distribution for 5CB in the mixture. The two rotational relaxation times of 5CB in the mixture, τ_{slow} and τ_{fast}, obtained by this fit, are plotted against the reciprocal of temperature T^{-1} in Fig. II-9 (so-called the Arrhenius plot). As seen in Fig. II-9, τ_{slow} rapidly increases in the vicinity of T_g with decreasing temperature while τ_{fast} is proportional to T^{-1}; therefore, the former shows the non-Arrhenius, that is, the WLF type of temperature dependence given by eq. II-4 while the latter exhibits the Arrhenius type of temperature dependence. For all other mixtures with different compositions, the τ_{slow} and τ_{fast} values were also determined

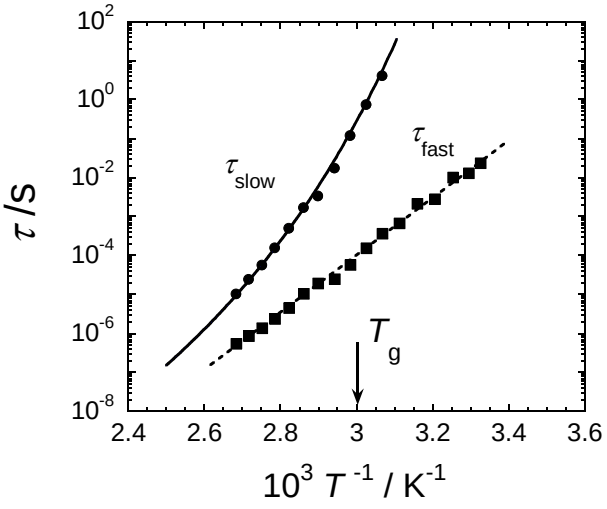

Figure II-9. Temperature dependences of dielectric relaxation times, τ_{slow} and τ_{fast}, for PS/5CB mixture at weight fraction of 5CB, W_{5CB} = 0.13.

and plotted as functions of $T-T_g$ in Fig. II-10 (A). It can be seen that both τ_{slow} and τ_{fast} form single-universal curves in this temperature range. This suggests that the fast and slow modes of 5CB are both related to the glass transition of the mixtures.

The dielectric intensities, $\Delta\varepsilon_{slow}$, $\Delta\varepsilon_{fast}$ and $\Delta\varepsilon_{total}$ ($=\Delta\varepsilon_{slow}+\Delta\varepsilon_{fast}$) obtained from the fitting procedure with eq. II-6 are summarized in Table II-1. It is likely that $\Delta\varepsilon_{total}$ and $\Delta\varepsilon_{theo}$ values are similar, meaning that both slow and fast modes are related to the rotational relaxation of 5CB. Furthermore, the similarity of $\Delta\varepsilon_{total}$ and $\Delta\varepsilon_{theo}$ indicates that 5CB molecules are well dispersed in the mixture without forming dimers or other higher order aggregates which change the effective dipole moment of 5CB molecule. From the data shown in Table II-1, it is noted that the relative intensities of the slow and fast modes depend on W_{5CB}: the relative intensity of the slow mode, $\phi_{slow} = \Delta\varepsilon_{slow}/\Delta\varepsilon_{total}$ is calculated to be 0.44 and 0.18 at $W_{5CB} = 0.067$ and 0.27, respectively. In the next section, the mechanism of the fast and slow modes will be explained in detail.

II-3-4. Relaxation mechanism of 5CB in PS/5CB mixtures

As described in the previous section, two relaxation modes (slow and fast modes) were observed in dielectric spectra for PS/5CB mixtures and both modes could be attributed to the rotational motion of 5CB. Now, the detailed relaxation mechanisms for these two modes will be discussed. It is obvious that the concentration fluctuation (CF) effect makes the relaxation time distribution broad, but cannot give bimodal distribution. Therefore, the observed bimodal relaxation spectra are never explained by the CF effect. Are there two kinds of 5CB species having the slow and fast relaxation times in PS/5CB mixtures? Concerning this issue, two possibilities are to be considered: (1) phase separation, and (2) formation of small aggregate of 5CB, like dimer, trimer, etc, due to dipole-dipole interactions. Hori et al.[1, 12] reported that the two components in the PS/5CB mixture are homogeneously

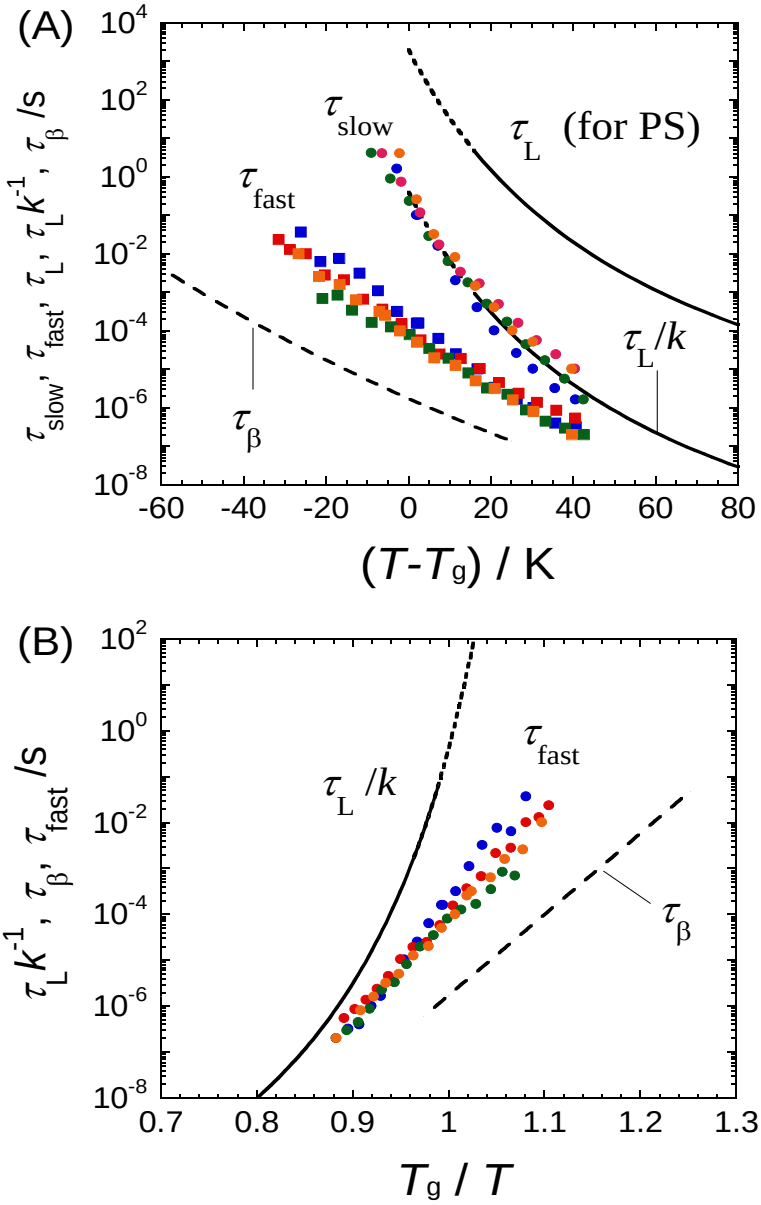

Figure II-10. (A): Temperature dependence of three relaxation times, τ_{slow}, τ_{fast}, and τ_L for PS/5CB mixtures at various compositions. Blue, red, green and orange symbols correspond to W_{5CB} = 0.07, 0.13, 0.19 and 0.27, respectively. The factor k = 5000 was used to superpose the viscoelastic relaxation time τ_L/k to the τ_{slow}. This k value is larger than the square of the Rouse mode number ($19^2 \approx 360$). The dashed line shows β relaxation time of bulk PS, τ_β, taken from the literature data.[13] (B): Temperature dependence of τ_{fast}, τ_L/k, and τ_β, which were plotted against T_g/T.

mixed within the composition range studied here, so that the mixtures did not undergo phase separation. Therefore, the possibility (1) of phase separation was excluded. The possibility (2) of the formation of small aggregates of 5CB molecules was also denied from the discussion in the previous section concerning the dielectric intensity based on eq. II-5. From these considerations, it is reasonable to think that the motion of a 5CB molecule takes place in two steps which correspond to slow and fast processes.

What are the relaxation mechanisms for the two rotational modes then? Rotational relaxation times of a rod-like molecule such as 5CB around long and short axes are known to be different.[14-15] However, the dielectric intensity corresponding to the rotational motion around long axis is very small in the isotropic state. Therefore, the observed two modes can not be attributed to the anisotropic rotational motion of 5CB. As will be discussed later, the slow and fast modes correspond to the rotation of whole 5CB molecule coupled with the α relaxation of PS and the fluctuation (wobbling) motion of 5CB permitted in a restricted free space by the less mobile PS chains. In the next section, the relaxation times of the slow and fast modes are compared with the PS chain relaxation to consider the 5CB dynamics in more detail.

II-3-5. Comparison of the dielectric and viscoelastic relaxation times

In Fig. II-10 (A), the slow relaxation time, τ_{slow}, showed the WLF type dependence on T and could be expressed by a universal function of $T-T_g$ as described in section II-3-3. This means that the slow mode of 5CB has a strong correlation with glass transition phenomena of the PS/5CB mixtures as Urakawa et al.[3] previously concluded. In general, glass transition is related to the segmental motion in bulk polymers, which is called the α relaxation, and the relaxation time becomes 1 ~ 100 s at T_g.[16] Since τ_{slow} at T_g takes about 1 s (cf. Fig. II-10 (A)), the slow mode of 5CB

around T_g has the same order of timescale with the α relaxation of PS.

The global (viscoelastic) relaxation time of PS is known to be proportional to the α relaxation time in the high temperature range ($T > T_g$+20 ~ 30 K).[17-19] In order to compare the component dynamics, the terminal relaxation time, τ_L, which is related to the global motion of PS chain, is also shown in Fig. II-10 (A) along with τ_{slow} and τ_{fast}. The temperature dependence of τ_{slow} seems to be similar to that of τ_L although the timescale of τ_{slow} is much shorter than τ_L. To examine the difference of τ_{slow} and τ_L, τ_L/k (k is a numerical number) is plotted in Fig. II-10 (A). By setting k = 5000, the dependence of τ_L/k on T could be superposed to that of τ_{slow} in the T range of $T > T_g$+20 K. This indicates that the slow mode of 5CB is cooperative with the PS chain motion. To examine the meaning of k (=5000), the Rouse relaxation time is compared with τ_L/k. From eq. II-3, the fastest Rouse mode corresponding to $p = N$ (N is the number of the Rouse segments) is regarded as a fundamental process for the global chain motion of polymers. Inoue et al. determined the molecular weight corresponding to the Rouse segment, M_s, for PS to be 850 from a rheo-optical method.[20-21] By using this M_s value, N for PS in this study ($M_w = 1.59\times10^4$) was estimated to be 18.7. This predicts the relaxation time of the fastest mode, $\tau_{seg(Rouse)}$ (= τ_L/N^2), to be $\tau_L/350$, which is longer than τ_{slow} (= $\tau_L/5000$). From this comparison and the same T dependence of τ_L and τ_{slow}, it can be concluded that, while the slow mode of 5CB reflects the smaller scale motion than the Rouse segment, the fundamental dynamic process for these two types of motion is the same in the high temperature range ($T > T_g$+20 K).

In contrast, T dependence of the fast mode is obviously different from that of the PS chain motion as shown in Figs. II-10 (A) and (B). This indicates that the fast mode is not cooperative with the PS chain dynamics. What is the origin of the fast relaxation of 5CB in the mixtures? In the previous studies,[3, 22-23] the fast mode was attributed to the spatially-restricted motion of 5CB in a “cage” mainly formed by PS

matrices. Since the fast mode is uncooperative with the α-relaxation of PS, it is natural that the temperature dependence of τ_{fast} will obey the Arrhenius type equation: $\tau = \tau_0 \exp(E_a/RT)$. Here, R is the gas constant, τ_0 is the relaxation time at limiting high temperature, and E_a is the activation energy. In Fig. II-10 (B) τ_{fast} data for all the PS/5CB mixtures are plotted against T_g/T. It seems that all the data can be approximately represented by a single straight line as predicted by the Arrhenius equation. The activation energies, $E_{a(fast)}$, determined from a slope in this plot were 120 ~ 180 kJ mol^{-1}, which are summarized in Table II-1. These activation energies are much larger than that of the rotational motion for 5CB in the pure and isotropic state (30 ~ 40 kJ mol^{-1})[24], which was determined by a dielectric measurement. Therefore, the fast mode is strongly affected by the existence of PS chain even though it is uncooperative with the α relaxation of the PS chain.

Dielectric β relaxation of bulk PS was reported by Yano and Wada[13] and was assigned to the motions of the smaller unit than that of the α relaxation of PS. However, the detailed mechanism for the β relaxation motion of PS is unclear. The β relaxation time of PS, τ_β, obeys the Arrhenius equation and has the activation energy, $E_{a(\beta)}$, of 126 kJ mol^{-1}. The activation energies for PS/5CB system except for the lowest composition (0.07) are close to the $E_{a(\beta)}$. The relationship between τ_{fast} and τ_β is shown in Fig. II-10 (A). The τ_{fast} value locates between α and β relaxations. When the abscissa axis is T_g/T, the data of τ_{fast} gather into a single line irrespective of the compositions as shown in Figs. II-10 (B). The similarity of the activation energy between τ_{fast} and τ_β suggests that the fast mode of 5CB might be governed by the same friction factor with the β relaxation of PS. The longer τ_{fast} value than τ_β suggests that the fast mode has larger dynamical scale than the β relaxation of PS.

The fraction of the dielectric relaxation intensity for the fast mode, defined as $\phi_{fast} = \Delta\varepsilon_{fast}/(\Delta\varepsilon_{fast}+\Delta\varepsilon_{slow})$, is calculated to be 0.56, 0.74, 0.77, and 0.82 for W_{5CB} = 0.067, 0.13, 0.19, and 0.27, respectively, at T_g+20 K from Table II-1.

Therefore, the relative intensity of the fast mode increases with increasing the concentration of 5CB at the same temperature from T_g, $T–T_g$, as seen in Fig. II-7 and also in Table II-1. Since the intensity of the fast mode reflects the amplitude of the fluctuating motion of 5CB under the restriction of the cage formed by PS matrix, the increase of ϕ_{fast} suggests that the cage size around 5CB molecule increases with W_{5CB}. PS component will mainly contribute to create the cage which restricts the rotational motion of 5CB molecules, and thus its size may increase with W_{5CB}. However, concerning the cage size, further quantitative analysis is difficult at present.

II-3-6. Dielectric relaxation of 5CT in PS/5CT mixtures

Fig. II-11 shows dielectric loss spectra of PS/5CT mixture at $W_{5CT} = 0.04$. By comparing the shapes of these spectra with those of PS/5CB shown in Fig. II-6, the ε'' curves of the PS/5CT mixture are unimodal and sharper than those of PS/5CB. This behavior was already reported[3] and the reason why the ε'' curves become unimodal is explained by the disappearance of the fast mode for PS/5CT system, i.e., the wobbling motion in a restricted cage becomes difficult for the large-size 5CT molecule. With increasing temperature, the peak position shifts to the higher frequency side and the shape of ε'' curves become narrower. Since the Cole-Cole function given by eq. II-6 could not perfectly fit these spectra shown in Fig. II-11 due to the asymmetry in the shape of the ε'' curves, the Havriliak-Negami function[25] given by eq. II-7 was used instead of eq. II-6, to fit the data.

$$\varepsilon^*(\omega) = \varepsilon_\infty + \frac{\Delta\varepsilon}{(1+(i\omega\tau_{HN})^\alpha)^\beta} \qquad \text{(II-7)}$$

Here, τ_{HN} is the characteristic relaxation time and β is an extra parameter not included in the Cole-Cole function, which represents the degree of asymmetry of the spectrum

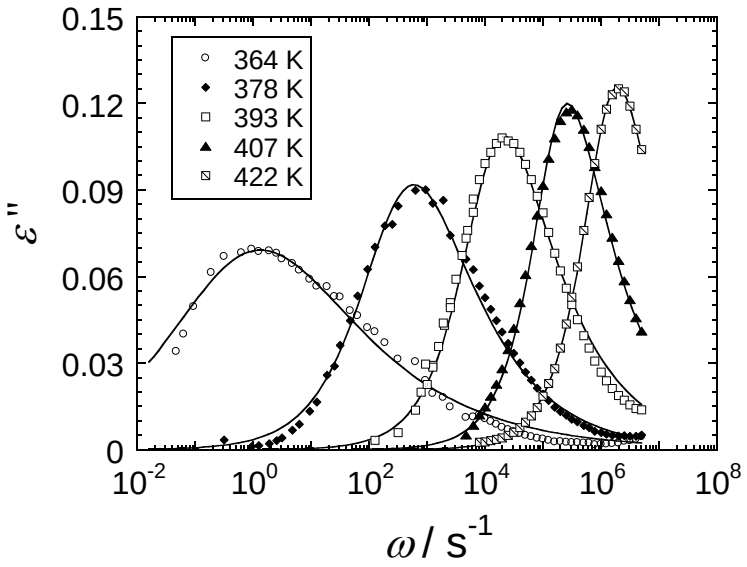

Figure II-11. Comparison of dielectric spectra for PS/5CT mixture (W_{5CB} = 0.04) at several temperatures. The solid lines are best fitted results by using eq. II-7.

shape. The fit curves are also shown by solid lines in Fig. II-11. The obtained parameters α and β were 0.45 and 0.60 for 364 K, and 0.95 and 0.55 for 407 K, respectively. β did not change so much but α decreased with decreasing temperature, meaning the distribution of the relaxation time became narrower with increasing temperature without changing the symmetry of the ε'' curves. The relaxation intensities, $\Delta\varepsilon$, were obtained to be 0.37 and 0.75 for PS/5CT mixtures with W_{5CT} = 0.04 and 0.11, respectively, from the fit of the data with eq. II-7. These intensities are close to $\Delta\varepsilon_{theo}$ (0.31 and 0.95 for W_{5CT} = 0.04 and 0.11, respectively) estimated by eq. II-5 with the dipole moment of 5CT (μ_{5CT} = 4.8 D), meaning that each 5CT molecule is well dispersed in PS matrices without aggregation in the same way with 5CB.

It is known that the relaxation time in the Havriliak-Negami function, τ_{HN}, does not correspond to the peak frequency, in the case of $\beta \neq 1$. The relaxation time,

τ_{max}, representing the peak frequency is given by the following equation[26],

$$\tau_{\max} = \tau_{HN}\left[\frac{\sin\left(\frac{\pi\alpha\beta}{2(\beta+1)}\right)}{\sin\left(\frac{\pi\alpha}{2(\beta+1)}\right)}\right]^{1/\alpha} \qquad \text{(II-8)}$$

From this equation, the average relaxation time of 5CT, τ_{5CT} (= τ_{max}) was determined as plotted against $T-T_g$ in Fig. II-12. The viscoelastic relaxation time divided by k, τ_L/k (here we set k = 2000 to superpose them), for PS/5CT mixtures also are compared in this figure. It is seen that the temperature dependence of τ_{5CT} is the same with that of τ_L, at least $T > T_g$+20 K, indicating that the rotational motion of 5CT is cooperative with the α dynamics of PS component. By comparing τ_{5CT} with τ_{slow} (for 5CB) which was shown in Fig. II-10, however, the k factors were 2000 and 5000 for 5CT and 5CB, respectively. This difference will be explained in the following section.

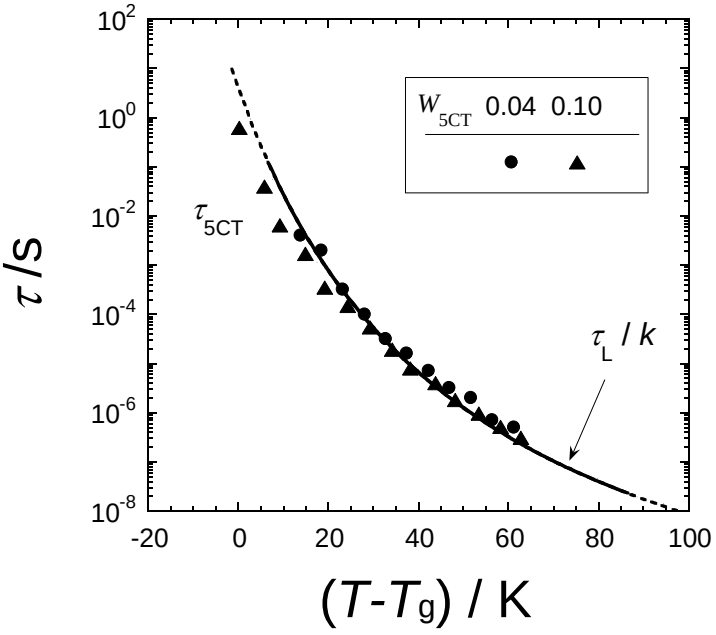

Figure II-12. Temperature dependence of relaxation τ_{5CT} for PS/5CT mixtures (W_{5CB} = 0.04 and 0.10). The solid line represents the τ_L/k data with k = 2000. The dashed line is the WLF function with c_1 = 13 and c_2 = 50 K at the reference temperature, $T_r = T_g$.

II-3-7. Timescale of cooperative motion for 5CB and 5CT

The relaxation times of 5CB and 5CT in the mixtures at a temperature difference from T_g, $T–T_g$, were slightly different: τ_{5CT} is 2.5 times longer than τ_{slow} of 5CB (the values of k for 5CT and 5CB are 2000 and 5000, respectively, as explained in Figs. II-10 and II-12). The difference in relaxation times is considered to be due to a difference in molecular sizes. Since 5CB and 5CT can be regarded as a rod-like molecule, the rotational relaxation time, τ, can be examined by using the following equation (rotational relaxation time for a rod in continuum media).[14]

$$\tau = \frac{\pi\eta L^3}{6k_B T\left(\ln(L/d) - \gamma\right)} \qquad \text{(II-9)}$$

Here, η is the viscosity coefficient of the media and γ is a correction factor (=0.8), L and d are the length of the long and short axes for the rod. According to this equation, the ratio of relaxation times, τ_{5CT}/τ_{slow}, is approximately proportional to $(L_{5CT}/L_{5CB})^3$. (Here, the aspect ratio, L/d, was assumed to be the same between 5CB and 5CT.) From the average lengths of the long axis (1.26 and 1.67 nm for 5CB and 5CT, respectively), the ratio, τ_{5CT}/τ_{slow}, becomes to be 2.3. This value is very close to the experimental value of 2.5. This result indicates that the difference in the relaxation time can be explained by the size difference of low-mass molecules. Furthermore, it can be said that the dynamics of 5CB and 5CT molecules are governed by the same effective viscosity (η in eq. II-9), which might be determined by the α motion of PS chain. The effective viscosity will be explained in chapter III.

II-4. Conclusion

In this chapter, the component dynamics in the mixtures of two rod-like low-mass molecules (4-pentyl-4'-cyanobiphenyl (5CB) and 4-pentyl-4'-cyanoter-

phenyl (5CT)) and polystyrene (PS) were examined by using dynamic viscoelastic relaxation (VR) and dielectric relaxation (DR) measurements. Temperature dependence of the viscoelastic terminal relaxation time, τ_L, of the mixtures reflecting the global motion of PS, could be represented by a single WLF equation by choosing the reference temperature $T_r = T_g$. Viscoelastic relaxation spectra for all PS/5CB and PS/5CT mixtures could be fitted by the Rouse model; the relaxation time distribution in the terminal region did not change so much with the composition.

PS/5CB mixture exhibited two rotational relaxation (slow and fast) modes in the DR spectra, both corresponding to 5CB motion, while PS/5CT mixture exhibited one rotational mode of 5CT. By comparing the temperature dependences of the rotational relaxation times of 5CB and 5CT in the mixtures with that of τ_L reflecting the PS chain dynamics in the mixture, it was concluded that the rotational motions of 5CB (slow mode) and 5CT were cooperative with the α dynamics of PS chain. In particular, the cooperative relaxation time of the low-mass molecules was found to be proportional to the cube of the length (long axis) for the molecules as predicted by the theory for rod-like molecules in a continuous medium. On the other hand, the fast mode in PS/5CB mixtures was attributed to the fluctuation of 5CB allowed in a restricted free volume (or a cage) formed mainly by PS component. The relaxation intensity of the fast mode depended on both temperature and composition which might change the cage size.

References

1. Hori, H.; Urakawa, O.; Adachi, K. *Polymer Journal* **2003,** 35, 721-727.
2. Yoshizaki, K.; Urakawa, O.; Adachi, K. *Macromolecules* **2003,** 36, 2349-2354.
3. Urakawa, O.; Ohta, E.; Hori, H.; Adachi, K. *Journal of Polymer Science Part B-Polymer Physics* **2006,** 44, 967-974.

4. Rouse, P. E. *Journal of Chemical Physics* **1953,** 21, 1272-1280.
5. Ferry, J. D.; Landel, R. F.; Williams, M. L. *Journal of Applied Physics* **1955,** 26, 359-362.
6. McCrum, N. G.; Read, B. E.; Williams, G., *Anelastic and Dielectric Effects in Polymeric Solids*. Dover Publications, Inc.: New York, 1967.
7. Onsager, L. *Journal of the American Chemical Society* **1936,** 58, 1486-1493.
8. Zgura, I.; Moldovan, R.; Beica, T.; Frunza, S. *Crystal Research and Technology* **2009,** 44, 883-888.
9. Debye, P.; Ramm, W. *Annalen Der Physik* **1937,** 28, 0028-0034.
10. Cole, K. S.; Cole, R. H. *Journal of Chemical Physics* **1941,** 9, 341-351.
11. Alvarez, F.; Alegria, A.; Colmenero, J. *Physical Review B* **1991,** 44, 7306-7312.
12. Nobukawa, S.; Urakawa, O.; Shikata, T.; Inoue, T. *Zairyo* **2009,** 58, 47-52.
13. Yano, O.; Wada, Y. *Journal of Polymer Science Part a-2-Polymer Physics* **1971,** 9, 669-686.
14. Doi, M.; Edwards, S. F., *The Theory of Polymer Dynamics*. Oxford University Press: New York, 1986.
15. Kundu, S. K.; Okudaira, S.; Kosuge, M.; Shinyashiki, N.; Yagihara, S. *Journal of Chemical Physics* **2008,** 129, 164509.
16. Kremer, F.; Schönhals, A., *Broadband Dielectric Spectroscopy*. Springer-Verlag: Berlin, 2003.
17. Adachi, K.; Hirano, H. *Macromolecules* **1998,** 31, 3958-3962.
18. Roland, C. M.; Ngai, K. L.; Santangelo, P. G.; Qiu, X. H.; Ediger, M. D.; Plazek, D. J. *Macromolecules* **2001,** 34, 6159-6160.
19. Roland, C. M.; Ngai, K. L.; Plazek, D. J. *Macromolecules* **2004,** 37, 7051-7055.
20. Inoue, T.; Mizukami, Y.; Okamoto, H.; Matsui, H.; Watanabe, H.; Kanaya, T.; Osaki, K. *Macromolecules* **1996,** 29, 6240-6245.
21. Inoue, T.; Matsui, H.; Osaki, K. *Rheologica Acta* **1997,** 36, 239-244.
22. Nobukawa, S.; Urakawa, O.; Shikata, T.; Inoue, T. *AIP Conference Proceedings* **2008,** 1027, 561-563.
23. Urakawa, O.; Nobukawa, S.; Shikata, T.; Inoue, T. *Nihon Reoroji Gakkaishi* **2010,** 38, 41-46.
24. Jadzyn, J.; Czechowski, G.; Legrand, C.; Douali, R. *Physical Review E* **2003,** 67.
25. Havriliak.S; Negami, S. *Polymer* **1967,** 8, 161-210.
26. Diaz-Calleja, R. *Macromolecules* **2000,** 33, 8924-8924.

Chapter III

Dynamics of Low-mass Molecule Dissolved in Polymers with Different Side-chain Structure

III-1. Introduction

In chapter II, molecular dynamics of polystyrene (PS) and rod-like low-mass molecules (LMs) in the mixtures were discussed based on the results of dielectric and viscoelastic relaxation measurements.[1-2] The comparison of component relaxation times demonstrated that the cooperative motion of LMs was faster than the shortest Rouse motion of PS, indicating that the Rouse mode is not a fundamental process for the cooperative dynamics. Therefore, it is necessary to identify what kind of dynamics of PS matrix is fundamental for the LM dynamics.

Urakawa et al.[3-4] studied the LMs size effect on the cooperative dynamics in LMs/PS mixtures. According to them, when LMs had the similar size to the Kuhn segment of PS, LMs moved cooperatively with the α dynamics of PS, which is related to the glass transition. In contrast, smaller LMs uncooperatively rotated in the mixtures. They estimated the two critical sizes where LMs dynamics became perfectly cooperative or uncooperative with PS dynamics. Since the Kuhn segment size depends on chemical structures of polymer, the critical sizes will depend on polymers. Furthermore, the cooperative dynamics of LMs will be affected by *inter*-molecular interactions which will possibly depend on the side-chain structure of polymers. However, the length scale of the α (glassy) relaxation is related to not only *intra*-molecular but also *inter*-molecular interactions between polymer chains. Therefore, the dynamical scale of the α relaxation will be different from the Kuhn

segment size which is associated with only the *intra*-molecular cooperativity.

In this chapter, 4-pentyl-4'-cyanobiphenyl (5CB) as the LM was used and dissolved in various polymers having different flexibilities, i.e., the different lengths of the Kuhn segment. The relationship between the 5CB dynamics and polymer chain flexibility was examined by using dielectric and viscoelastic relaxation measurements. By comparing timescales of component dynamics from the glass to flow regions for the mixtures, the length scale of the glassy (α) unit for polymer chains is examined. The length scale of the α (glassy) relaxation unit is discussed in relation to the Kuhn segment size.

III-2. Experimental

Materials Polystyrene (PS), poly(4-methyl styrene) (P4MS), poly(4-*tert*-butyl styrene) (PtBS), and poly(1,2-butadiene) (1,2-PB) were synthesized by a living anion polymerization of vinyl monomers (styrene, 4-methyl styrene, 4-*tert*-butyl styrene, and 1,3-butadiene) with *sec*-butyl lithium (Sigma-Aldrich) as an initiator in benzene or *n*-heptane solution. The weight-average molecular weight, M_w, and molecular weight distribution, M_w/M_n were determined by gel-permeation-chromatography (GPC) as shown in Table III-1. Here, M_n is the number-average molecular weight. 4-Pentyl-4'-cyanobiphenyl (5CB, purity > 97 %) was purchased from Wako Pure Chemical Industries, Ltd and used as received. Chemical structures of polymers and 5CB are shown in Fig. III-1.

To prepare mixture samples, polymer and 5CB were first dissolved in benzene at a weight ratio of about 95/5 and then the solvent (benzene) was removed by freeze-dry method. To remove any air bubbles, all samples were annealed above T_g at low-pressure atmosphere for about half a day. Since 5CB is not perfectly nonvolatile, the compositions of the mixtures could not be precisely controlled by weighting. Therefore, the weight fraction of 5CB, W_{5CB}, was determined before/after

each measurement by ^{1}H-NMR spectroscopy using EXcalibur-270 (JEOL Ltd., Tokyo, Japan) or Mercury-300 (Varian, California, USA) for deuterio-chloroform solutions in which the small portion of the mixture film was dissolved. The compositions were confirmed to be almost constant during all measurements, and are shown in Table III-2.

Table III-1. Weight-average molecular weight, M_w, molecular weight distribution, M_w/M_n, glass transition temperature, T_g, the Kuhn segment length, l_K, and dielectric relaxation intensity, $\Delta\varepsilon$, for PS, P4MS, PtBS, and 1,2-PB.

	M_w /10^4	M_w/M_n	T_g / K	l_K / nm *	$\Delta\varepsilon$ (373 K)**
PS	1.59	1.05	373	1.79	0.038
P4MS	11.1	1.08	387	2.17	0.0074
PtBS	4.51	1.06	419	2.30	0.0064
1,2-PB	3.0	1.05	275	1.55	0.096

* determined from literature data[5-6] with characteristic ratio C_∞ or mean-square-radius $\langle S^2 \rangle$

** estimated by Onsager equation with dipole moment values calculated by WinMopac software (Fujitsu, Japan)

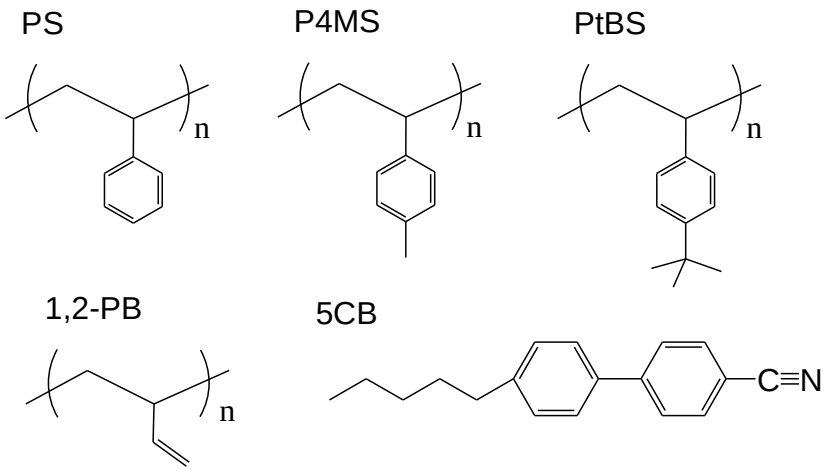

Figure III-1. Chemical structures of polystyrene (PS), poly(4-methyl styrene) (P4MS), poly(4-*tert*-butyl styrene) (PtBS), poly(1,2-butadiene) (1,2-PB), and 4-pentyl-4'-cyanobiphenyl (5CB).

Table III-2. Weight fraction of 5CB and T_g for various polymer/5CB mixtures. Dielectric intensities, $\Delta\varepsilon_{slow}$, $\Delta\varepsilon_{fast}$, and $\Delta\varepsilon_{total}$ (= $\Delta\varepsilon_{slow}$ + $\Delta\varepsilon_{fast}$), which were obtained at T_g+20 K by fitting the data with eq. III-1, are shown. Apparent activation energies for the fast mode of 5CB, $E_{a,h}$ and $E_{a,l}$, are also shown.

mixture	W_{5CB}	T_g / K	$\Delta\varepsilon_{theo}$ ($\Delta\varepsilon_{theo,5CB}$)	$\Delta\varepsilon_{slow}$	$\Delta\varepsilon_{fast}$	$\Delta\varepsilon_{total}$	$E_{a,l}$ / kJ mol^{-1}	$E_{a,h}$ / kJ mol^{-1}
PS	0.067	348	0.69 (0.65)	0.36	0.51	0.87	155±10	205±10
P4MS	0.035	373	0.34 (0.34)	0.09	0.34	0.44	85±10	210±20
PtBS	0.048	389	0.31 (0.31)	0.05	0.45	0.50	80±10	185±20
1,2-PB	0.056	267	0.62 (0.50)	0.65	-	0.65	-	-

Measurements A dielectric relaxation (DR) measurement was performed using in combination with an LCR meter (4284A, Hewlett Packard, USA) and a Fast-Fourier-Transfer (FFT) Analyzer (VC-2440, Hitachi, Japan), or an impedance analyzer (β analyzer, Novocontrol Technologies GmbH & Co. KG, Germany). Temperature and frequency ranges were $300-430$ K and 1 mHz $-$ 3 MHz, respectively. Temperature dependence of dielectric permittivity for all mixtures was measured at frequencies of 12 Hz − 200 kHz with an LCR meter (1693, Quad Tech Inc., USA) by increasing temperature from 100 K to 450 K at a heating rate of 0.3 K min^{-1}.

A dynamic viscoelastic relaxation measurement for the same samples for DR was performed using an oscillatory rheometer (Physica MCR 301, Anton Paar GmbH, Austria) equipped with 4 mm parallel plates after the DR measurement. The temperature and angular frequency ranges were $258-453$ K and $0.1-100$ s^{-1}, respectively.

The glass transition temperature, T_g for each mixture was determined using a differential scanning calorimeter (DSC 6220, EXSTAR-6000 Seiko Instruments Inc., Japan). After the viscoelastic measurements, T_g values were checked again to confirm that the composition of mixtures did not change. The determined T_g values for polymers and mixtures are shown in Table III-1 and III-2, respectively.

III-3. Results and Discussion

III-3-1. Dielectric relaxation behaviors of PS/5CB, P4MS/5CB and PtBS/5CB mixtures

To discuss the side-chain effect on the LM dynamics in polymer/LM mixtures, dielectric relaxation behavior of 5CB dissolved in PS, P4MS or PtBS matrix was compared. Urakawa et al.[4] suggested that the cooperative dynamics of LMs with the dielectric α dynamics of PS was related to the size ratio of the long axis of LMs to the Kuhn segment of PS. The lengths of the Kuhn segment, l_K, for the polymers used in this study were estimated from the literature data[5-6] by using following relationship between the unperturbed mean-square end-to-end distance, $\langle R^2 \rangle$, and the fully-extended end-to-end distance, R_{max},

$$l_K = \frac{\langle R^2 \rangle}{R_{max}} = \frac{C_\infty n b^2}{nh} = C_\infty \frac{b^2}{h} \qquad \text{(III-1)}$$

Here, C_∞ is the characteristic ratio, n and b are respectively the number and length of C-C bonds in the main chain, and h is the projection length of the C-C bonds to the polymer chain axis. By using b (0.154 nm), h (= $b \sin(\theta/2)$, θ is the C-C bond angle and 109.5°), and reported C_∞ values, l_K values for PS, P4MS, and PtBS were respectively estimated to be 1.79, 2.17, and 2.30 nm as listed in Table III-1. The Kuhn segment size depends on the pendant group structure of polymers. The dynamics of 5CB dissolved in the polymer as a probe is expected to be different among the mixtures because it depends on not only the probe size but also the Kuhn segment size of the polymer, as explained by Urakawa et al.[4]

Dielectric permittivity and loss, ε' and ε'', respectively, were measured as functions of angular frequency, ω, for PS/5CB, P4MS/5CB and PtBS/5CB mixtures. The dielectric relaxations in those systems almost only reflect the reorientation of 5CB

molecules as mentioned in chapter II. Fig. III-2 compares the results of dielectric loss of the three mixtures. The weight fraction of 5CB, W_{5CB}, for all the mixtures was fixed at 0.05. For all mixtures, dielectric relaxation appears in the wide temperature range below and above the T_g. The major peak observed in PS/5CB above T_g becomes weaker with increasing the side chain bulkiness of the polymer (PS < P4MS < PtBS). In particular, for PtBS/5CB system, the low temperature peak becomes higher than the high temperature peak, meaning that the bulky *tert*-butyl group strongly affects the dielectric relaxation behavior of the mixture. In general, the dielectric relaxation of pure polymers appears in the audio frequency range at temperatures just above T_g and this relaxation corresponds to the α-motion which is referred to as segmental motion. Therefore, the relaxation peaks observed above T_g in Fig. III-2 can be ascribed to the α relaxation of polymers. However, PS, P4MS and PtBS show much weaker dielectric response than 5CB as will be discussed later, so that the high temperature peaks of all mixtures do not reflect the α segmental motion of the polymers but the rotational motion of 5CB. For the same reason, the relaxation below T_g can also be assigned to the 5CB relaxation.

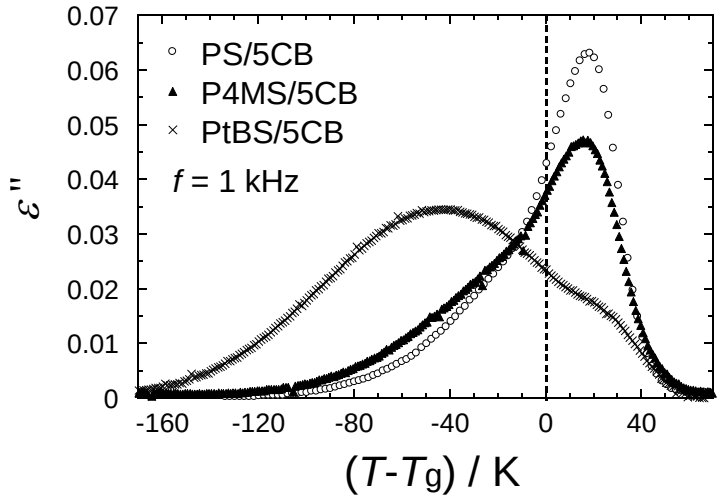

Figure III-2. Temperature dependence of dielectric loss, ε", for the mixtures of PS/5CB, P4MS/5CB and PtBS/5CB with W_{5CB}=0.05 at a frequency of 1 kHz. The abscissa axis is the difference between the measured temperature and the T_g of each mixture.

Fig. III-3 (A) shows the frequency dependence of ε' and ε'' for PS/5CB, P4MS/5CB and PtBS/5CB mixtures measured at T_g+2 K. Dielectric loss, ε'', curves are very broad and obviously bimodal. In the top panel, $\varepsilon'-\varepsilon_\infty$ values are plotted, where ε_∞ is the limiting dielectric permittivity at high frequencies. The dielectric intensity, $\Delta\varepsilon$, is given by the difference between ε' at low frequencies ($\varepsilon'(\omega = 0)$) and ε_∞ ($\Delta\varepsilon = \varepsilon'(0)-\varepsilon_\infty$). In the inset of this figure, the values of $\Delta\varepsilon$ are plotted against the weight fraction of 5CB, W_{5CB}. The linear relationship between $\Delta\varepsilon$ and W_{5CB} holds, meaning that the observed broad dielectric relaxation can be attributed only to 5CB molecules.

The Onsager theory[7] given by eq. II-5 can relate an electric dipole moment, μ, to $\Delta\varepsilon$ as follows,

$$\Delta\varepsilon = \varepsilon(0) - \varepsilon_\infty = \frac{\rho\phi_i N_A}{M}\frac{\mu^2}{9\varepsilon_0 k_B T}\frac{(2+\varepsilon_\infty)^2}{2+\varepsilon_\infty/\varepsilon(0)} \qquad \text{(III-2)}$$

Here, T is the absolute temperature, k_B is the Boltzmann constant, ε_0 is the electric constant (or the vacuum permittivity), N_A is Avogadro's number, and ρ is the density. M and ϕ_i are the molecular weight and the volume fraction of a polar molecule i having the electric dipole moment, μ, in the mixture, respectively. From the dipole moments, μ, for 5CB (4.4 D, 1 D = 3.33564×10^{-30} C m) and monomer units of PS (0.21 D), P4MS (0.09 D) and PtBS (0.11 D), which were estimated with WinMopac software (Fujitsu, Japan), the dielectric intensities, $\Delta\varepsilon_{theo}$, for components were theoretically calculated and shown in Table III-1 and III-2. For the calculation, ε_∞ values were approximated to be the same with those for the pure polymer because the 5CB concentration was low. By comparing $\Delta\varepsilon$ values between polymers and 5CB components, which are tabulated in Table III-1 and III-2, it is seen that the contributions of PS, P4MS and PtBS components to the dielectric response are

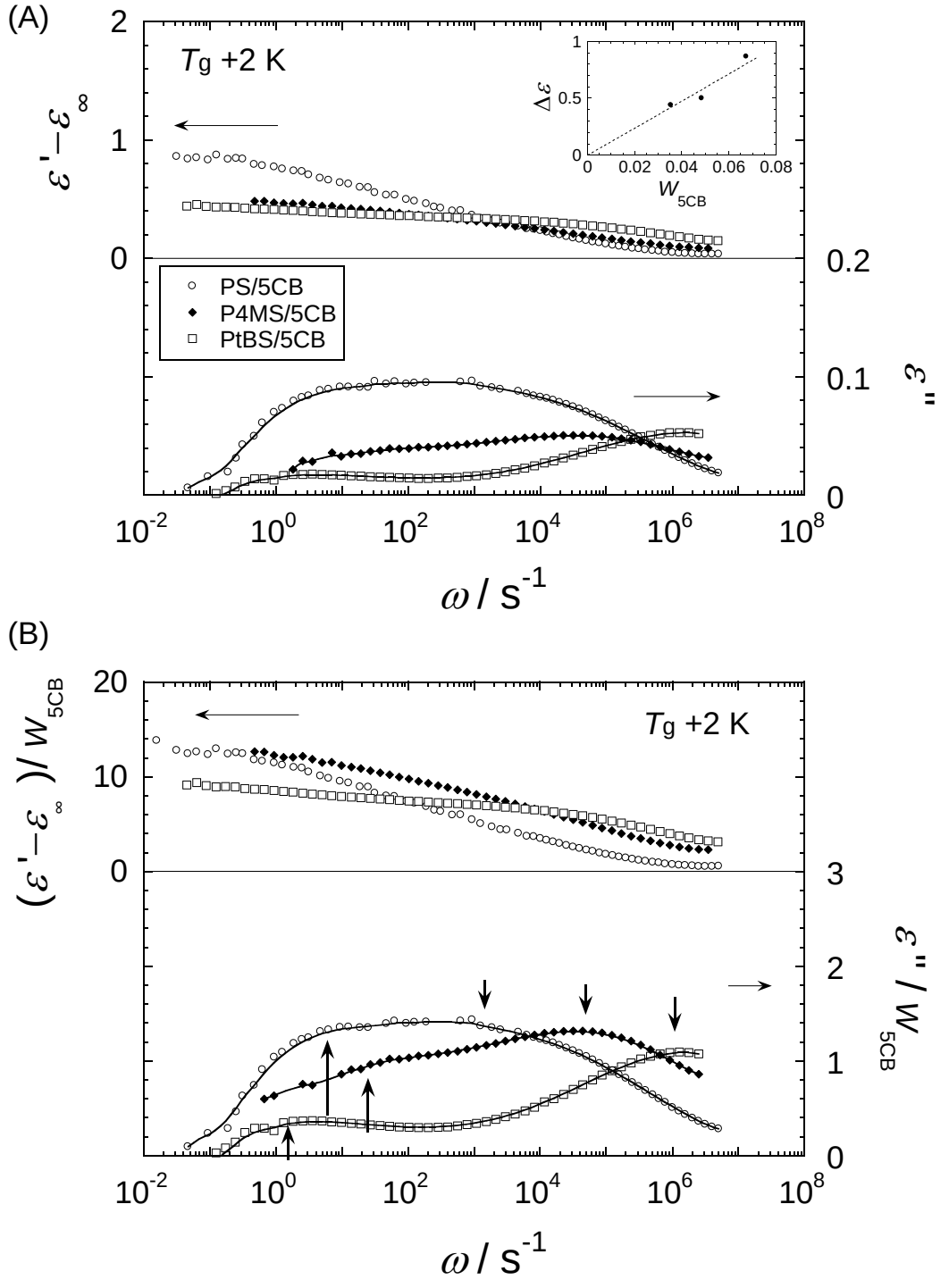

Figure III-3. (A) Angular frequency, ω, dependences of dielectric permittivity and loss, ε' and ε'', for PS/5CB, P4MS/5CB and PtBS/5CB mixtures at T_g+2 K. The vertical axis on the left side indicates the difference between the ε' and the limiting permittivity at high frequency, ε_∞. The inset shows the relationship between $\Delta\varepsilon$ and W_{5CB}. (B) Frequency dependence of dielectric relaxation data divided by each weight fraction of 5CB, W_{5CB}, for mixtures. The arrows indicate the peak frequencies for slow and fast relaxations.

negligibly small compared to that of 5CB. In addition, as already mentioned, the linear relation, $\Delta\varepsilon \propto \phi_{5CB}$ ($\propto W_{5CB}$), strongly indicates that the observed dielectric responses is assigned to only the 5CB contribution based on eq. III-2.

For the quantitative comparison, $\varepsilon' - \varepsilon_\infty$ (= $\Delta\varepsilon'$) and ε'' values divided by W_{5CB} are shown in Fig. III-3 (B). It is seen that the values of $\Delta\varepsilon'/W_{5CB}$ at the limiting low frequencies were comparable for all mixtures. All dielectric curves look bimodal and the high and low peak frequencies are indicated by the up and down arrows, respectively. The observed results here qualitatively agree with those presented in chapter II, in which the 5CB component in PS/5CB mixtures exhibited two rotational motions with different timescales. The slow and fast modes were assigned to the cooperative motion with PS segmental motion and the fluctuation in restricted space, respectively. By closely looking at the data shown in Fig. III-3 (B), it is clear that the peak frequency of the slow modes locate at almost the same position while the fast mode peak shift to higher frequency with increasing the side-chain size (PS < P4MS < PtBS). Furthermore, the intensity of the slow mode becomes weaker with increasing the side chain size and vice versa for the fast mode.

III-3-2. Dielectric relaxation intensity and time for three mixtures

Since the obtained spectra were broad and bimodal, they could not be analyzed by a single relaxation function (the Debye type function).[8] In this study, the broad dielectric spectra are analyzed by the sum of two Cole-Cole type function[9] given by eq. II-6. All the experimental data were fitted by this equation, and τ and $\Delta\varepsilon$ for the slow and fast modes were determined as well as PS/5CB system described in chapter II. Fig. III-4 displays a typical result of the fit for the PtBS/5CB mixture at 390.7 K. The arrows show the relaxation frequencies corresponding to τ_{slow}^{-1} and τ_{fast}^{-1}. The α values for both modes were smaller than unity ($0.3 < \alpha < 0.7$) indicating relatively broad relaxation time distribution. Fig. III-5 shows both α_{slow}

and α_{fast} values plotted against $T–T_g$. Both the values monotonously decrease with decreasing temperature, indicating that the relaxation time distributions for both the slow and fast modes become broader at lower temperature.

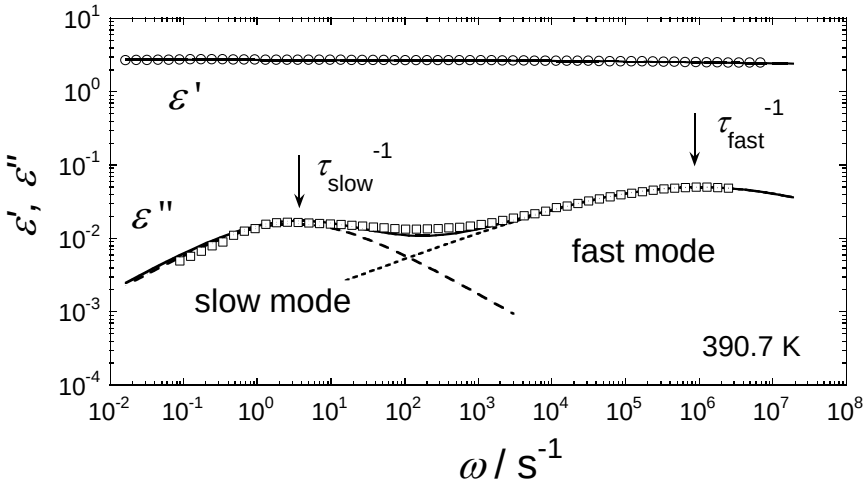

Figure III-4. A typical dielectric spectrum of PtBS/5CB mixture at 390.7 K. The solid and dotted lines represent the best fit results by using eq. II-6.

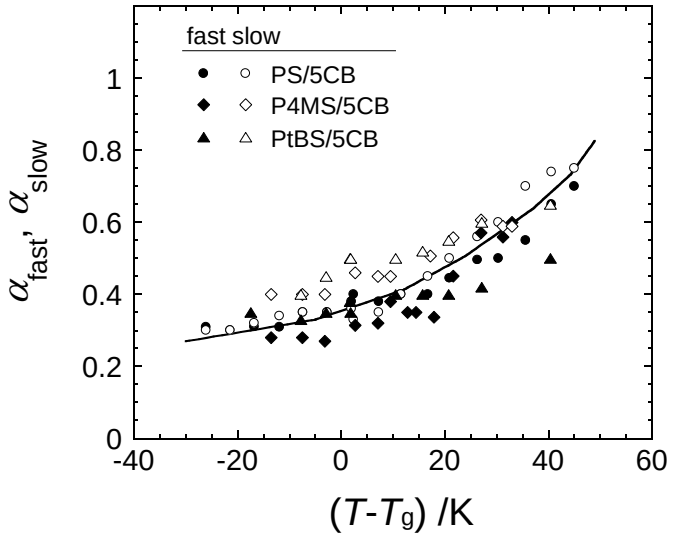

Figure III-5. Temperature dependence of α_{fast} and α_{slow} for various mixtures. The temperature axis is normalized by each T_g.

As seen in Tables III-1 and III-2, the dielectric relaxation intensities of slow and fast modes of 5CB, $\Delta\varepsilon_{slow}$ and $\Delta\varepsilon_{fast}$ are much larger than those expected for polymers. Therefore, as already mentioned in the previous section, only the 5CB relaxations are observed in these dielectric spectra. The dielectric relaxation times, τ_{slow} and τ_{fast}, for PS/5CB, P4MS/5CB and PtBS/5CB mixtures are shown as the functions of $T–T_g$ in Fig. III-6. The τ_{slow} value becomes longer with decreasing T and reaches about 1 s at $T = T_g$. These behaviors are similar for all mixtures. It is also seen that the temperature dependence of τ_{slow} is almost universal as a function of $T–T_g$ but slight deviation is seen for PtBS/5CB system, as will be discussed later. On the other hand, the temperature dependence of τ_{fast} is dependent on the polymer species and always weaker than that of τ_{slow}, meaning that 5CB has two kinds of rotational processes. In the next section, the relaxation modes of 5CB will be discussed.

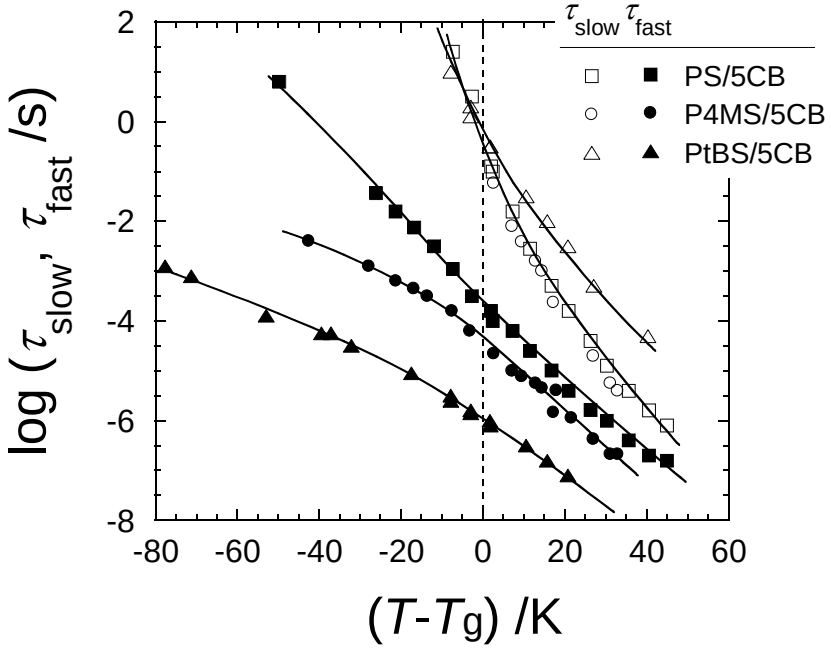

Figure III-6. Temperature dependence of slow and fast relaxation times for 5CB, τ_{slow} and τ_{fast} in PS/5CB, P4MS/5CB and PtBS/5CB mixtures. The horizontal axis is normalized by T_g for the mixtures.

III-3-3. Comparison of dielectric and viscoelastic spectra

Viscoelastic spectra of the mixtures from the glassy to flow regions are shown in Fig. III-7, which includes dielectric spectra obtained at the same reference temperature for comparison. The complex elastic moduli, $G^* = G' + iG''$, in which G' and G'' are elastic and loss moduli, respectively, were obtained by using the time-temperature superposition (TTS) principle from viscoelastic data at several temperatures with a shift factor, a_T. The viscoelastic spectra of PS/5CB and PtBS/5CB mixtures do not clearly show the rubbery plateau region, because of the lower M_w of polymers than the entanglement molecular weight, M_e (1.7×10^4 for PS, 3.7×10^4 for PtBS).[10] For those systems, the terminal region of the G^* could be well-explained by the Rouse theory[11] which gives a good prediction for the viscoelastic behavior of non-entanglement polymers. On the other hand, the spectrum of P4MS/5CB exhibits the rubbery plateau due to the entanglement effect because the M_w is higher than M_e, which is 1.9×10^4 calculated under the assumption that P4MS has the same number of entanglement units with PS.

At higher frequency, G' reached to 10^9 Pa which is the typical value for the glassy materials. The peak in G'' appears for all mixtures around this area. Inoue et al. reported that the glassy (G) mode generally observed in the viscoelastic relaxation spectra is mainly due to the torsional motions of the main chain.[12-13] Roland et al. determined the α (segmental) relaxation time related to the glass transition, τ_G, from the inverse of loss modulus peak.[14]

Since we focus on the cooperativity of the glass transition between polymers and 5CB, the dielectric and viscoelastic relaxation times between components are compared. The arrows shown in Fig. III-7 indicate the peak frequency corresponding to the inverse of the relaxation times, τ_G (for polymers), and τ_{slow}, τ_{fast} (for 5CB) for each mixture. From this figure, it is found that τ_{slow} is 3~14 times shorter than τ_G, suggesting that the slow mode of 5CB reflects a faster motion than the glassy

dynamics of polymers. In contrast, since the τ_{fast} locates deeply inside the glassy region for mixtures, the fast mode should correspond to 5CB motion in restricted space by the glassy matrix.

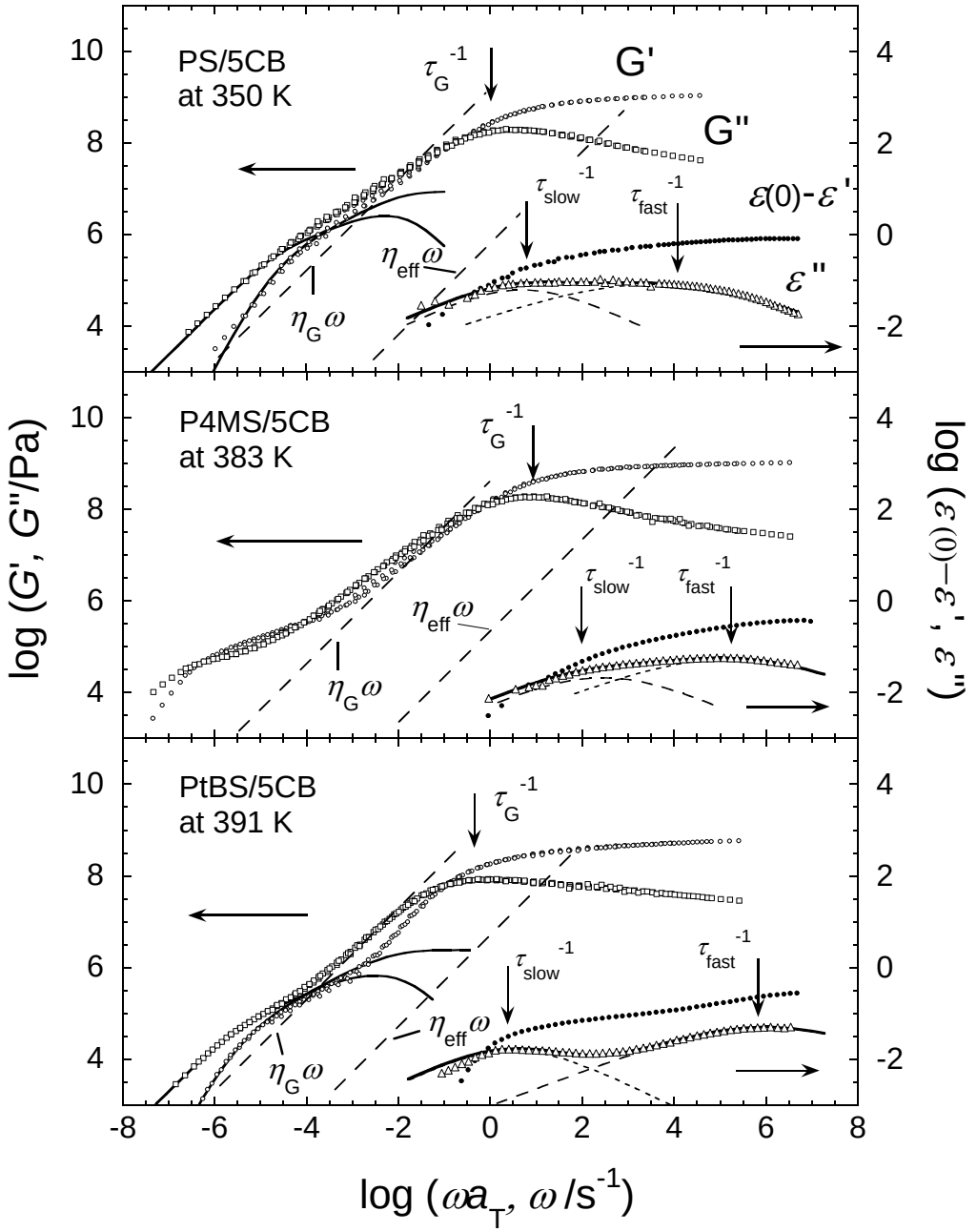

Figure III-7. Comparison of dielectric and viscoelastic spectra for PS/5CB, P4MS/5CB and PtBS/5CB mixtures at the same temperature. The arrows indicate the peak frequencies for dielectric and viscoelastic losses for each data. The solid lines for G^* were the Rouse model spectra given by eqs. II-1–II-3. The solid and dotted lines for ε^* were the fitted results by eq. II-6.

III-3-4. Slow mode of 5CB and glass relaxation of polymers

By utilizing the TTS principle, τ_G data over a wide temperature range were obtained and shown in Fig. III-8 along with τ_{slow} as functions of $T–T_g$. Inoue et al. separated the viscoelastic spectra of homopolymer systems into rubbery (R) and glassy (G) modes and demonstrated that the R and G modes had different temperature dependences (different shift factors, a_T(R) and a_T(G)). Since the R mode is governed by the orientation of chain segments, the viscoelastic data of the R component can be understood by coarse-grained models such as the Rouse[11] and tube[15] models. Although the determined a_T at the high temperature (in the rubber ~ flow region) should corresponds to that for the R mode, the T dependences of a_T(R) and a_T(G) in this region are expected to be the same, based on the data reported by Roland et al.[14] This means that the obtained nominal shift factors will approximately correspond to the a_T(G). Fig. III-8 reveals that τ_{slow} traces the same T-dependence with τ_G, suggesting that the slow mode of 5CB is dominated by the same friction factor with the G mode of polymers. Since τ_{slow} is shorter than τ_G as mentioned above, the length scale of the motional unit corresponding to the maximum of G'' will be larger than the 5CB size (1.26 nm). The estimation of the relevant length scale for the G mode will be made as follows.

In chapter II, the molecular-size dependence of the rotational relaxation time for rod-like molecules was discussed based on the rotational diffusion theory.[15] Rotational diffusion constant of a rod-like molecule, $D_{r,rod}$, is given by,

$$D_{r,rod} = \frac{3k_B T\left(\ln(L/d) - \gamma\right)}{\pi\eta L^3} \qquad \text{(III-3)}$$

Here, η is the viscosity coefficient of the media and γ is a correction factor (=0.8), L and d are the lengths of the long and short axes for the rod. The rotational time of the rod-like molecule observed by DR methods, $\tau_{r,rod}^{DR}$, is calculated with D_r as

$$\tau_{\mathrm{r,rod}}^{\mathrm{DR}} = \frac{1}{2D_{\mathrm{r}}} = \frac{\pi\eta L^3}{6k_{\mathrm{B}}T\left(\ln(L/d) - \gamma\right)} \qquad \text{(III-4)}$$

In this equation, η will represent the effective matrix viscosity, η_{eff}, in the glassy region. By using the molecular size of 5CB, L (1.26 nm) and d (0.215 nm), η_{eff}, for the rotational motion of 5CB can be estimated from eq. III-4. On the other hand, rheological viscosity of the matrix polymer in the glassy region, η_{G}, corresponding to $G_{\infty}'\tau_{\mathrm{G}}$ as shown in Fig. III-5, can be determined. Here, G_{∞}' is the storage modulus at the limiting high frequency. The ratio of these two viscosities, $\eta_{\mathrm{G}}/\eta_{\mathrm{eff}}$, is given by the following equation.

$$\frac{\eta_{\mathrm{G}}}{\eta_{\mathrm{eff}}} = \frac{G_{\infty}'\pi L^3}{6k_{\mathrm{B}}T\left(\ln(L/d) - \gamma\right)} \frac{\tau_{\mathrm{G}}}{\tau_{\mathrm{slow}}} \qquad \text{(III-5)}$$

The relaxation time ratios, $\tau_{\mathrm{G}}/\tau_{\mathrm{slow}}$, were obtained to be 14 (±5), 13 (±4), and 2.5 (±1) for PS/5CB, P4MS/5CB, and PtBS/5CB mixtures, respectively. By using these values, the $\eta_{\mathrm{G}}/\eta_{\mathrm{eff}}$ values were estimated from eq. III-5 to be 3.1×10^3, 2.6×10^3, and 4.0×10^2 for PS/5CB, P4MS/5CB, and PtBS/5CB mixtures, respectively. The large $\eta_{\mathrm{G}}/\eta_{\mathrm{eff}}$ values (>> 1) indicate that the cooperative rotational motion of 5CB was not directly related to the matrix viscosity, η_{G}. However, the temperature dependences of them are the same. This result suggests that these two relaxation modes have the same fundamental dynamical process with the relaxation time shorter than or comparable to τ_{slow}, since τ_{slow} is shorter than τ_{G}.

When the rotational time, $\tau_{\mathrm{r,rod}}$, becomes longer than the glassy relaxation time, τ_{G}, the rotational dynamics of the rod-like molecule will reflect the matrix viscosity, η_{G}. On the other hand, as described above, when $\tau_{\mathrm{r,rod}}$ is shorter than τ_{G}, the rotational dynamics of the rod is related to the effective viscosity, η_{eff}. Therefore,

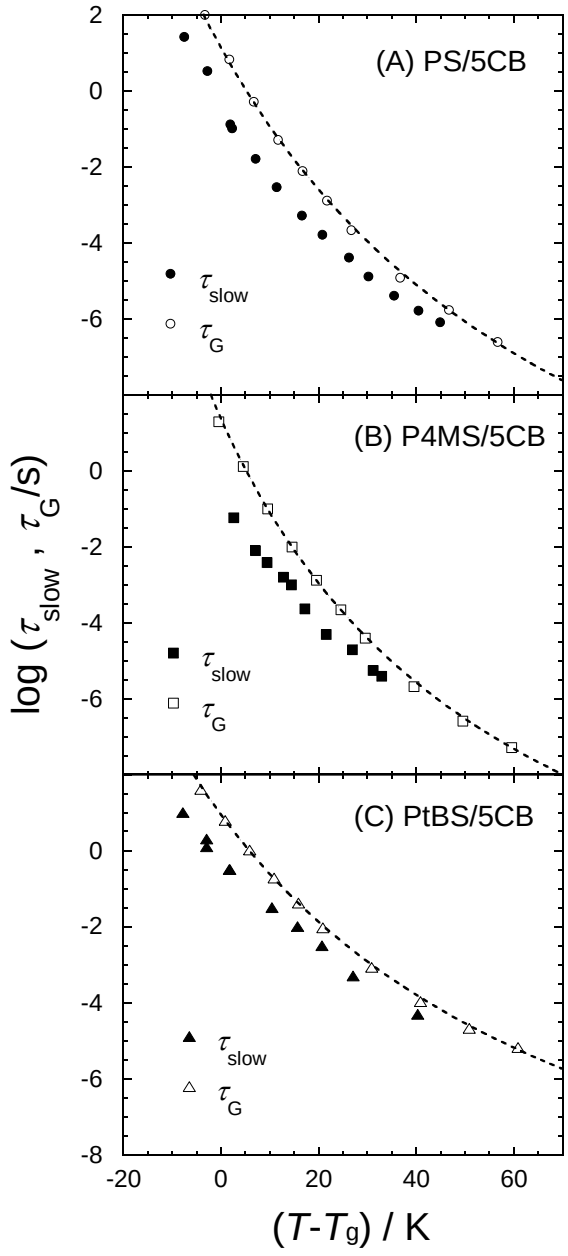

Figure III-8. Temperature dependence of the relaxation times for viscoelastic G mode of polymers and dielectric slow mode of 5CB, τ_G and τ_{slow}, respectively. (A) PS/5CB, (B) P4MS/5CB, (C) PtBS/5CB mixtures. The dotted lines are best fit-results by using the WLF function[16], $\tau = \tau_{ref} \exp[-c_1(T-T_{ref})/(c_2 + T-T_{ref})]$ with proper numbers of parameters for each mixture.

there will be the critical length of the rod-like molecule, L_c, for which the effective viscosity in eq. III-4 becomes glassy matrix viscosity, η_G. As mentioned in chapter II, for the rod-like molecules dissolved in the polymer matrix, the rotational relaxation time, τ_r, is approximately proportional to L^3. The critical length of the rod-like LM, L_c, can be estimated from this power law relation as the value when τ_r becomes equal to $3\tau_G$ (the numerical factor 3 comes from the difference between dielectric and viscoelastic relaxation times). When η_{eff} is considered to be independent of the LM length and the aspect ratio, L/d, is constant, the critical length, L_c, is given by,

$$L_c = L_{5CB}\left(\frac{3\tau_G}{\tau_{5CB}}\right)^{1/3} \qquad \text{(III-6)}$$

From this relationship, L_cs for the mixtures with PS, P4MS, and PtBS are estimated to be 4.4 (±0.5), 4.3 (±0.4), and 2.5 (±0.3) nm, respectively. Is the critical length of LM related to the glassy dynamical scale of polymer matrices?

Cooperative rearranging region (CRR) idea was introduced by Adam and Gibbs to explain the glass transition behavior.[17] CRR is related to the glassy dynamics of polymeric materials. Ellison et al. reported the length scales of cooperative rearranging region (CRR), ξ_{CRR}, for PS, P4MS and PtBS to be 3.5, 3.3, and 2.6 nm by DSC measurements.[18] Surprisingly, the CRR sizes, ξ_{CRR}, are fairly well correlated with L_c values, suggesting that the CRR will be closely related to the rotational dynamics of the rod-like LM having the critical length, L_c. Therefore, the critical length of the LM, L_c, will represent the CRR size of glassy polymers, ξ_{CRR}. Interestingly, the order of the L_c values (4.4, 4.3 and 2.5 nm in PS, P4MS and PtBS mixtures) is not the same with that of the Kuhn segment length (1.79, 2.17, and 2.30 nm for PS, P4MS, and PtBS). This result indicates that the cooperative rotational motion of rod-like LM is not related to the Kuhn segment dynamics, which

is determined by the *intra*-molecular interaction, but related to the cooperative glassy dynamics of polymers, which is governed by the *inter*-molecular interaction between the polymer and the rod-like LM.

III-3-5. Fast mode of 5CB and glass transition

The fast mode of 5CB in mixtures was independent of the local chain motion of polymer components and was assigned to be fluctuation (wobbling motion) in a restricted space as discussed in chapter II and previous studies.[2, 4] In order to discuss the effect of the Kuhn segment size on dielectric relaxation behavior of the fast mode, the dielectric intensity $\Delta\varepsilon_{fast}$ normalized by W_{5CB} and the relaxation time, τ_{fast}, are plotted against T/T_g in Figs. III-9 and III-10, respectively. As a general trend, increase of $\Delta\varepsilon_{fast}$ with increasing temperature was observed in Fig. III-9. By considering that the dielectric intensity reflects the largeness of the movable space for the rotational motion of LMs, the increase of $\Delta\varepsilon_{fast}$ indicates that the restriction for the fluctuation motion of LMs is weakened at higher temperature. This is natural because the free volume increases with temperature for glass forming materials.[19-20]

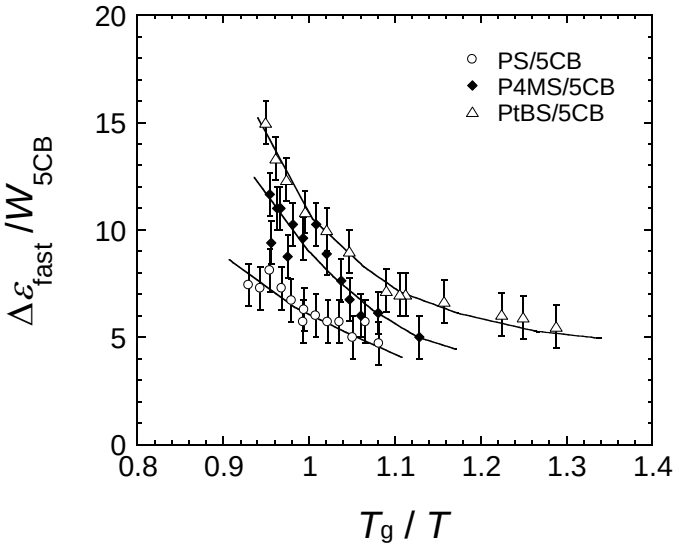

Figure III-9. The T_g-scaled Arrhenius plot of the normalized relaxation intensity of the fast mode, $\Delta\varepsilon_{fast}/W_{5CB}$, for PS/5CB, P4MS/5CB and PtBS/5CB mixtures.

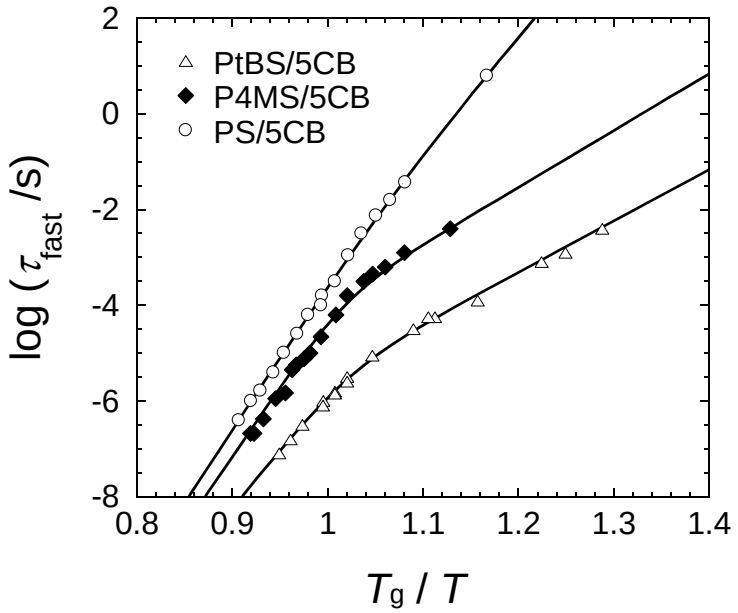

Figure III-10. The T_g-scaled Arrhenius plot of the fast relaxation time, τ_{fast}, against T_g /T for PS/5CB, P4MS/5CB and PtBS/5CB mixtures. The solid lines represent best fit results by the double Arrhenius function given by eq. III-7.

Since the total dielectric intensity per one molecule is approximately constant among three different mixtures, $\Delta\varepsilon_{fast}/W_{5CB}$ reflects the contribution of the fast mode to total 5CB rotational motion. As seen in Fig. III-9, the values of $\Delta\varepsilon_{fast}/W_{5CB}$ increases in the order of PS, P4MS, and PtBS, i.e., in the order of the Kuhn segment length or side chain bulkiness. Urakawa et al. reported that the fast mode intensity increased with decreasing the LM size in the same PS matrix.[2, 4] By taking into account all the results, the size ratios of the LM to the Kuhn segments will possibly determine the strength of the fast mode. As another possibility, the side chain bulkiness of polymers will contribute to increase the free space which will enhance the fluctuation motion of LMs.

Fig. III-10 shows the plot of τ_{fast} against T_g/T. The T_g/T dependence looks like the double step Arrhenius type: two linear lines can be drawn. The temperatures at which the slopes changes seem to locate in the vicinity of T_g for all the mixtures,

indicating that the fast mode is *indirectly* affected by the glass transition. This behavior apparently resembles to the temperature dependence of specific volume or density, and is also reported in the β relaxation of a probe molecules in the PS/probe system (van den Berg et al.[21]) and the secondary relaxation in amorphous poly(methyl methacrylate) (Bergman et al.[22]). Here, it is assumed that the T dependence of the relaxation time, τ, can be expressed by the reciprocal sum of the two Arrhenius equations,

$$\tau = \left[\frac{1}{\tau_{\mathrm{h}}^{\infty} \exp(-E_{\mathrm{a,h}} / RT)} + \frac{1}{\tau_{\mathrm{l}}^{\infty} \exp(-E_{\mathrm{a,l}} / RT)} \right]^{-1} \qquad \text{(III-7)}$$

where E_{a} and τ^{∞} are the apparent activation energy and the limiting relaxation time at high temperature. The subscripts, "h" and "l", represent higher and lower temperature regions than T_{g}. Two activation energies, $E_{\mathrm{a,h}}$ and $E_{\mathrm{a,l}}$, estimated from eq. III-7 are tabulated in Table III-2. $E_{\mathrm{a,h}}$ was similar among all the mixtures while $E_{\mathrm{a,l}}$ decreased in the order of PS, P4MS and PtBS. As discussed before, the restricted space of 5CB becomes wider with increasing temperature probably related to the increase of the free volume. Therefore, the difference of the activation energies above and below T_{g} will be possibly related to the change in the thermal expansion coefficients of the surrounding free volume.

III-3-6. Component dynamics in 1,2-PB/5CB system

In this section, the cooperative rotational motion of an LM in a flexible polymer/LM mixture is discussed. Poly(1,2-butadiene) (1,2-PB) is more flexible than styrene polymers as described in the previous sections. The Kuhn length of 1,2-PB is 1.55 nm which is almost similar to the 5CB size (1.26 nm), and the size ratio of the LM to the Kuhn segment is 0.82. This ratio was 0.93 in the case of PS/5CT in

which the fast mode of 5CT disappeared. If the size ratio was the key parameter to determine whether the fast relaxation mode appeared or not, 1,2-PB/5CB mixture (W_{5CB} of 0.05) is also expected to exhibit only the cooperative slow mode. Actually, as shown in Fig. III-11, the dielectric dispersion curve of 1,2-PB/5CB is unimodal no to the PS/5CB mixture and similar to that of PS/5CT. The height of the dielectric loss peak for 1,2-PB/5CB is slightly higher than PS/5CT, mainly due to the difference in molar concentration of LMs (weight fraction is matched in this comparison). Fig. III-12 shows the dielectric relaxation curves of 1,2-PB/5CB at various temperatures. The shapes of ε'' curves for 1,2-PB/5CB become broader with decreasing temperature. This behavior is similar to that of PS/5CT presented in Fig. II-11, indicating that the rotational relaxation of 5CB in 1,2-PB can also be analyzed by the Havriliak-Negami function described in eq. II-7. From this analysis, the rotational relaxation times of 5CB, τ_{5CB}, for 1,2-PB/5CB were determined as explained below.

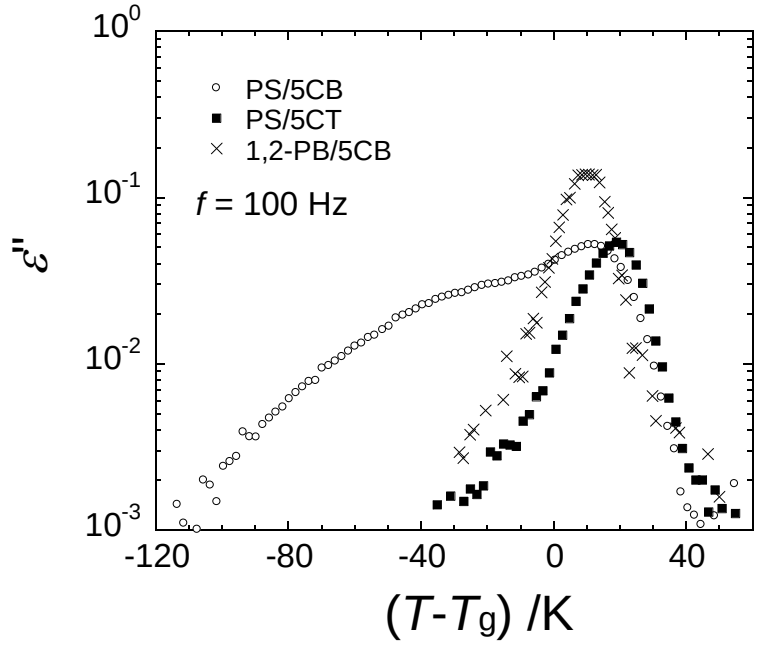

Figure III-11. Temperature dependence of dielectric loss, ε'', of PS/5CB, PS/5CT and 1,2-PB/5CB mixtures at 100 Hz. Temperature axis is normalized by each T_g.

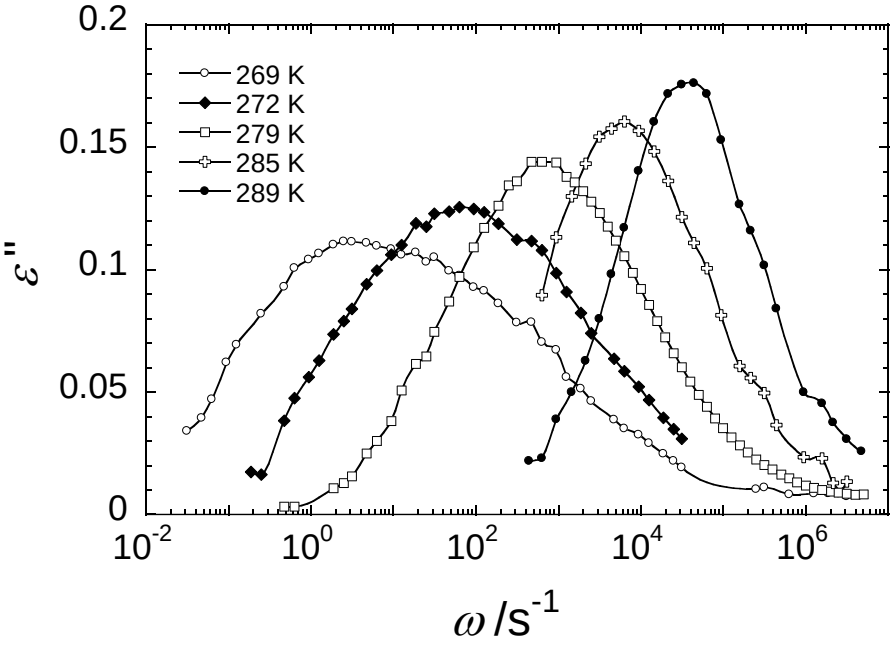

Figure III-12. Angular frequency, ω, dependence of dielectric loss, ε'', for 1,2-PB/5CB system at various temperatures. Solid lines are drawn for eye guides.

In order to investigate the polymer component dynamics in the mixture, the complex moduli over wide range of temperature were determined. Fig. III-13 shows the viscoelastic composite curves of the 1,2-PB/5CB mixture and bulk 1,2-PB at the reference temperature T_r = 40 °C. Since 1,2-PB in this study has higher molecular weight ($M_w = 3.0\times10^4$) than the molecular weight between entanglements[5] ($M_e \sim 3.8\times10^3$), the rubbery plateau region appears in the ω range of $10\sim10^4$ s^{-1}. The shapes of the two viscoelastic curves look similar, but the peak position of G'' shifts slightly to the higher frequency side by mixing 5CB. This shift is due to the decrease of T_g (cf. Tables III-1 and III-2). The relaxation time of the glass mode, τ_G, at various temperatures was determined as the inverse of the peak frequency. This mode is known to be similar to the dielectric α-relaxation. The τ_G data are plotted against $T-T_g$ in Fig. III-14 along with the rotational relaxation time of 5CB, τ_{5CB}. It can be seen that the temperature dependencies of τ_G and τ_{5CB} are almost the same but the timescales are different: τ_{5CB} is longer than τ_G. The relaxation time ratio, τ_{5CB}/τ_G, for

1,2-PB/5CB mixture is about 10 while τ_{slow}/τ_G (τ_{slow} corresponds to τ_{5CB}) for other mixtures described in the previous sections is smaller than unity. From the analysis using eq. III-6, the critical length of LM in 1,2-PB matrix, L_c is estimated to be 0.84 nm, which is a half of the Kuhn length, l_K, (1.55 nm). By assuming that L_c approximately corresponds to the cooperative glassy unit of polymers as mentioned in section III-3-4, the smaller L_c than l_K means that the *inter*-molecular cooperativity is weaker than the *intra*-molecular cooperativity for 1,2-PB,. This result is different from that for PS, P4MS, and PtBS systems described before.

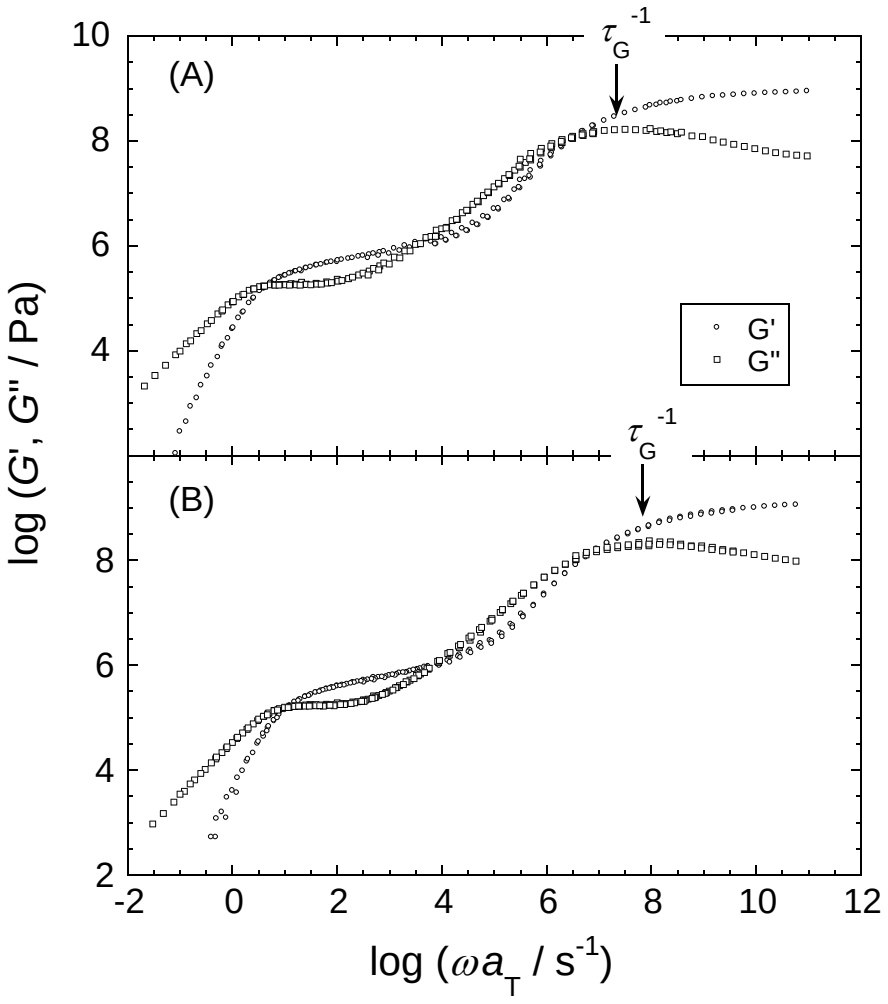

Figure III-13. Composite curves of elastic and loss moduli, *G*' and *G*", for (A) 1,2-PB and (B) 1,2-PB/5CB mixture at the reference temperature of 40 °C.

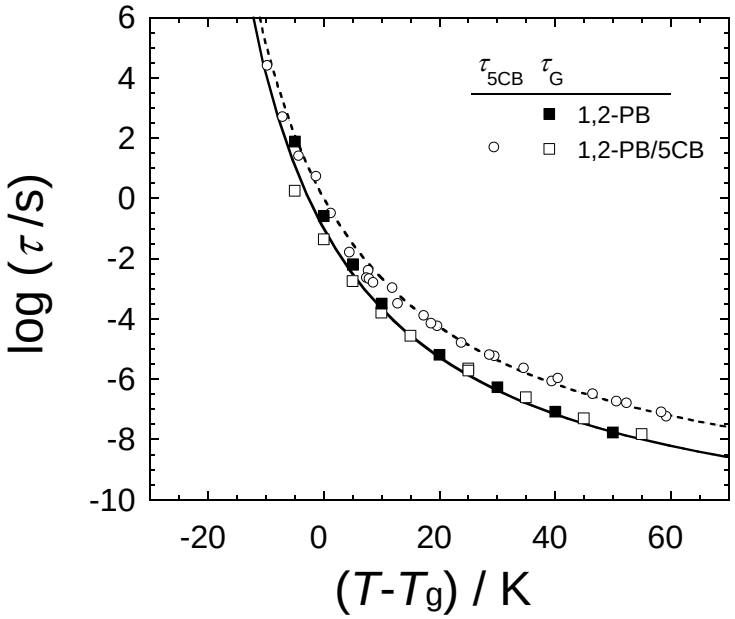

Figure III-14. Temperature dependence of relaxation times, τ_{5CB} and τ_G, for 1,2-PB and 1,2-PB/5CB mixture. The solid and dotted curves are fit-results by WLF function (eq. II-4) with the same c_1 and c_2 values.

The length scales for the glassy dynamics of various polymer mixtures used in this study are summarized in Table III-3. The Kuhn length, l_K, reflects the internal rotational potential along the C-C bond which is due to the *intra*-molecular interaction between adjacent monomeric units. In contrast, the critical length, L_c, corresponding to the glassy unit scale of polymers will be affected by not only the *intra*-molecular but also the *inter*-molecular interactions. Therefore, when polymers such as PS and P4MS have long L_c and short l_K, the *inter*-molecular cooperativity will be higher. In contrast, when polymers such as PtBS have short L_c and long l_K, the *intra*-molecular cooperativity will be dominant. Since 1,2-PB exhibited the small length scales for both units, both the *intra*- and *inter*-molecular cooperativities will not be so strong.

How is the relation between the glass transition temperature, T_g, and the polymer structures? It is generally expected that inflexible (rigid) polymers tend to

have higher T_g. In addition, it is also reasonable to think that polymers with higher dynamic cooperativity will exhibit higher T_g. From the comparison of T_g, l_K, and CRR values shown in Table III-3, there seems to be a correlation between l_K and T_g but no correlation between the CRR size and T_g. The difference between l_K and L_c is considered to be originated from the different contribution of the *intra*- and *inter*-molecular interactions for the glassy dynamics. Unfortunately, because of the limited number of polymers examined here, it is difficult to clarify how the *inter*- and *intra*-molecular interactions contribute to the T_g values.

Table III-3. T_g, l_K, and the CRR size, ξ_{CRR}, for PtBS, P4MS, PS and 1,2-PB taken from literature data[5, 18]. The critical length, L_c, of LM in the mixtures was estimated from eq. III-6.

	T_g [a]/ K	l_K [a] /nm	ξ_{CRR} [b] /nm	L_c /nm
PtBS	419	2.30	2.6	2.5
P4MS	387	2.17	3.3	4.3
PS	373	1.79	3.5	4.4
1,2-PB	275	1.55	-	0.84

a) already shown in Table III-1 b) data estimated by Ellison et al. based on the DSC measurements[18]

III-4. Conclusion

In this chapter, the dynamics of 4-pentyl-4'-cyanobiphenyl (5CB) used as a rod-like low-mass molecule and polymers having various side-chains in mixtures with the 5CB concentration of 5 wt% were examined in the wide temperature and frequency ranges by the viscoelastic relaxation (VR) and dielectric relaxation (DR) measurements. Polymers examined were polystyrene (PS), poly(4-methyl styrene) (P4MS), poly(4-*tert*-butyl styrene) (PtBS) and poly(1,2-butadiene) (1,2-PB).

The DR curves of PS/5CB, P4MS/5CB, and PtBS/5CB mixtures reflected only the rotational motion of 5CB and showed two rotational modes (fast and slow modes)

of 5CB in the mixtures. The slow and fast modes were ascribed to the cooperative rotational motion of 5CB with the α (segmental) motion of the polymer and the wobbling (fluctuation) motion of 5CB molecule, respectively. The fast mode intensity increased with decreasing the chain flexibility (increasing the Kuhn segment length), suggesting that the size mismatch of component characteristic lengths (molecular size of 5CB and the Kuhn length of polymer) might enhance the fast mode of 5CB. This result was consistent with the previously reported data.[4] The temperature dependence of the slow mode relaxation time, τ_{slow}, was stronger than that of τ_{fast}. The glassy relaxation time of polymers, τ_G, estimated from the viscoelastic relaxation measurements, showed almost the same temperature dependence with τ_{slow}. This result means that the slow mode of 5CB is cooperative with the α-motion (responsible for the glass mode) of polymers. The DR data of 1,2-PB/5CB exhibited one relaxation mode of 5CB which corresponded to the slow mode for other mixtures.

The slow modes of 5CB in PS/5CB, P4MS/5CB and PtBS/5CB, and the rotational mode of 5CB in 1,2-PB/5CB were concluded to be cooperative with the glassy motion of polymers, although the timescale of τ_{5CB} or τ_{slow} did not agree with that of τ_G. Assuming that the rotational motion of 5CB in the mixture could be described by the theory which predicts the rotational diffusion of rod-like structures in a continuous medium, the critical length, L_c, of the rod-like molecule, of which the rotational time corresponds to the α relaxation time of polymers, was estimated. The L_c scales were comparable to the CRR (cooperative rearranging region) scales taken from literature, suggesting that the critical size of the rod-like LM corresponds to the dynamical scale of the glassy polymers. The obtained lengths for polymers were not matched with the Kuhn length, indicating that the glassy dynamics is governed not only by the *intra*-molecular segmental motion but also by the *inter*-molecular cooperative motion.

Concerning the fast mode relaxation time, τ_{fast}, they exhibited the two steps of

the Arrhenius type dependence on temperature. The change of the slopes in the Arrhenius plot was commonly observed in the vicinity of T_g. The fast mode relaxation intensity increased with increasing temperature. From these results, it was concluded that the wobbling motion of LM was affected by the "cage" size which would be dependent on temperature.

References

1. Nobukawa, S.; Urakawa, O.; Shikata, T.; Inoue, T. *AIP Conference Proceedings* **2008,** 1027, 561-563.
2. Urakawa, O.; Nobukawa, S.; Shikata, T.; Inoue, T. *Nihon Reoroji Gakkaishi* **2010,** 38, 41-46.
3. Hori, H.; Urakawa, O.; Adachi, K. *Polymer Journal* **2003,** 35, 721-727.
4. Urakawa, O.; Ohta, E.; Hori, H.; Adachi, K. *Journal of Polymer Science Part B-Polymer Physics* **2006,** 44, 967-974.
5. Fetters, L. J.; Lohse, D. J.; Milner, S. T.; Graessley, W. W. *Macromolecules* **1999,** 32, 6847-6851.
6. Maconnachie, A.; Fried, J. R.; Tomlins, P. E. *Macromolecules* **1989,** 22, 4606-4615.
7. Onsager, L. *Journal of the American Chemical Society* **1936,** 58, 1486-1493.
8. Debye, P.; Ramm, W. *Annalen Der Physik* **1937,** 28, 0028-0034.
9. Cole, K. S.; Cole, R. H. *Journal of Chemical Physics* **1941,** 9, 341-351.
10. Fetters, L. J.; Lohse, D. J.; Richter, D.; Witten, T. A.; Zirkel, A. *Macromolecules* **1994,** 27, 4639-4647.
11. Rouse, P. E. *Journal of Chemical Physics* **1953,** 21, 1272-1280.
12. Inoue, T.; Matsui, H.; Osaki, K. *Rheologica Acta* **1997,** 36, 239-244.
13. Inoue, T. *Nihon Reoroji Gakkaishi* **2000,** 28, 167-175.
14. Roland, C. M.; Ngai, K. L.; Plazek, D. J. *Macromolecules* **2004,** 37, 7051-7055.
15. Doi, M.; Edwards, S. F., *The Theory of Polymer Dynamics*. Oxford University Press: New York, 1986.
16. Williams, M. L.; Landel, R. F.; Ferry, J. D. *Journal of the American Chemical Society* **1955,** 77, 3701-3707.

17. Adam, G.; Gibbs, J. H. *Journal of Chemical Physics* **1965,** 43, 139-146.
18. Ellison, C. J.; Mundra, M. K.; Torkelson, J. M. *Macromolecules* **2005,** 38, 1767-1778.
19. Li, H. L.; Ujihira, Y.; Nanasawa, A. *Journal of Radioanalytical and Nuclear Chemistry-Articles* **1996,** 210, 533-541.
20. Kanaya, T.; Tsukushi, T.; Kaji, K.; Bartos, J.; Kristiak, J. *Physical Review E* **1999,** 60, 1906-1912.
21. van den Berg, O.; Wubbenhorst, M.; Picken, S. J.; Jager, W. F. *Journal of Non-Crystalline Solids* **2005,** 351, 2694-2702.
22. Bergman, R.; Alvarez, F.; Alegria, A.; Colmenero, J. *Journal of Chemical Physics* **1998,** 109, 7546-7555.

Chapter IV
Orientational Correlation of Rod-like Molecule to Polymer Chain

IV-1. Introduction

Nematic interaction (NI) works between anisotropic rod-like molecules and makes them tend to align in the same direction. Even for flexible polymer chains, due to the anisotropic shape of its segment, NI affects the orientation relaxation behavior.[1-4] Theoretical expression for the NI applicable to entangled polymeric systems was proposed by Doi et al.[1] and extended to polymer blends by Zawada et al.[3] In this chapter, the Zawada's theory is further modified to apply it to polymer/LM mixtures and evaluate the NI parameter between LM and polymer chains from experimental data for polystyrene (PS)/4-pently-4'-cyanobiphenyl (5CB) and PS/4-pently-4'-cyanoterphenyl (5CT) systems.

In polymeric materials, the degree of molecular orientation can be determined by several methods: birefringence,[5-6] infrared linear dichroism,[7] neutron scattering[8] and other optical measurements.[9-10] Among them, the birefringence technique sensitively detects anisotropic orientation for polymeric materials. This method is utilized to determine the degree of molecular orientation in polymer/LM mixture systems.

Birefringence of polymeric materials originates from molecular orientations which relax through two types of dynamical modes: so called rubbery (R) and glassy (G) modes.[5-6] Simultaneous dynamic viscoelastic and birefringence measurements make it possible to separate the relaxation spectra into two component contributions based on the modified stress optical rule (MSOR) proposed by Inoue et al.[6]. The R component originates from the chain orientation of polymers while the G component is

considered to be due to twisting orientation of repeating units.[6]

From the concentration dependence of the stress-optical coefficient of the R mode, C_R, NI parameters in PS/5CB and PS/5CT systems are determined based on the new equation. Finally, I discuss the relationship between the nematic effect and the cooperative dynamics in the mixtures by using the determined NI parameters along with the results described in chapter II.

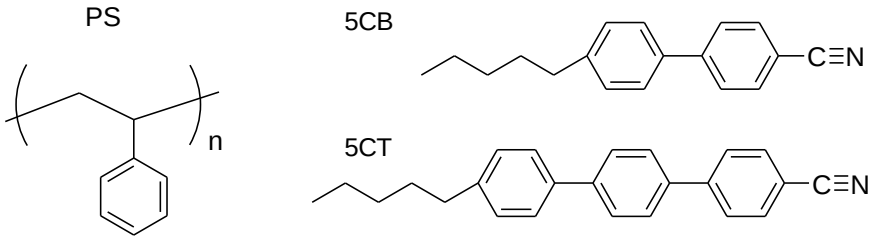

Figure IV-1. Chemical structures of polystyrene (PS), 4-pentyl-4'-cyanobiphenyl (5CB) and 4-pentyl-4'-cyanoterphenyl (5CT).

IV-2. Theoretical Background

IV-2-1. Modified stress-optical rule

Tensile strain, e, induces polymer chain orientation and consequently birefringence, Δn is observed. Δn is define as the difference between two refractive indexes, $n_{//}$ and $n_{\perp}$, in the directions parallel and perpendicular to the stretching direction.

$$\Delta n = n_{//} - n_{\perp} \tag{IV-1}$$

Δn is proportional to the tensile stress, σ, for homopolymer melts in the relaxation process, and this empirical relationship is called stress-optical rule (SOR). The strain-optical coefficient, O (=$\Delta n/e$), is also proportional to Young's modulus, E (=σ/e),

with the same proportional constant, *C*:

$$\Delta n(t) = C\,\sigma(t) \quad \text{and} \quad O(t) = CE(t) \tag{IV-2}$$

Here, *C* is called the stress-optical coefficient. However, in the glass-to-rubber transition region of polymeric materials, the SOR does not hold. Concerning this phenomenon, Inoue et al.[5-6, 11-12] proposed a modified SOR (MSOR), i.e., the stress and birefringence can be described by the sum of two components, rubbery and glassy components (denoted by the subscripts R and G, respectively).

$$E^*(\omega) = E^*_{\mathrm{R}}(\omega) + E^*_{\mathrm{G}}(\omega) \tag{IV-3}$$

$$O^*(\omega) = O^*_{\mathrm{R}}(\omega) + O^*_{\mathrm{G}}(\omega) = C_{\mathrm{R}}E^*_{\mathrm{R}}(\omega) + C_{\mathrm{G}}E^*_{\mathrm{G}}(\omega) \tag{IV-4}$$

Here, $E^*(\omega)$ ($=E'(\omega)+\mathrm{i}E''(\omega)$) is the complex Young's modulus and $O^*(\omega)$ ($=O'(\omega)+\mathrm{i}O''(\omega)$) is the complex strain-optical coefficient. C_{G} is defined as $\lim_{\omega\to\infty} = O''(\omega)/E''(\omega)$. From $E^*(\omega)$ and $O^*(\omega)$ data, the $E^*_{\mathrm{R}}(\omega)$ and $E^*_{\mathrm{G}}(\omega)$ can be separately determined *via* eqs. IV-3 and IV-4. C_{R} reflects the orientation of polymer chain (segment), and this value depends on the longitudinal anisotropy of polarizability tensor for the repeat units of polymers. In contrast, C_{G} is related to the transverse anisotropy of the polarizability tensor.[6, 11-12]

IV-2-2. Nematic interaction and stress-optical coefficient in polymer/LM mixtures

Doi et al.[1] proposed the theory to account for the effect of NI on polymer dynamics. Zawada et al.[3] extended this theory to apply to miscible binary polymer mixtures. In this section, a new equation applicable to polymer/LM systems will be proposed based on Zawada's approach.

The orientation of the entanglement strands (of the length a) are characterized by orientation distribution, S_{ij} (i or j stands for one of the direction, x, y, or z in the Cartesian coordinate), of the unit vector, **r** (r_x, r_y, r_z), parallel to the vector connecting two adjacent entanglement points which is schematically shown in Scheme IV-1 (A): $S_{ij} \equiv <r_i r_j - \delta_{ij}/3>$, where δ_{ij} stands for the Kroneker δ. For an entangled polymer system, the deviatoric part of the stress tensor is related to the orientation distribution by

$$\sigma_{ij} = 3k_B T \frac{x}{N_e} S_{ij} \tag{IV-5}$$

$$\mathbf{S} = \begin{pmatrix} S_{xx} & S_{xy} & S_{xz} \\ S_{yx} & S_{yy} & S_{yz} \\ S_{zx} & S_{zy} & S_{zz} \end{pmatrix} = \begin{pmatrix} r_x r_x - 1/3 & r_x r_y & r_x r_z \\ r_y r_x & r_y r_y - 1/3 & r_y r_z \\ r_z r_x & r_z r_y & r_z r_z - 1/3 \end{pmatrix}$$

where k_B is the Boltzmann constant, T is absolute temperature, x is the number of the freely jointed (Kuhn) bonds per unit volume, and N_e is the number of the Kuhn bonds in the entanglement strand. In contrast, the deviatoric part of refractive index tensor, n_{ij}, can be directly related to the local orientation distribution q_{ij} of the unit vector of the Kuhn bonds, **u** (u_x, u_y, u_z), which is shown in Scheme IV-1 (B), ($q_{ij} = <u_i u_j - \delta_{ij}/3>$) through a coefficient corresponding to the intrinsic birefringence Δn_0:

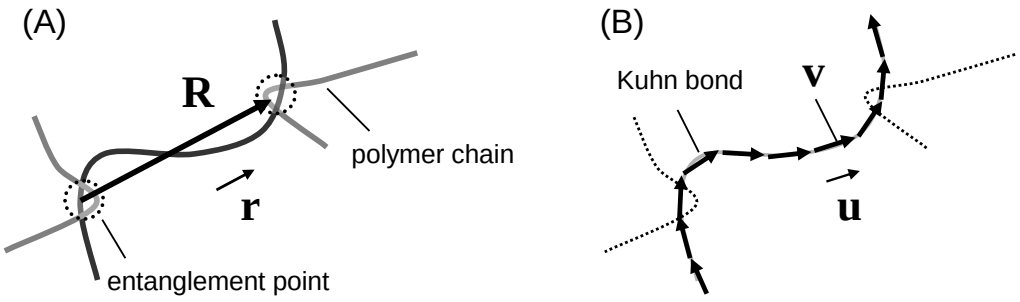

Scheme IV-1. Schematic illustration of (A) the unit vector parallel to the vector connecting two adjacent entanglement points, **r** (= **R**/|**R**|), and (B) the unit vector of the Kuhn bonds, **u** (= **v**/|**v**|).

$$n_{ij} = \Delta n_0 q_{ij} \tag{IV-6}$$

$$\mathbf{q} = \begin{pmatrix} q_{xx} & q_{xy} & q_{xz} \\ q_{yx} & q_{yy} & q_{yz} \\ q_{zx} & q_{zy} & q_{zz} \end{pmatrix} = \begin{pmatrix} u_x u_x - 1/3 & u_x u_y & u_x u_z \\ u_y u_x & u_y u_y - 1/3 & u_y u_z \\ u_z u_x & u_z u_y & u_z u_z - 1/3 \end{pmatrix}$$

According to Doi et al.[1], the orientational distribution of the Kuhn bonds, q_{ij}, is affected by the surrounding orientational field due to the nematic interaction and the two orientational distribution tensors for entangled polymers are related by the following equation.

$$q_{ij} = \frac{3l^2}{5N_e{}^2 b^2} S_{ij} + \varepsilon q_{ij} \tag{IV-7}$$

where b is the Kuhn length, l is the length measured along the primitive chain pass between two entanglement points or between two slip-links ($l = N_e b^2/a$) and ε ($0 \le \varepsilon \le 1$) is the nematic interaction (NI) parameter meaning the strength of the orientational coupling between a given probe polymer and its surroundings. The first term of the right-hand side in eq. IV-7 represents the effect of slip-link constraints, and the second term the effect of orientational coupling. To simplify the equation, the term $3l^2/(5N_e{}^2 b^2)$ is replaced by K and eq. IV-7 is rewritten as

$$q_{ij} = \frac{1}{1-\varepsilon} K S_{ij} \tag{IV-8}$$

Note that S_{ij} of LM component is considered to be zero since the LM size is generally smaller than entanglement strands and the vector **r** (connecting two entanglement points) of LMs cannot be defined. For the uniaxial deformation, the stress-optical coefficient, C, is given from eqs. IV-2, IV-5, IV-6, and IV-8 as,

$$C = \frac{\Delta n}{\sigma} = \frac{n_{zz} - n_{xx}}{\sigma_{zz} - \sigma_{xx}}$$
$$= \frac{\Delta n_0}{3k_B T \frac{x}{N_e}} \frac{q_{zz} - q_{xx}}{S_{zz} - S_{xx}} = \frac{\Delta n_0}{3k_B T \frac{x}{N_e}} \frac{K}{1-\varepsilon} \qquad \text{(IV-9)}$$

The stress-optical coefficient without nematic interaction, C^0, is related to the C as

$$C^0 = (1-\varepsilon)C \qquad \text{(IV-10)}$$

For polymer/LM (A/B) mixtures, eq. IV-8 takes on more complicated forms due to coupling between different species (polymer and LM) in addition to the coupling between the same species. Following the approaches of Doi et al.[1] and Zawada et al.[3], q_{ij} of the each component in polymer/LM mixture is given by

$$q_{ij,A} = K_A S_{ij,A} + \phi_A \varepsilon_{A,A} q_{ij,A} + \phi_B \frac{x_B}{x_A} \varepsilon_{A,B} q_{ij,B} \qquad \text{(IV-11)}$$

$$q_{ij,B} = \phi_B \varepsilon_{B,B} q_{ij,B} + \phi_A \frac{x_A}{x_B} \varepsilon_{B,A} q_{ij,A} \qquad \text{(IV-12)}$$

where the NI parameter, *e.g.* $\varepsilon_{A,B}$ represents the coupling of component A (polymer) with the orientational field of component B (LM), and ϕ_A (or ϕ_B) is the volume fraction of component A (or B). It is noteworthy that eq. IV-12 does not contain S_{ij} term (corresponding to the slip link constraint) and the orientation of LMs is affected only by the orientational coupling with both orientated polymer chains and LMs themselves.

From eq. IV-6 and the additivity rule, the deviatoric part of the refractive index

tensor of A/B mixture, $n_{ij,mix}$, may be expressed as

$$n_{ij,mix} = \phi_A \Delta n_{0,A} q_{ij,A} + \phi_B \Delta n_{0,B} q_{ij,B} \tag{IV-13}$$

As for $\sigma_{ij,mix}$, only the polymer component generates the stress (LM does not contribute to the stress), and thus

$$\sigma_{ij,mix} = 3k_B T \frac{x_A}{N_{e,A}} \phi_A S_{ij,A} \tag{IV-14}$$

From eqs. IV-9 – IV-14, and relations of $\Delta n = n_{zz} - n_{xx}$ and $\sigma = \sigma_{zz} - \sigma_{xx}$ (z axis is the stretching direction), the following equation is obtained. (see Appendix IV-1)

$$\Delta n_{mix} = \left[\frac{1 + \phi_B \varepsilon_{B,A} \dfrac{\Delta n_{0,B}}{\Delta n_{0,A}} \dfrac{x_A}{x_B} \Big/ (1 - \phi_B \varepsilon_{B,B})}{1 - \phi_A \varepsilon_{A,A} - \phi_A \phi_B \varepsilon_{A,B} \varepsilon_{B,A} / (1 - \phi_B \varepsilon_{B,B})} C_A^{\,0} \right] \sigma_{mix} \tag{IV-15}$$

Eq. IV-15 indicates that the stress-optical coefficient, C_R, of polymer/LM mixtures corresponding to the term in the bracket is a function of the composition, intrinsic parameters for pure components ($\Delta n_{0,x}$), and four NI parameters $\varepsilon_{A,A}$, $\varepsilon_{B,B}$, $\varepsilon_{A,B}$, and $\varepsilon_{B,A}$.

Intrinsic birefringence, Δn_0, corresponding to the birefringence for the perfectly-oriented molecules to the stretching direction, is defined as $\Delta n_0 = \Delta n / P_2$, where P_2 is the orientation function and $P_2 = (3\langle\cos^2\theta\rangle - 1)/2$, with θ being the angle between the molecular axis and the stretching direction. Without NI, P_2 is calculated from the strain, e, based on the assumption of a pseudo-affine deformation (see Appendix IV-2). This calculated value is defined as $P_2^{\,0}$. When NI works between chains, P_2 becomes larger than $P_2^{\,0}$ due to the failure of the pseudo-affine assumption.

Apparent intrinsic birefringence, defined by $\Delta\tilde{n}_0 \equiv \Delta n / P_2^0 (= (\Delta n / e)(e / P_2^0))$, is experimentally determined by the following equation,

$$\Delta\tilde{n}_0 = \frac{5}{3} O_{\mathrm{R}}'(\infty) = \frac{5}{3} C_{\mathrm{R}} E_{\mathrm{R}}'(\infty) \tag{IV-16}$$

Here, relations of $O = \Delta n/e$ and $e/P_2{}^0 = 5/3$ (see Appendix IV-2) were used. $E_{\mathrm{R}}'(\infty)$ is the limiting modulus of the rubbery component at high frequency, which can be estimated from the decomposed E_{R}' spectra. If there is no NI, $\Delta\tilde{n}_0$ becomes Δn_0. Therefore, Δn_0 of a single component polymer can be determined as (5/3) $C_{\mathrm{R}}{}^0 E_{\mathrm{R}}'(\infty)$.

From eqs. IV-15 and IV-16, apparent intrinsic birefringence of polymer/LM (A/B) mixtures $\Delta\tilde{n}_0$ is written as

$$\Delta\tilde{n}_{0,mix} = \frac{\phi_A \left(\Delta n_{0,A} + \dfrac{\phi_B \varepsilon_{B,A} \Delta n_{0,B}\, x_A / x_B}{1 - \phi_B \varepsilon_{B,B}} \right)}{1 - \phi_A \varepsilon_{A,A} - \dfrac{\phi_A \phi_B \varepsilon_{A,B} \varepsilon_{B,A}}{1 - \phi_B \varepsilon_{B,B}}} \tag{IV-17}$$

In the derivation of this equation, the relation of $E_{\mathrm{R},mix}'(\infty) = \phi_A E_{\mathrm{R},A}'(\infty)$, which is known to be valid for polymer/LM systems in the Rouse region (corresponding to the polymer chain motion inside the entanglement points) was used, because of the following reasons: all the observed data in this study were in the higher frequency region than the frequency where entanglement plateau appears, and the LM component (B) motion does not contribute to Young's modulus in the R-mode. In analyzing the data in the entanglement region, eq. IV-15 must be used instead of eq. IV-17. In this study, the magnitude of the inter-component NI parameter $\varepsilon_{B,A}$ or $\varepsilon_{A,B}$ (actually these two values are assumed to be the same) for PS/5CB mixtures is examined by using eq. IV-17.

IV-3. Experimental

Materials Polystyrene (PS), 4-pentyl-4'-cyanobiphenyl (5CB, purity > 97 %), and 4-pentyl-4'-cyanoterphenyl (5CT, purity > 97 %) were purchased from Wako Pure Chemicals Industries, Ltd. Their chemical structures are shown in Fig. IV-1. PS was purified by reprecipitation of the PS/dioxane (good solvent) solution into ethanol (non-solvent). The weight average-molecular-weight (M_w) and the molecular weight distribution index (M_w/M_n) of PS were 1.55×10^5 and 3.1, respectively. All mixture samples were prepared by freeze-drying method from benzene solutions. The dried samples were pressed into sheets with the size of 25 mm × 5 mm × 1mm at temperatures above T_g+50 K, for the dynamic viscoelastic and birefringence measurements.

Although 5CB and 5CT are not volatile, a little bit weight loss was sometimes observed especially during the freeze-drying process. Therefore, the weight fractions of 5CB and 5CT, W_{5CB} and W_{5CT}, of all the mixtures were determined by ^{1}H-NMR measurement using EXcalibur-270 (JEOL Ltd., Tokyo, Japan) or Mercury-300 (Varian, California, USA) in the same way with the chapters II and III. NMR spectra of the samples were checked after the viscoelastic and birefringence measurements and it was confirmed that W_{5CB} and W_{5CT} were constant during the measurements within the experimental error.

Methods Dynamic viscoelastic and birefringence measurements were carried out with an oscillatory tensile rheometer (Rheospectoler DVE-3, Rheology Co. Ltd., Kyoto, Japan) equipped with an optical system at several temperatures between T_g –5 K and T_g +30 K in the frequency range of 1 ~ 130 Hz ($6.3 \sim 8.2\times10^2$ s^{-1}).

A differential scanning calorimeter (DSC EXSTAR-6000, Seiko Instruments Inc., Chiba, Japan) was operated to determine the glass transition temperature T_g for each sample. The value of T_g was estimated as the inflection point of the DSC trace

Table IV-1. Weight fractions of 5CB or 5CT, W_{5CB} or W_{5CT}, and glass transition temperatures, T_g, for PS/5CB and PS/5CT mixtures.

Code	W_{5CB} or W_{5CB}	T_g / K
PS	0	368.2
PS/5CB	0.049	359.2
	0.127	335.4
	0.206	316.4
PS/5CT	0.031	372.2
	0.049	368.8
	0.086	358.5

for the glass transition process upon heating with the scan rate of 10 K min^{-1}. Values of T_g and W_{5CB} are summarized in Table IV-1.

IV-4. Results and Discussion

IV-4-1. Viscoelastic and birefringence behaviors of PS and PS/5CB mixtures

First of all, the result for PS/5CB mixtures will be discussed. Fig. IV-2 shows the composite curves of $E^*(\omega)$ and $O^*(\omega)$ for pure PS (A) and PS/5CB mixtures (B)~(D) at reference temperatures, $T_r = T_g$+20 K. It is well-known that time-temperature superposition principle does not hold in the glass-to-rubber transition region of amorphous polymers.[13-15] Actually $E^*(\omega)$ and $O^*(\omega)$ data measured at different temperature were not superposable in a precise sense. However in these figures, all the data were roughly superposed to see the global shapes of the $E^*(\omega)$ and $O^*(\omega)$ spectra. For the quantitative discussion, the master curves for separated E_R^* and E_G^*, which are superposable,[14-15] will be presented in the next section. The (+) and (–) symbols in Fig. IV-2 represent the sign of O^* data. The different signs at high and low frequencies mean the relevant motional units are different at high and low frequencies since they should have different stress-optical coefficients.[5-6, 11-12]

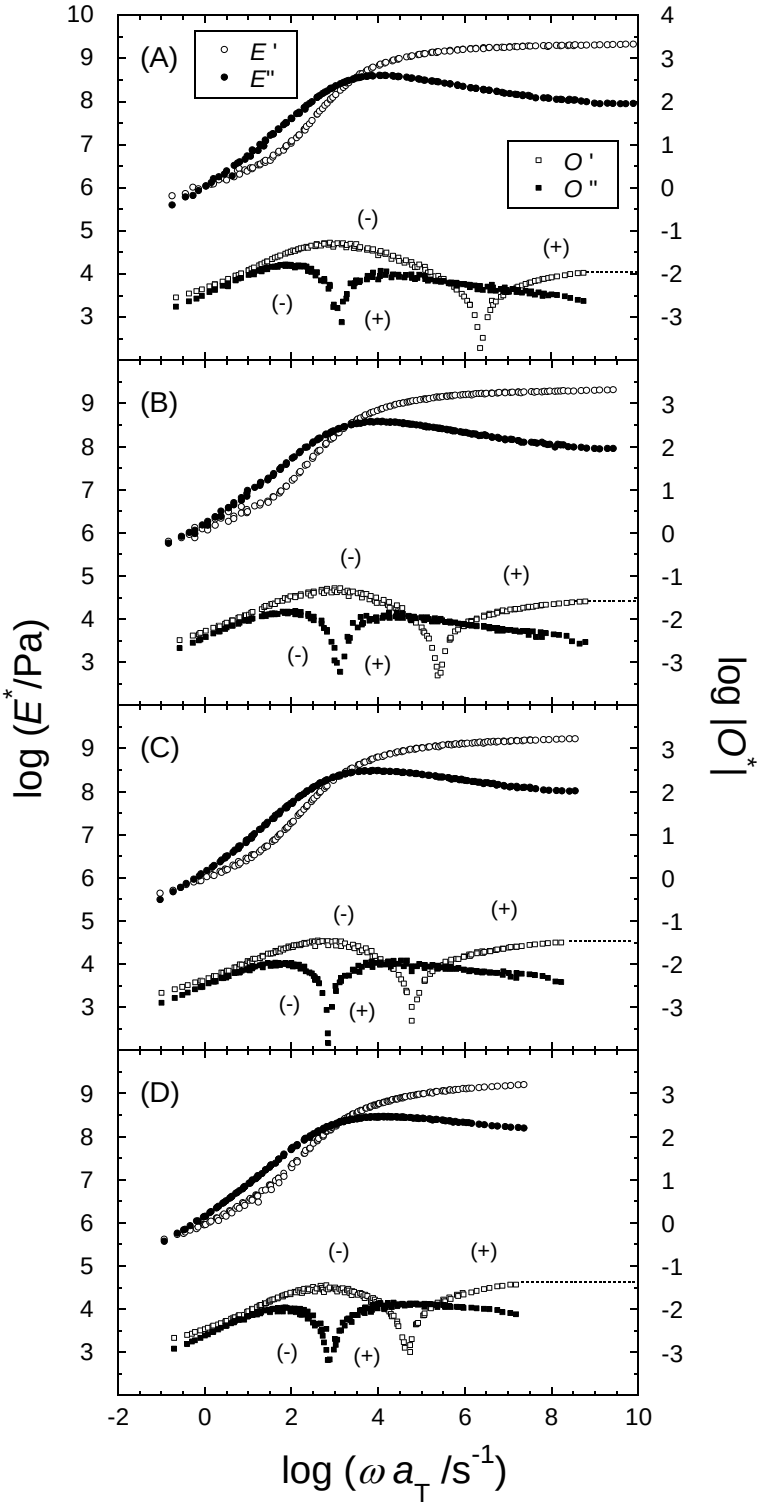

Figure IV-2. Composite curves of complex Young's modulus, $E^*=E'+iE''$, and complex strain-optical coefficient, $O^*=O'+iO''$, for PS (A) and PS/5CB mixtures with W_{5CB}=0.05(B), 0.13(C), and 0.20(D) at reference temperatures, 388, 379, 355, and 336 K, respectively, which correspond to T_g+20 K.

The shapes and locations of E^* curves are almost the same for all samples compared at $T = T_g$+20 K (T_g varies 368 ~ 316 K for $W_{5CB} = 0 \sim 0.20$ as shown in Table IV-1). This means that the mechanical relaxation spectra of PS/5CB mixtures can be approximately regarded as a universal function of $T–T_g$. In contrast, O' spectra can be seen to depend on W_{5CB} especially as to position of the apparent valley of log $|O'|$ curves where the sign in O' changes. The apparent minimum in the log $|O'|$ curve shifts to the lower frequency side with increasing W_{5CB}. This is because the magnitude of O' of the mixture in the glass-plateau region at the highest frequency slightly increases with W_{5CB} and the opposite signs at low and high frequency regions make such slight change visible. The increase of high-ω plateau in O' with W_{5CB} as shown by dotted-lines in Fig. IV-2 (corresponding to the increase of C_G as will be shown in Fig. IV-5) is attributable to the higher intrinsic birefringence of 5CB than PS as will be discussed in sections V-4-4 and V-4-5.

IV-4-2. Application of a modified stress-optical rule

The breakdown of time-temperature superposition principle (TTS) in the transition region originates from different temperature dependencies of the two relaxation modes (rubbery and glassy modes). Inoue et al. showed that TTS holds for each mode.[14-15] As described previously, the two relaxation components can be separated into two modes based on MSOR (eqs. IV-3 and IV-4) in principle at each temperature. Firstly, two stress optical coefficients C_R and C_G at the highest and at the lowest temperatures, respectively, were determined, where only the R or G mode was dominantly observed in both the stress and birefringence data. Thus determined two coefficients were tentatively assumed to be independent of T. After reasonable separation into the two modes were attained for all the data at each temperature with temperature independent C_R and C_G, only the C_R is assumed to be inversely proportional to T as C shown in eq. IV-9, in which C_R corresponds to C.

$$C_{\mathrm{R}}(T) = C_{\mathrm{R}}(T')\frac{T'}{T} \qquad \text{(IV-18)}$$

Then, the separation procedure and the TTS for each mode with temperature-dependent C_R were reexamined. As a result, it was found that the correction of C_R by eq. IV-18 did not practically give a significant change of the shapes of both E_R^* and E_G^* spectra as well as the shift factors. However, for the comparison of C_R values determined at widely separated temperatures, it was judged that this correction was necessary and used eq. IV-18 for the application of the MSOR. On the other hand, C_G was assumed to be independent of T. The MSOR with temperature-dependent C_R worked well for all the systems (W_{5CB}=0~0.20) and successfully separated $E^*(\omega)$ into R and G components as shown in Fig. IV-3: E_R' and E_R" in the high frequency region are proportional to ω^0 and ω^{-1} (high frequency terminal behavior) while E_G' and E_G" in the low frequency region are proportional to ω^2 and ω^1 (low frequency terminal behavior).

After the separation of $E^*(\omega)$ data into the rubbery (E_R^*) and glassy (E_G^*) components at each temperature, master curves were constructed for each mode. The vertical shift for E_R^* was assumed to be proportional to T according to the rubber elasticity theory but as for E_G^* no vertical shift was applied. The results (master curves) are shown in Fig. IV-3. TTS held for both modes of all the samples, indicating that dynamic heterogeneity (concerning the heterogeneity of the component dynamics[16-29]) is very low for these mixtures. This is consistent with our previous dielectric and viscoelastic results, *i.e.* the rotational motion of 5CB is coupled with the segmental relaxation of PS.[30-32] However, the shapes of E_R^* and E_G^* curves are slightly dependent on W_{5CB}: slight broadening of both spectra with increasing W_{5CB} is observed. This would be due to the concentration fluctuation effect.

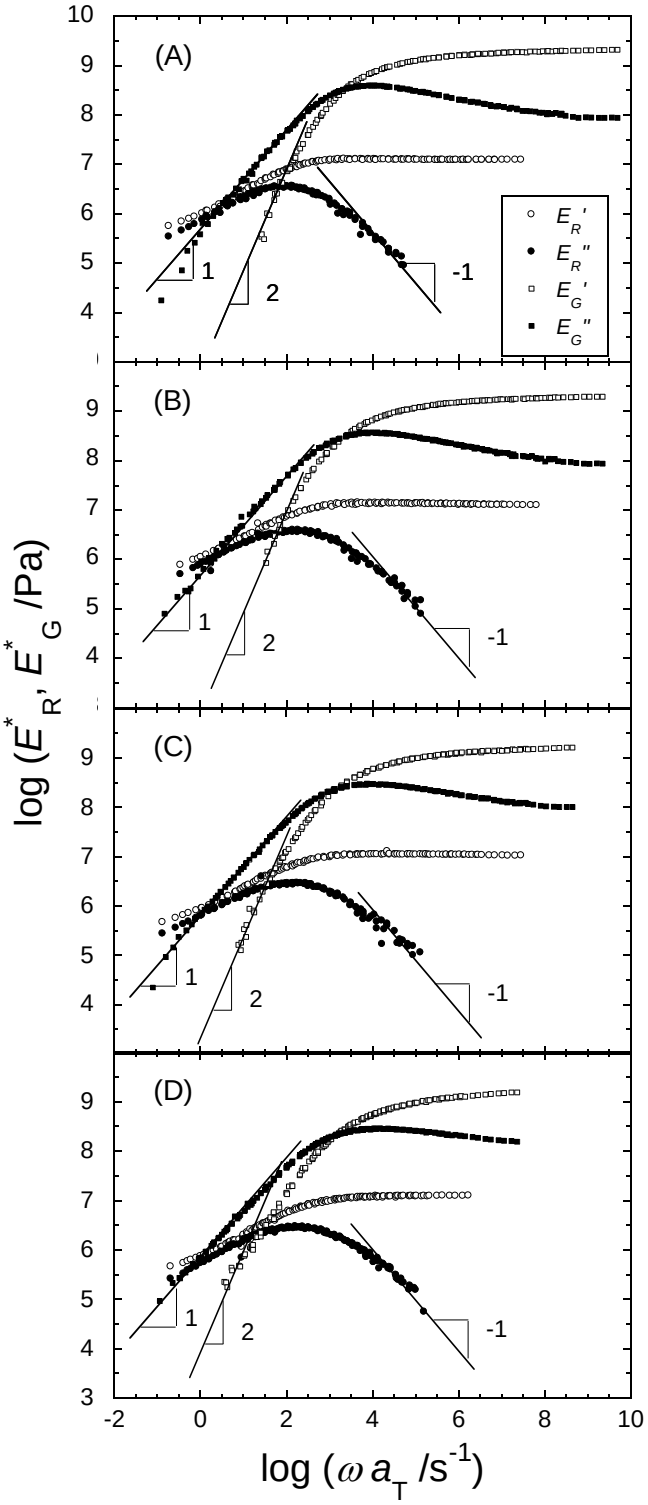

Figure IV-3. Decomposed rubbery and glassy viscoelastic spectra, E^*_R and E^*_G, respectively, for PS (A) and PS/5CB mixtures with W_{5CB}=0.05(B), 0.13(C), and 0.20(D) at $T = T_g$+20 K. The slopes shown in figure represent ω dependences of E_R' at limiting high frequency, and E_G', and E_G" at limiting low frequency.

Temperature dependences of the obtained shift factors a_T for the R and G modes to construct the composite curves are shown in Fig. IV-4. The reference temperature was set to be T_g+20 K. All the shift factors a_T for each mode overlap each other. This means that the temperature dependencies of the R and G mode relaxations can be reduced by T_g irrespective of the mixture composition. The difference between the two kinds of a_T's (R-and G-modes) is consistent with the data reported by Inoue et al.[14-15]

IV-4-3. Rotational motion of 5CB and nematic interaction

In chapter II, the length scales of dynamical unit for 5CB and PS were compared.[30, 32] The average length of the long axis of 5CB is 1.3 nm relevant to the main relaxation (rotational motion) of 5CB, which is slightly smaller than the viscoelastic (Rouse) segmental size of PS, 1.9 nm.[11, 33-34] The R mode reflects the large scale motion of polymers (larger than or equal to the size of the viscoelastic

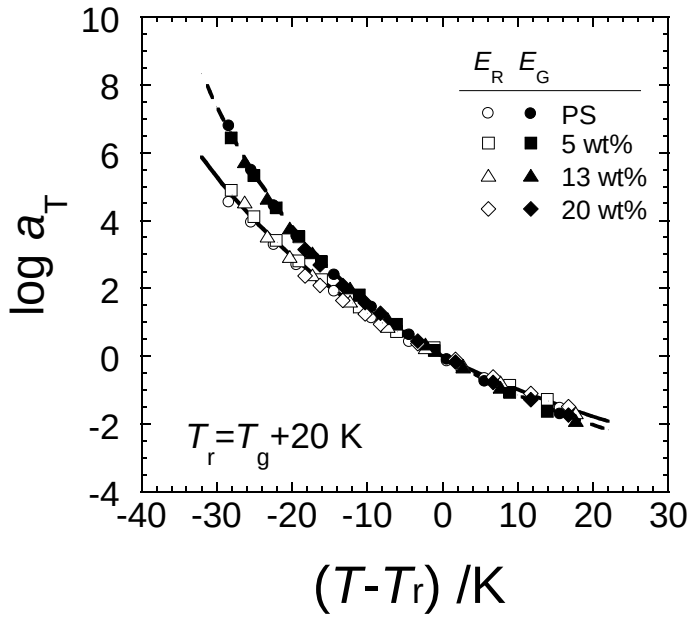

Figure IV-4. Shift factors of the glass and rubber modes for pure PS and PS/5CB mixtures as functions of reduced temperature T-T_r with T_r=T_g+20 K.

segment) and the G mode reflects the local motions of the smaller size units than the Rouse segment. Therefore, the rotational motion of 5CB will mainly appear in the G mode. Furthermore the increase of C_G values with W_{5CB} suggests that the cooperative orientation of the long axis of 5CB with the local orientation of PS inside its segment will occur in the G mode since 5CB has larger intrinsic birefringence than PS. However, the rotational relaxation of 5CB could not complete in the G mode and a part of the orientation still remains in the rubber mode due to the NI with the partially orientated (unrelaxed) PS chain.

In the following sections, the degree of the residual orientation of 5CB in the R mode will be evaluated by analyzing the concentration dependence of C_R.

IV-4-4. Concentration dependence of C_R and C_G

Fig. IV-5 shows the concentration dependence of C_R and C_G. (For pure PS, $C_R = -4.7\times10^{-9}$ Pa^{-1} at 373 K and $C_G = 3.2\times10^{-11}$ Pa^{-1}. These values agree well with the reported ones.[5]) Both C_R and C_G increase with the 5CB concentration. As mentioned before, the polarizability of the long axis of 5CB is larger than that of the short axis and thus the intrinsic birefringence of 5CB is positive. Therefore, the increase of both C_R and C_G with W_{5CB} indicates the orientation of the long axis of 5CB to the stretching direction. As for the increase of C_R (decrease in the magnitude), cooperative orientation of 5CB molecule with PS chain segment through the NI is thought to be the cause. In contrast, the increase of C_G originates from the orientation of 5CB molecule to the stretching direction under (pseudo-)affine deformation resulting in an enhancement of the positive birefringence of PS in the G-mode. If 5CB component does not contribute to either stress or birefringence in both modes, just working as a diluent, C_R and C_G will take constant values against W_{5CB}. It is obvious that this is not the case from Fig. IV-5.

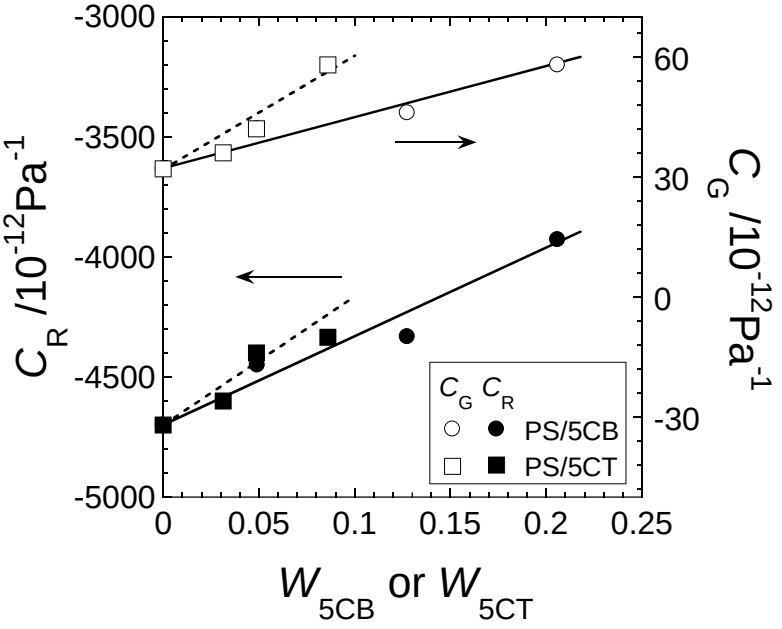

Figure IV-5. Concentration dependence of C_R and C_G for PS/5CB and PS/5CT mixtures at 373 K. The solid and dotted lines are drawn for eye guides.

IV-4-5. Concentration dependence of $\Delta\tilde{n}_0$

Fig. IV-6 shows the W_{5CB} dependence of $\Delta\tilde{n}_0$ experimentally determined with eq. IV-16. W_{5CB} is approximately equal to ϕ_{5CB}, since the densities of PS and 5CB are similar. The thin solid line in this figure indicates the proportional relation, i.e., $\Delta n_{0,PS}(1-\phi_{5CB})$, which corresponds to all NI parameters in eq. IV-17 being zero and means that the dilution of PS chain by mixing 5CB induces the decrease of the absolute value of $\Delta\tilde{n}_0$. It is seen that experimental $\Delta\tilde{n}_0$ value is larger than the thin solid line, indicating the existence of the interaction between PS and 5CB.

In order to fit the data with eq. IV-17, the following assumptions were made to reduce the floating parameters: (1) $\varepsilon_{PS,5CB} \approx \varepsilon_{5CB,PS}$, (2) x_{PS}/x_{5CB}~1 (this is a reasonable approximation because the densities of PS and 5CB are similar and the sizes of PS segment and 5CB molecule are not so different), and (3) $\varepsilon_{PS,PS}$=0.26 which was experimentally determined by Tassin et al.[35]

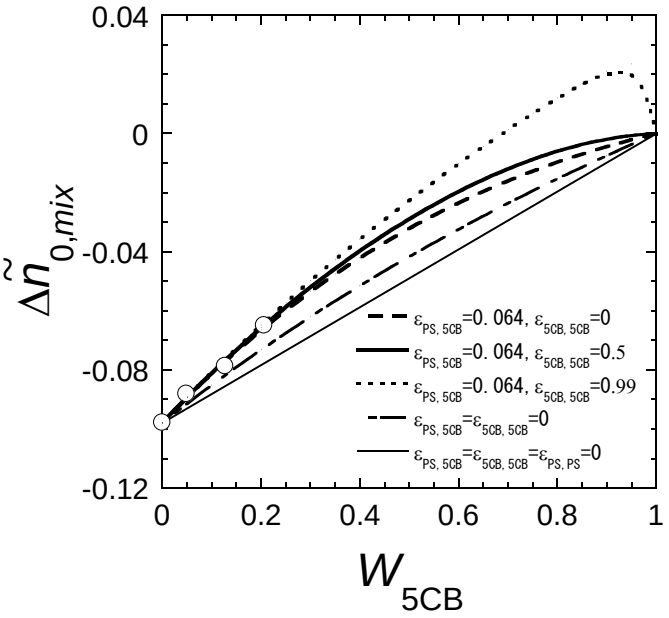

Figure IV-6. Concentration dependence of $\Delta\tilde{n}_{0,mix}$ for PS/5CB mixtures. The curves are the calculated results by eq. IV-17 with the parameters indicated in the figure.

$\Delta n_{0,PS}$ can be related to the C_{PS} (= -4.7×10^{-9} Pa^{-1}) through the eqs. IV-10 and IV-16, and the formula of $\Delta n_{0,PS} = -0.098\times(1-\varepsilon_{PS,PS})$ is obtained including the NI parameter. Since the intrinsic birefringence of 5CB, $\Delta n_{0,5CB}$, was unknown, the value was calculated from the difference between two polarizabilities in the parallel and perpendicular directions to the long axis of 5CB molecule. The polarizability, α, is given by the Lorentz-Lorenz equation:

$$\frac{n^2-1}{n^2+2}\frac{M}{\rho}=\frac{4}{3}\pi N_A\alpha \qquad \text{(IV-19)}$$

where n, M, ρ, and N_A are refractive index, molecular weight, density, and Avogadro's number, respectively. Differentiation of eq. IV-19 by α leads to the expression for the intrinsic birefringence, Δn_0, as follows.[36]

$$\Delta n_0 \cong \frac{2}{9}\pi \frac{(n^2+2)^2}{n}\frac{\rho N_A}{M}\Delta\alpha \qquad \text{(IV-20)}$$

where $\Delta\alpha$ is defined as the difference between parallel and perpendicular polarizabilities ($P_{//}$ and $P_{\perp}$) to the stretching axis ($\Delta\alpha = \alpha_{//} - \alpha_{\perp}$). The $\Delta\alpha_{5CB}$ was calculated by using WinMopac software (Fujitsu) and $\Delta n_{0,5CB}$ was determined to be 0.48. It is reported that homogeneously aligned 5CB nematic liquid crystal on the rubbed surface shows birefringence of about 0.21.[37] The orientation of 5CB in the nematic state will not be perfect, and thus the experimental value may be smaller than the calculated one. In this paper, this calculated value ($\Delta n_{0,5CB} = 0.48$) was used.

Finally, eq. IV-17 contains two parameters $\varepsilon_{PS,5CB}$ and $\varepsilon_{5CB,5CB}$. It was found that $\varepsilon_{PS,5CB}$ is much more sensitive than $\varepsilon_{5CB,5CB}$ to the calculated result of $\Delta\tilde{n}_{0,mix}$ at low ϕ_{5CB} (or W_{5CB}). The dotted, thick solid, and dashed curves in Fig. IV-6 demonstrate the results of calculation with $\varepsilon_{5CB,5CB} = 0$, 0.5, and 0.99, respectively, at fixed $\varepsilon_{PS,5CB}$ (=0.064). It is seen that the variation of $\varepsilon_{5CB,5CB}$ does not give significant change in $\Delta\tilde{n}_{0,mix}$ at low ϕ_{5CB}. This is because eq. IV-17 at low ϕ_B can be approximated by the following equation:

$$\Delta\tilde{n}_{0,mix} \approx \frac{\phi_A\left(\Delta n_{0,A} + \phi_B \varepsilon_{A,B}\Delta n_{0,B}\right)}{1-\phi_A\varepsilon_{A,A}} \qquad \text{(IV-21)}$$

In contrast, the variation of $\varepsilon_{PS,5CB}$ value is sensitive to the $\Delta\tilde{n}_{0,mix}$ and the optimum value was found. The obtained result was $\varepsilon_{PS,5CB}$=0.070 (at $\varepsilon_{5CB,5CB} = 0$), $\varepsilon_{PS,5CB} = 0.064$ (at $\varepsilon_{5CB,5CB} = 0.5$), and $\varepsilon_{PS,5CB} = 0.058$ (at $\varepsilon_{5CB,5CB} = 0.99$). The thick solid curve in the figure corresponds to the result using the optimum value. The dash-dotted curve indicates the case of $\varepsilon_{PS,5CB} = 0$ (and $\varepsilon_{5CB,5CB} = 0$). It is seen that the variation of $\varepsilon_{PS,5CB}$ sensitively alter the calculated result. Note that this

dash-dotted curve is different from the proportional relation (thin solid line) because the NI between PS-PS, which is weakened with increasing W_{5CB}, is taken into account in this case. From these results, the inter-component NI parameter between PS and 5CB ($\varepsilon_{PS,5CB}$) can be determined to be 0.064 with ±10% accuracy. $\varepsilon_{PS,5CB}$ (0.064) is about a quarter of $\varepsilon_{PS,PS}$ (0.26), meaning that 5CB does not orient parallely to the PS chain so much.

IV-4-6. Birefringence behavior of PS/5CT mixtures

Fig. IV-7 (A) shows the result of viscoelastic and birefringence measurement for PS/5CT mixture at $W_{5CT} = 0.05$. The MSOR given by eqs. IV-3 and IV-4 also worked well for PS/5CT system, and thus the viscoelastic curves could be separated into R and G components. The decomposed curves of R and G components are shown in Fig. IV-7 (B). C_R and C_G values of PS/5CT used for the separation are given in Fig. IV-5. Concentration dependence of C_R and C_G for PS/5CT mixtures was stronger than that for PS/5CB mixtures, indicating that the orientation of 5CT correlates more strongly with PS chain orientation than that of 5CB. The intrinsic birefringence $\Delta\tilde{n}_0$ of PS/5CT obtained in the same way with the case of PS/5CB is shown in Fig. IV-8. As expected, it is seen that $\Delta\tilde{n}_0$ of PS/5CT is larger than that of PS/5CB compared at the same weight fraction. NI parameter between PS and 5CT, $\varepsilon_{PS,5CT}$ was determined to be 0.080 with ±10% accuracy by using eqs. IV-17 and IV-20. This value is larger than $\varepsilon_{PS,5CB}$ (0.064). This will be caused by the fact that the long axis of 5CT (1.67 nm) is longer than that of 5CB (1.26 nm).

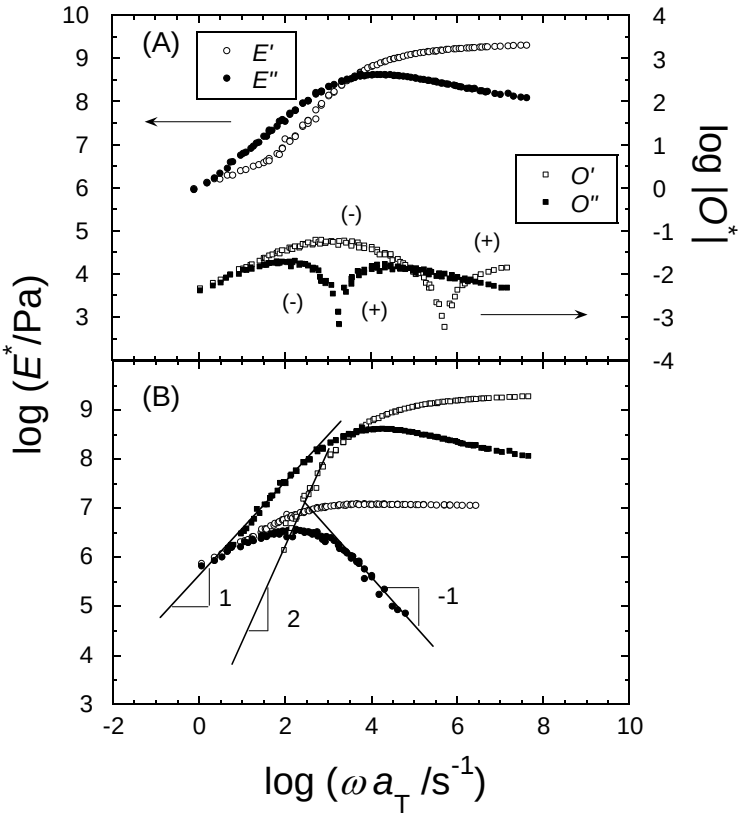

Figure IV-7. (A) Composite curves of complex Young's modulus, $E^*=E'+iE''$, and complex strain-optical coefficient, $O^*=O'+iO''$, for PS/5CT mixture at $W_{5CT} = 0.049$. The (+) and (–) symbols indicate the signs for optical data, O' and O''. (B) Decomposed curves of rubbery and glassy components, E^*_R and E^*_G.

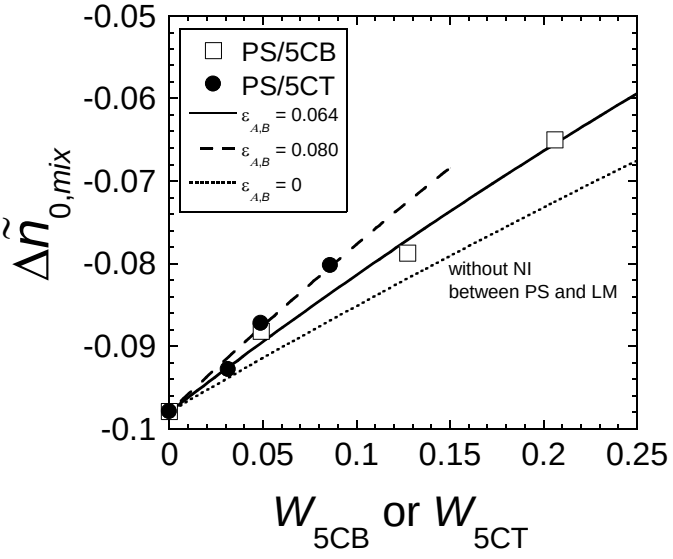

Figure IV-8. Concentration dependence of $\Delta\tilde{n}_{0,mix}$ for PS/5CT and PS/5CB mixtures. The solid and broken curves are the fitted results by eq. IV-17 with $\varepsilon_{A,B}$ as a parameter. The subscript A and B in $\varepsilon_{A,B}$ denote PS and 5CB (or 5CT) components, respectively. $\varepsilon_{A,A}$ ($\varepsilon_{PS,PS}$) was fixed to be 0.26.

IV-4-7. Comparison of nematic interactions for PS-5CB and PS-5CT

The determined $\varepsilon_{PS,5CB}$ (=0.064) and $\varepsilon_{PS,5CT}$ (=0.080) are 1/3~1/4 of $\varepsilon_{PS,PS}$ (=0.26)[38], which was determined through the infrared absorption dichroism measurements for mixtures of low molecular weight deuterio-PS (dPS) and high molecular weight protio-PS. This indicates the weaker nematic interaction acting between PS-5CB (and PS-5CT) than between PS-dPS, suggesting that dynamically homogeneous behaviors of PS/5CB and PS/5CT systems[30, 32] studied in chapter II are not directly related to the NI between the components. As described as "speculation" in the introduction, it can be suggested that the strong NI is not required for the cooperative component dynamics. The origin of the dynamic homogeneity in PS/5CB and PS/5CT mixtures may be in the large size of 5CB and 5CT molecules. As Urakawa et al suggested,[30,32] it can be concluded that there is a critical size above which the LM dynamics became cooperative with that of PS segments.

From a practical viewpoint, small $\varepsilon_{PS,5CB}$ and $\varepsilon_{PS,5CT}$ values indicate that 5CB and 5CT cannot effectively compensate the birefringence of PS. As can be seen in eq. IV-21, if $\Delta n_{0,A}$ and $\Delta n_{0,B}$ have opposite signs and $\varepsilon_{A,B}$ is large enough, the birefringence of the mixture can become zero even at lower LM concentration. This means that the inter-component NI parameter $\varepsilon_{A,B}$ as well as the intrinsic birefringence of each component plays a significant role in controlling the polymer birefringence by mixing LMs. Actually, eq. IV-21 indicates that the product of $\varepsilon_{A,B}\Delta n_{0,B}$ determines the $\Delta\tilde{n}_{0,mix}$. Therefore, the evaluation of $\varepsilon_{A,B}$ is important not only in newly creating zero-birefringent polymer/LM mixtures but also in understanding already reported results for such mixtures in which only the intrinsic birefringence values of the components have been mainly focused on.[35]

The small $\varepsilon_{PS,5CB}$ and $\varepsilon_{PS,5CT}$ values suggest that NI strength depends on the chemical structure: NI between different chemical species might be weak. The difference in the shapes and/or sizes between PS segments and LM molecules will also

be a possible origin for the small value of $\varepsilon_{A,B}$. As a future work, it will be necessary to consider the correlation between the chemical structure and the $\varepsilon_{A,B}$ value.

IV-5. Conclusions

In this chapter, the result of simultaneous measurements of dynamic birefringence and viscoelastic relaxation are presented for PS/5CB and PS/5CT mixtures. By applying the MSOR, C_R and C_G values were determined as functions of 5CB or 5CT concentrations. The C_R value was negative and increased (absolute value of C_R decreased) with increasing the 5CB or 5CT concentration, indicating the partial orientation of the mesogenic low-mass molecules to the orientation direction of PS segments through the nematic interaction (NI).

The inter-component NI parameter in PS/5CB and PS/5CT mixtures is determined by using a newly proposed equation. The NI parameter, $\varepsilon_{PS,5CB}$ and $\varepsilon_{PS,5CT}$ were 0.064 ± 0.006 and 0.080 ± 0.010, respectively, being smaller compared with the value of $\varepsilon_{PS,PS}$ (0.26). The weak NI between PS and 5CB (or 5CT) suggested that NI strength between different components in miscible mixtures depends on their chemical structures including the size and/or shape differences. From the result that the NI parameter was small in the dynamically homogeneous mixture, it was concluded that there is no direct correlation between dynamic cooperativity and orientational coupling.

The derived equations in this chapter (eqs. IV-17 and IV-21) indicated that the larger $\varepsilon_{A,B}$, the more effectiveness to control the birefringence of the mixture. This means that the determination of $\varepsilon_{A,B}$ is very important in creating zero-birefringent polymer/LM mixtures.

Appendix IV-1.

From eqs. IV-11 and IV-12, the local orientation distributions of components A

and B, $q_{ij,A}$ and $q_{ij,B}$, are given as,

$$q_{ij,A} = \frac{1}{(1-\phi_A\varepsilon_{A,A}) - \phi_A\phi_B\varepsilon_{A,B}\varepsilon_{B,A}/(1-\phi_B\varepsilon_{B,B})} K_A S_{ij,A} \qquad \text{(A-IV-1)}$$

$$q_{ij,B} = \frac{\phi_A \dfrac{x_A}{x_B}\varepsilon_{B,A}/1-\phi_B\varepsilon_{B,B}}{(1-\phi_A\varepsilon_{A,A}) - \phi_A\phi_B\varepsilon_{A,B}\varepsilon_{B,A}/(1-\phi_B\varepsilon_{B,B})} K_A S_{ij,A} \qquad \text{(A-IV-2)}$$

By using these equations in eq. IV-13, the following equation is obtained.

$$n_{ij,mix} = \left[\frac{1+\phi_B\varepsilon_{B,A}\dfrac{\Delta n_{0,B}}{\Delta n_{0,A}}\dfrac{x_A}{x_B}\Big/(1-\phi_B\varepsilon_{B,B})}{1-\phi_A\varepsilon_{A,A}-\phi_A\phi_B\varepsilon_{A,B}\varepsilon_{B,A}\big/(1-\phi_B\varepsilon_{B,B})} \right] \Delta n_{0,A}\phi_A K_A S_{ij,A} \qquad \text{(A-IV-3)}$$

Here, from eqs. IV-9 and IV-14, the term in the right hand, $\Delta n_{0,A}\ \phi_A\ K_A\ S_{ij,A}$, is given by

$$\Delta n_{0,A}\phi_A K_A S_{ij,A} = (1-\varepsilon_{A,A}) C_A \sigma_{ij,mi} \qquad \text{(A-IV-4)}$$

Since the stress and birefringence, σ and Δn, are defined to be $\sigma = \sigma_{zz} - \sigma_{xx}$ and $\Delta n = n_{zz} - n_{xx}$ (z axis is the stretching direction), respectively, the birefringence of the mixture can be obtained from eqs. A-IV-3 and A-IV-4 as,

$$\Delta n_{mix} = \left[\frac{1+\phi_B\varepsilon_{B,A}\dfrac{\Delta n_{0,B}}{\Delta n_{0,A}}\dfrac{x_A}{x_B}\Big/(1-\phi_B\varepsilon_{B,B})}{1-\phi_A\varepsilon_{A,A}-\phi_A\phi_B\varepsilon_{A,B}\varepsilon_{B,A}\big/(1-\phi_B\varepsilon_{B,B})} \right] (1-\varepsilon_{A,A}) C_A \sigma_{mi} \qquad \text{(A-IV-5)}$$

By using eq. IV-10, eq. IV-15 is obtained.

$$\Delta n_{mix} = \left[\frac{1+\phi_B \varepsilon_{B,A} \dfrac{\Delta n_{0,B}}{\Delta n_{0,A}} \dfrac{x_A}{x_B} \Big/ (1-\phi_B \varepsilon_{B,B})}{1-\phi_A \varepsilon_{A,A} - \phi_A \phi_B \varepsilon_{A,B} \varepsilon_{B,A} / (1-\phi_B \varepsilon_{B,B})} C_A^{\,0} \right] \sigma_{mix} \qquad \text{(IV-15)}$$

Appendix IV-2.[36, 39]

The second order orientation function, $P_2(\theta)$, is given by,

$$P_2(\theta) = \frac{3\langle \cos^2 \theta \rangle - 1}{2} \qquad \text{(A-IV-6)}$$

Here, θ is the angle between the unit vector of the structure unit and the stretching direction (z). In the pseudo-affine model, a polymeric material is affinely stretched to the z-axis with the stretching ratio, λ. As a result, the unit vector **u** parallel to a polymer segment is transformed to **U**:

$$\mathbf{U} = \begin{pmatrix} \lambda^{-1/2} & 0 & 0 \\ 0 & \lambda^{-1/2} & 0 \\ 0 & 0 & \lambda \end{pmatrix} \mathbf{u} = \begin{pmatrix} \lambda^{-1/2} & 0 & 0 \\ 0 & \lambda^{-1/2} & 0 \\ 0 & 0 & \lambda \end{pmatrix} \begin{pmatrix} u_x \\ u_y \\ u_z \end{pmatrix} \qquad \text{(A-IV-7)}$$

The unit vector, **u**, using polar coordinate expression as shown in Fig. A-IV-1, is given by

$$\mathbf{u} = \begin{pmatrix} u_x \\ u_y \\ u_z \end{pmatrix} = \begin{pmatrix} \cos\varphi \sin\theta \\ \sin\varphi \sin\theta \\ \cos\theta \end{pmatrix} \qquad \text{(A-IV-8)}$$

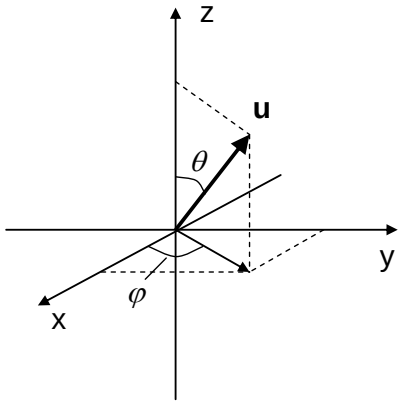

Figure A-IV-1. Schematic representation of a vector **u** which orients to z axis to some extent. θ and φ are angles which specify the **u** direction.

From the inner product of **U** and a unit vector parallel to the z axis, $\cos^2\theta$ can be obtained as follows.

$$\mathbf{U}\cdot\begin{pmatrix}0\\0\\1\end{pmatrix}=|\mathbf{U}|\cos\theta \tag{A-IV-9}$$

$$\cos^2\theta=\left[\frac{\lambda\cos\theta}{|\mathbf{U}|}\right]^2=\frac{\lambda^2\cos^2\theta}{\lambda^2\cos^2\theta+\lambda^{-1}\sin^2\theta} \tag{A-IV-10}$$

The averaged value, $\langle\cos^2\theta\rangle$, is given by the integration in respect to θ and φ,

$$\begin{aligned}\langle\cos^2\theta\rangle&=\frac{\int_0^{\pi}\sin\theta d\theta\int_0^{2\pi}d\varphi\left(\dfrac{\lambda^2\cos^2\theta}{\lambda^2\cos^2\theta+\lambda^{-1}\sin^2\theta}\right)}{\int_0^{\pi}\sin\theta d\theta\int_0^{2\pi}d\varphi}\\&=\frac{\lambda^3}{\lambda^3-1}\left(1-\frac{1}{\sqrt{\lambda^3-1}}\arctan\left(\sqrt{\lambda^3-1}\right)\right)\\&\approx\lambda^3\left(\frac{1}{3}-\frac{\lambda^3-1}{5}\right)=(1+e)^3\left(\frac{1}{3}-\frac{(1+e)^3-1}{5}\right)\\&\sim(1+3e+\cdots)\left(\frac{1}{3}-\frac{3}{5}e+\cdots\right)\sim\frac{1}{3}-\frac{3}{5}e+e=\frac{1}{3}+\frac{2}{5}e\end{aligned} \tag{A-IV-11}$$

Here, under small stretching ratio, $\lambda-1$ is approximately replaced by strain *e*. From eqs. (A-IV-6) and (A-IV-11), the second order orientation function is obtained as a function of *e*,

$$P_2(\theta)=\frac{3\langle\cos^2\theta\rangle-1}{2}\approx\frac{3}{5}e \tag{A-IV-12}$$

References

1. Doi, M.; Pearson, D.; Kornfield, J.; Fuller, G. *Macromolecules* **1989,** 22, 1488-1490.
2. Doi, M.; Watanabe, H. *Macromolecules* **1991,** 24, 740-744.
3. Zawada, J. A.; Fuller, G. G.; Colby, R. H.; Fetters, L. J.; Roovers, J. *Macromolecules* **1994,** 27, 6851-6860.
4. Zawada, J. A.; Fuller, G. G.; Colby, R. H.; Fetters, L. J.; Roovers, J. *Macromolecules* **1994,** 27, 6861-6870.
5. Inoue, T.; Okamoto, H.; Osaki, K. *Macromolecules* **1991,** 24, 5670-5675.
6. Inoue, T. *Nihon Reoroji Gakkaishi* **2000,** 28, 167-175.
7. Hoffmann, U.; Pfeifer, F.; Okretic, S.; Volkl, N.; Zahedi, M.; Siesler, H. W. *Applied Spectroscopy* **1993,** 47, 1531-1539.
8. LeDuc, P.; Haber, C.; Bao, G.; Wirtz, D. *Nature* **1999,** 399, 564-566.
9. Ube, T.; Aoki, H.; Ito, S.; Horinaka, J.; Takigawa, T. *Polymer* **2007,** 48, 6221-6225.
10. Ube, T.; Aoki, H.; Ito, S.; Horinaka, J.; Takigawa, T.; Masuda, T. *Polymer* **2009,** 50, 3016-3021.
11. Inoue, T.; Mizukami, Y.; Okamoto, H.; Matsui, H.; Watanabe, H.; Kanaya, T.; Osaki, K. *Macromolecules* **1996,** 29, 6240-6245.
12. Inoue, T.; Matsui, H.; Osaki, K. *Rheologica Acta* **1997,** 36, 239-244.
13. Plazek, D. J. *Journal of Physical Chemistry* **1965,** 69, 3480-3487.
14. Inoue, T.; Onogi, T.; Yao, M. L.; Osaki, K. *Journal of Polymer Science Part B-Polymer Physics* **1999,** 37, 389-397.
15. Inoue, T.; Onogi, T.; Osaki, K. *Journal of Polymer Science Part B-Polymer Physics* **2000,** 38, 954-964.
16. Colby, R. H. *Polymer* **1989,** 30, 1275-1278.
17. Alegria, A.; Colmenero, J.; Ngai, K. L.; Roland, C. M. *Macromolecules* **1994,** 27, 4486-4492.
18. Chung, G. C.; Kornfield, J. A.; Smith, S. D. *Macromolecules* **1994,** 27, 964-973.
19. Chung, G. C.; Kornfield, J. A.; Smith, S. D. *Macromolecules* **1994,** 27, 5729-5741.
20. Leroy, E.; Alegria, A.; Colmenero, J. *Macromolecules* **2002,** 35, 5587-5590.
21. Urakawa, O.; Fuse, Y.; Hori, H.; Tran-Cong, Q.; Yano, O. *Polymer* **2001,** 42, 765-773.
22. Haley, J. C.; Lodge, T. P.; He, Y. Y.; Ediger, M. D.; von Meerwall, E. D.;

Mijovic, J. *Macromolecules* **2003,** 36, 6142-6151.
23. Hirose, Y.; Urakawa, O.; Adachi, K. *Macromolecules* **2003,** 36, 3699-3708.
24. Lutz, T. R.; He, Y. Y.; Ediger, M. D.; Cao, H. H.; Lin, G. X.; Jones, A. A. *Macromolecules* **2003,** 36, 1724-1730.
25. Haley, J. C.; Lodge, T. P. *Colloid and Polymer Science* **2004,** 282, 793-801.
26. Urakawa, O.; Ujii, T.; Adachi, K. *Journal of Non-Crystalline Solids* **2006,** 352, 5042-5049.
27. Colmenero, J.; Arbe, A. *Soft Matter* **2007,** 3, 1474-1485.
28. Lodge, T. P.; McLeish, T. C. B. *Macromolecules* **2000,** 33, 5278-5284.
29. Watanabe, H.; Urakawa, O. *Korea-Australia Rheology Journal* **2009,** 21, 235-244.
30. Urakawa, O.; Ohta, E.; Hori, H.; Adachi, K. *Journal of Polymer Science Part B-Polymer Physics* **2006,** 44, 967-974.
31. Nobukawa, S.; Urakawa, O.; Shikata, T.; Inoue, T. *AIP Conference Proceedings* **2008,** 1027, 561-563.
32. Urakawa, O.; Nobukawa, S.; Shikata, T.; Inoue, T. *Nihon Reoroji Gakkaishi* **2010,** 38, 41-46.
33. Fetters, L. J.; Lohse, D. J.; Richter, D.; Witten, T. A.; Zirkel, A. *Macromolecules* **1994,** 27, 4639-4647.
34. Fetters, L. J.; Lohse, D. J.; Milner, S. T.; Graessley, W. W. *Macromolecules* **1999,** 32, 6847-6851.
35. Tagaya, A.; Iwata, S.; Kawanami, E.; Tsukahara, H.; Koike, Y. *Applied Optics* **2001,** 40, 3677-3683.
36. Oh, G. K.; Inoue, T. *Rheologica Acta* **2005,** 45, 116-123.
37. Koysal, O.; San, S. E.; Ozder, S.; Ecevit, F. N. *Measurement Science & Technology* **2003,** 14, 790-795.
38. Tassin, J. F.; Baschwitz, A.; Moise, J. Y.; Monnerie, L. *Macromolecules* **1990,** 23, 1879-1881.
39. Ward, I. M. *Journal of Polymer Science Part C-Polymer Symposium* **1977**, 1-21.

Chapter V
Summary

In this thesis, the cooperative dynamics in rod-like low-mass molecules (rod-like LMs)/polymer mixtures was investigated by using dielectric and viscoelastic relaxation measurements. The orientational correlation between low-mass component and polymer chain was quantitatively evaluated by using a rheo-optical measurement.

In chapter II, dynamics of two rod-like low-mass molecules (4-pentyl-4'-cyanobiphenyl (5CB) and 4-pentyl-4'-cyanoter- phenyl (5CT)) and polystyrene (PS) in the mixtures were examined by using dynamic viscoelastic relaxation (VR) and dielectric relaxation (DR) measurements. 5CB in the mixture showed two rotational relaxations (slow and fast modes) in the DR spectra while 5CT exhibited one rotational relaxation. By comparing the temperature dependence of the relaxation time for the slow mode of 5CB or 5CT with the terminal relaxation time reflecting the global motion of the PS chain, which was estimated from the VR spectra, the rotational motions of 5CB (slow mode) and 5CT were found to be cooperative with the local (α) dynamics of PS chain. Particularly, the cooperative relaxation time of the rod-like LMs was found to be proportional to the cube of the length (long axis) for the molecules as predicted by the theory for rod-like molecules in a continuous medium. On the other hand, the fast mode in PS/5CB mixtures was attributed to the fluctuation of 5CB allowed in a restricted free volume (or a cage) formed mainly by PS component. The relaxation intensity of the fast mode depended on both temperature and composition which might change the cage size.

In chapter III, the effect of the side-chain structure of polymers on the rotational dynamics of 5CB was examined in the wide temperature and frequency ranges by the VR and DR measurements for the polymer/5CB mixtures with the 5CB concentration of 5 wt%. As polymer components, PS, poly(4-methyl styrene) (P4MS), poly(4-*tert*-butyl styrene) (PtBS) and poly(1,2-butadiene) (1,2-PB) were examined in this study. The DR spectra of PS/5CB, P4MS/5CB, and PtBS/5CB mixtures showed the two rotational relaxations (slow and fast modes) of 5CB while those of 1,2-PB/5CB mixture exhibited the one relaxation of 5CB. In the same way with that described in chapter II, it was concluded that the slow mode of 5CB in PS/5CB, P4MS/5CB, and PtBS/5CB mixtures and the rotational motion of 5CB in 1,2-PB/5CB were the cooperative motion with the α-motion (responsible for the glass mode) of polymers while the fast mode is the fluctuation motion of 5CB in the restricted space. The increase of the fast mode intensity with decreasing the chain flexibility (increasing the Kuhn segment length) was observed, suggesting that the size mismatch of component characteristic lengths (molecular size of 5CB and the Kuhn length of polymers) might enhance the fast mode of 5CB.

Absolute values of the cooperative relaxation time of 5CB, τ_{slow} or τ_{5CB}, did not agree with the glassy (α) relaxation time, τ_G, of polymers although the temperature dependences of them were the same. Based on the rotational diffusion theory for a rod-like LM, the length scale of the glassy polymer dynamics was evaluated as the critical length for the rod-like LM of which the rotational time was the same with τ_G. By comparing the obtained glassy length with the Kuhn segment length, it was concluded that the glassy dynamics is governed not only by the *intra*-molecular segmental motion but also by the *inter*-molecular cooperative motion.

The fast mode relaxation times, τ_{fast}, exhibited the Arrhenius type dependence on temperature but the activation energy changed in the vicinity of T_g of all the mixtures which exhibited the fast mode relaxation of 5CB. The fast mode relaxation

intensity increased with increasing temperature. From these results, it was concluded that the fluctuation motion of the rod-like LM such as 5CB was affected by the "cage" size which would be dependent on temperature.

In chapter IV, the orientational correlation between the components in PS/5CB and PS/5CT mixtures was evaluated by simultaneous measurements of dynamic birefringence and viscoelastic relaxation, and the effect of the nematic interaction (NI) was quantitatively examined. By applying the MSOR, the values of C_R and C_G were determined as functions of the 5CB or 5CT concentration. These values are determined by anisotropic polarizabilities of rubbery units (the Rouse segments) and glassy units for polymer chains, respectively, but are affected by the NI. From the concentration dependence of the C_R value, it was concluded that the mesogenic low-mass molecules (5CB and 5CT) partially aligned parallel to the orientation direction of PS segments through the NI. The inter-component NI parameter in PS/5CB and PS/5CT mixtures is determined by using a newly proposed equation. The NI parameter, $\varepsilon_{PS,5CB}$ and $\varepsilon_{PS,5CT}$ were 0.064 ± 0.006 and 0.080 ± 0.010, respectively, being smaller compared with the value of $\varepsilon_{PS,PS}$ (0.26). The weak NI between PS and 5CB (or 5CT) suggested that NI strength between different components in miscible mixtures depended on their chemical structures including the size and/or shape differences. From the result that the NI parameter was small in the dynamically homogeneous mixture, it was suggested that there is no direct correlation between dynamic cooperativity and orientational coupling.

List of Publications

1. "Dynamics in Low Mass Molecules Dissolved in Polymers"
   Urakawa, O. Nobukawa, S. Shikata, T. Inoue, T. *Journal of the Society of Rheology, Japan* **2010**, 38, 41-46
2. "Evaluation of Nematic Interaction Parameter between Polymer Segments and Low-Mass Molecules in Mixtures"
   Nobukawa, S. Urakawa O. Shikata, T. Inoue, T. *Macromolecules* **2010**, 43, 6099-6105
3. "Cooperative Dynamics in Polystyrene and Low-Mass Molecule Mixtures",
   Nobukawa, S. Urakawa, O. Shikata, T. Inoue, T. *Macromolecules*, **2011**, 44, 8324-8332
4. "Dynamics of a probe molecule dissolved in several polymer matrices with different side chain structures: Determination of correlation length relevant to glass transition"
   Nobukawa, S. Urakawa, O. Shikata, T. Inoue, T. *Macromolecules* **2013**, 46, 2206-2215

Related paper

5. "Component Dynamics in Polystyrene/4-Pentyl-4'-cyanobiphenyl Blend"
   Nobukawa, S. Urakawa, O. Shikata, T. Inoue, T. *AIP Conference Proceedings* **2008**, 1027, 561-563

Other Papers

6. "Small-Angle Neutron Scattering Study on the Miscibility and Concentration Fluctuation of Hydrogen-Bonded Polymer Blends"
   Urakawa, O. Ikuta, H. Nobukawa, S. Shikata, T. *J. Polym. Sci. Part B: Polym. Phys.* **2008**, 46, 2556-2565
7. "Miscibility Control of Polystyrene and 4-Pentyl-4'-cyano-biphenyl by Partial *p*-Hydroxymethylation"
   Nobukawa, S. Urakawa, O. Shikata, T. Inoue, T. *Zairyo* **2009**, 58**,** 47-52
8. "Origin of High Segmental Mobility at Chain Ends of Polystyrene"
   Miwa, Y. Shimada, S. Urakawa, O. Nobukawa, S. *Macromolecules* **2010**, 43**,** 7192-7199
9. "Dynamics and Hydrogen-bonding of Benzylalcohol in Toluene Solution"
   Nobukawa, S. Urakawa, O. Shikata, T. Inoue, T. to be submitted